Dynamic Characteristics of a Vertical Axis Vane Type Wind Turbine

By

Zulfa Ferdous

St. No. 100710018F

A Thesis

Submitted to the

Department of Mechanical Engineering

In partial Fulfillment of the requirements for the degree

Of

Masters of Science in MECHANICAL ENGINEERING

Department of Mechanical Engineering

Bangladesh University of Engineering and Technology

Dhaka

June 2011

RECOMMENDATION OF THE BOARD OF EXAMINERS

The board of Examiners hereby recommends to the Department of Mechanical Engineering, Bangladesh University of Engineering and Technology, Dhaka, the acceptance of the thesis titled "Dynamic Characteristics of a Vertical Axis Vane Type Wind Turbine", submitted by Zulfa Ferdous, Roll No: 100710018F, Session: October 2007, in partial fulfillment of the requirements for the degree of Master of Science in Mechanical Engineering on June , 2011.

1. _____

Dr. Md. Quamrul Islam (Supervisor) Chairman
Professor
Department of Mechanical Engineering
BUET, Dhaka – 1000

2. _____

Dr. M. Mahbubul Alam (Ex-Officio) Member
Professor & Head
Department of Mechanical Engineering
BUET, Dhaka – 1000

3. _____

Dr. Amalesh Chandra Mandal Member
Professor
Department of Mechanical Engineering
BUET, Dhaka – 1000

4. _____

Dr. Mohammad Mamun Member
Associate Professor
Department of Mechanical Engineering
BUET, Dhaka – 1000

5. _____

Dr. M. Hosney Ara Begum Member
Senior Engineer (External)
BCSIR, Dhaka

CERTIFICATE OF RESEARCH

This is to certify that the work presented in this thesis is an outcome of the investigation carried out by the author under the supervision of Dr. Md. Quamrul Islam, Professor, Department of Mechanical Engineering, Bangladesh University of Engineering and Technology (BUET), Dhaka.

Dr. Md. Quamrul Islam	Zulfa Ferdous
Supervisor	Author

ACKNOWLEDGEMENT

I would like to express my sincerest gratitude and indebtedness to DR. M. Quamrul Islam, Professor, Department of Mechanical Engineering, Bangladesh University of Engineering and Technology, Dhaka, for his valuable suggestions, advice and guidance from the very beginning of the work. His initiatives, encouragement, patience and invaluable supervision are gratefully acknowledged. I am also indebted to him for providing me with necessary information, papers, giving me valuable ideas and opinions that helped me to complete the work smoothly.

Sincere thanks are offered to Superintendent and Chief Instructors and Technicians of Machine Shop, Welding and Sheet Metal Shop, BUET for their co-operation in fabricating and assembling different parts and components of the experimental set-up. I am thankful to the Lab instructor of Fluid Mechanics lab, Lab Instructor of Heat Transfer lab, Lab Instructor of Foundry Shop, Senior Lab Instructor of Solid Mechanics lab, Lab Instructor of Solid Mechanics Laboratory of Mechanical Engineering Department, BUET, for their assistance in fabrication and manufacturing of different components of the experimental set-up.

My appreciation is extended to my father and mother for their constant inspiration and encouragement, my brothers for their co operation in different stages. Specially, I would like to express my heartiest gratitude to my kids for their sacrifices and my husband for his inspiration and all sorts of supports.

ABSTRACT

The present research work concerns with the dynamic conditions of vertical axis vane type rotor at different Reynolds number. The investigation on wind loading and aerodynamic effects on the four, five and six bladed vertical axis vane type rotors have been conducted with the help of a subsonic wind tunnel together with the experiment set-up of the vane type rotor and a spring balance. The experiment was carried out in the open circuit subsonic wind tunnel by placing the rotor at its exit section. For different bladed rotor the flow velocities were varied from 5 m/s to 9 m/s covering the Reynolds numbers up to 1.2 x 10^5.

For the purpose of analyzing the dynamic conditions of rotor, the rpm of multi-bladed rotor at different loading conditions and the difference in tensions between two ends of the friction belt for different Reynolds number were measured. Finally, from these data, the changes in Tip Speed Ratio, Power coefficient and Torque coefficient with the increase in load were determined at different Reynolds number of multi-bladed rotor.

The nature of predicted dynamic aerodynamic characteristics has been analyzed by comparing them with existing research works. For comparison power coefficient versus tip speed ratio of the present measurement and previous researcher's works has been plotted on the same graph. It is seen that there is a close correlation between the present result and those obtained from the existing research works and the nature of all compared curves are similar to previous ones.

TABLE OF CONTENTS

LIST OF FIGURES

LIST OF SYMBOLS

C_P Power Coefficient, $C_p = \frac{P_t}{\frac{1}{2}\rho V^3 A}$

P_t Power extracted by the turbine

A Rotor disc area, HD

D Diameter of the rotor

H Height of the rotor

V Free stream wind speed

C_q Torque Coefficient, $Cq = \frac{T_t}{\frac{1}{2}\rho V^2 AR}$

T_t Actual torque the shaft can develop

R Radius of the turbine rotor

d Diameter of the blade

F_L Lift force acting on a blade

F_D Drag force acting on a blade

F_N Normal force acting on a blade

F_T Tangential force acting on a blade

V_{rel} Relative velocity

R Reynolds number, VD/ν

Greek Symbols:

ρ Air density

λ Tip speed ratio, $R\Omega/V_\infty$

Ω Angular speed of the rotor

ν Kinematic viscosity of air

σ Blade solidity

1 INTRODUCTION

1.1 General

Energy has become synonymous with today‘s civilization. With the advancement of modern science rapid developement is seen in all aspect of life, so the demand of energy is increasing in geometric rate. The most conventional energy source like oil, hydro, coal, natural gas, nuclear etc. are used as fuels all around the world. Among these conventional fuels, only hydro is renewable in nature and the other sources are non renewable and causes of air pollution and green house effect. In the consequence, environmental pollution has reached in an alarming level all over the world. As the sources of conventional energy is not only being exhausted very rapidly but also causing serious threats to the existence of mankind, people are rethinking about the use of environment friendly as well as renewable energy resources in large scale. Replacing the conventional fuels with Renewable energy sources include wind energy, solar(photovoltaic) systems, solar thermal systems, biomass energy (wood and other plant fuels), geothermal energy, fuel cell, municipal waste etc. The costs of many of these technologies have come down considerably in recent years, particularly wind energy, which is now competitive with conventional power sources in regions with strong winds.

The science of exploitation of wind power is not a new one. For the past few centuries, people are extracting energy from the wind in various ways. One means for converting wind energy to a more useful form is through the use of windmills. Recently, due to the fuel crisis, this science is gaining more popularity. Wind energy has become very lucrative now-a-days due to its reliability. The European Wind Energy Association (EWEA) estimates that between 20 GW and 40 GW of offshore wind energy capacity will be operating in the European Union by 2020. A fully developed European offshore wind resource could deliver a capacity of several hundred GW to supply our future energy demands. Over the years people are extracting wind energy in various ways. One of the means for converting the wind energy to a more useful form is through the use of windmills.

There are various types of windmills. The most common one is the horizontal axis wind turbine. Another type is the vertical axis wind turbine. The primary attraction of the vertical axis wind turbine is the simplicity of its manufacture compared to that of horizontal axis wind turbine. Among the different vertical axis wind turbine, the Vertical Axis Vane Type Wind Turbine is a slow running wind machine and has relatively lower efficiency. Still it is being used in the developing countries because of its simple design, easy and cheap technology for construction and good starting torque characteristics at low wind speed. It is independent of wind direction for generation of power and it also works even at low speed.

1.2 History of Wind Energy

Human beings have used wind energy for thousands of years. Ancient Persians used wind energy to pump water before the birth of Christ. The world was explored by wind-driven ships long before engines were invented. As recently as the 1920s, over a million wind turbines pumped water and provided electricity to farms in North America and Europe.

The current interest in wind energy was started by the need to develop clean, sustainable energy systems that can be relied on for the long-term future. Modern aerodynamics and engineering have improved wind turbines. Wind Energy is providing reliable, cost-effective, pollution-free energy for individual, community and national applications.

1.3 Sources of Wind Energy

Wind energy is an indirect form of solar energy. The sun radiaetes wind energy is an indirect form of solar energy. The sun radiates 1014 kJ/sec of energy to the earth. Sufficient amount of energy is continuously transferred from the sun to the air of earth. Some of the sun's energy is absorbed directly by air. Most of the energy of the sun is first absorbed by the surface of the earth and then transferred to air by convection. Between 1-2% of the solar radiation that reaches the earth is converted into wind energy. Global wind pattern depends mainly on the earth's rotation around its own axis, ocean current and cosmic gravitational pulls. However, the prime cause of local wind is different. The Earth is unevenly heated by the sun, such that the poles receive less energy from the sun than the equator; along with this, dry land heats up (and cools down) more quickly than the seas do. Cold air over the sea then replaces the rising air. The diagram below shows how this 'system' works. The differential heating drives a global atmospheric convection system reaching from the Earth's surface to the stratosphere which acts as a virtual ceiling. Most of the energy stored in these wind movements can be found at high altitudes where continuous wind speeds of over 160 km/h (99 mph) occur. Eventually, the wind energy is converted through friction into diffuse heat throughout the Earth's surface and the atmosphere.

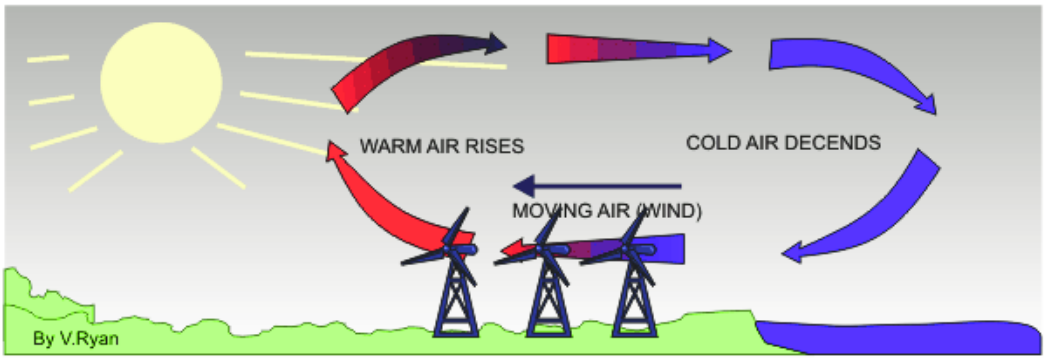

Figure 1. 1: How wind turbine works

1.4 Nature of Wind Energy

Wind energy is the kinetic energy that is present in moving air; this kinetic energy in turn derives from the heating of the atmosphere, earth and oceans by the sun. The amount of energy in the wind depends mainly on wind speed, but is also affected slightly by the density of the air, which is determined by the air temperature, barometric pressure and altitude.

For any wind turbine, the power and energy output increases dramatically as the wind speed increases. Therefore, the most cost-effective wind turbines are located in the windiest areas. Wind speed is affected by the local terrain and increases with height above the ground, so wind turbines are usually mounted on tall towers.

1.5 Costs of Wind Energy

The cost of wind energy is determined by:

- The initial cost of the wind turbine nstallation.
- The interest rate of the money invested.
- The amount of energy produced.

Any wind turbine that is installed in a very windy area generates less expensive electricity than the same unit installed in a less windy area. So it's important to assess the wind at the potential site.

Modern wind turbine generators cost about $1500 per kilowatt for wind farms that use multiple-unit arrays of large machines. Smaller individual units cost up to $3000 per kilowatt. In good wind areas, the costs of generating electricity range between five and ten cents per kilowatt hour. That cost is somewhat higher than the costs associated with an electrical facility, but wind energy costs are decreasing every year, whereas most conventional generation costs continue to increase.

In remote areas, generating electricity with diesel generators can exceed $0.25 per kilowatt hour. So in good wind areas, electricity that is generated by the wind is clearly cost effective. When compared to the money that is charged by electrical companies, wind energy costs are nearly competitive. And that is without accounting for the environmental and health benefits of using a non-polluting source of energy.

1.6 Wind Energy Around the World

Worldwide development of wind energy expanded rapidly since early 1990s. Most of the investment was spent in Europe where conventional electricity costs are higher and where political motivation to reduce greenhouse gas pollution is greater. At the end of April 1999, 10,000 megawatts of wind-generated electricity produced some 22.5 TWh of electricity. That is sufficient electricity for all the industrial, commercial and domestic electrical requirements of

about two cities the size of Madrid, Spain – a total of about 8 million people. The average annual growth rate from 1994 to 2001 of the world installed capacity of wind power was 31%, making the wind industry one of the fastest growing. Unlike the last surge in wind power development during 1970s and early 1980s, which was due mainly to the oil embargo of the OPEC countries, the current wave of wind energy development is driven by many forces that make it favorable. These include its tremendous environmental, social and economic benefits, its technological maturity and the deregulation of electricity markets throughout the world, public support and government incentives. The global wind turbine industry comprises about a dozen major firms located in Europe with annual revenues of about of $100M per year. The Danish wind turbine industry is larger than their fishing and agricultural industries combined.

1.7 Benefits of Wind Energy

Wind energy is an ideal renewable energy because:

- It is a pollution free, infinitely sustainable form of energy.
- It does not require fuel
- It doesn’t create greenhouse gases
- It doesn’t produce toxic or radioactive waste

Wind energy is quiet and doesn't present any significant hazard to birds or other wildlife. When large arrays of wind turbines are installed on farmland, only about 2% of the land area is required for the wind turbines. The rest is available for farming, livestock and other uses. Landowners often receive payment for the use of their land which enhances their income and increases the value of the land. Ownership of wind turbine generators by individuals and the community allows people to participate directly in the preservation of our environment.

Each megawatt-hour of electricity that is generated by wind energy helps to reduce the 0.8 to 0.9 tonnes of greenhouse gas emissions that are produced by coal or diesel fuel generation each year.

1.8 Wind Turbine

All grid-connected commercial wind turbines today are built with a propeller-type rotor on a horizontal axis (i.e. a horizontal main shaft). Most horizontal axis turbines built today are two or three-bladed, although some have fewer or more blades. The purpose of the rotor is to convert the linear motion of the wind into rotational energy that can be used to drive a generator.

The wind passes over both surfaces of the airfoil shaped blade but passes more rapidly over the longer (upper) side of the airfoil, thus creating a lower-pressure area above the airfoil. The pressure differential between top and bottom surfaces results in aerodynamic lift. In an aircraft wing, this force causes the airfoil to rise, lifting the aircraft off the ground. Since the blades of a wind turbine are constrained to move in a plane with the hub as its center, the lift force causes rotation about the hub. In addition to the lift force, a drag force perpendicular to the lift force

impedes rotor rotation. A prime objective in wind turbine design is for the blade to have a relatively high lift–to-drag ratio. This ratio can be varied along the length of the blade to optimize the turbine's energy output at various wind speeds.

Wind mills that were used to grind grain are an example of early uses of wind energy. Modern uses of wind energy include generation of electricity and pumping water. Current wind energy machines are called wind turbine generators, wind pumps or more generally, wind turbines.

1.9 Global Wind Energy Utilization Scenario

Wind energy "penetration" refers to the fraction of energy produced by wind compared with the total available generation capacity. At present, a few grid systems have penetration of wind energy above 5%: Denmark (values over 19%), Spain and Portugal (values over 11%), Germany and the Republic of Ireland (values over 6%). For instance, in the morning hours of 8 November 2009, wind energy produced covered more than half the electricity demand in Spain, setting a new record, and without problems for the network.

The Danish grid is heavily interconnected to the European electrical grid, and it has solved grid management problems by exporting almost half of its wind power to Norway. The correlation between electricity export and wind power production is very strong.

There are now many thousands of wind turbines operating, with a total capacity of 157,899 MW of which wind power in Europe accounts for 48% (2009). World wind generation capacity more than quadrupled between 2000 and 2006, doubling about every three years. 81% of wind power installations are in the US and Europe. The share of the top five countries in terms of new installations fell from 71% in 2004 to 62% in 2006, but climbed to 73% by 2008 as those countries—the United States, Germany, Spain, China, and India—have seen substantial capacity growth in the past two years.

By 2010, the World Wind Energy Association expects 160 GW of capacity to be installed worldwide, up from 73.9 GW at the end of 2006, implying an anticipated net growth rate of more than 21% per year.

Denmark generates nearly one-fifth of its electricity with wind turbines—the highest percentage of any country—and is ninth in the world in total wind power generation. Denmark is prominent in the manufacturing and use of wind turbines, with a commitment made in the 1970s to eventually produce half of the country's power by wind.

In recent years, the US has added more wind energy to its grid than any other country, with a growth in power capacity of 45% to 16.8 GW in 2007. Wind power generation in the U.S. was up 31.8% in February, 2007 from February, 2006. The average output of one MW of wind power is equivalent to the average electricity consumption of about 250 American households. According to the American Wind Energy Association, wind will generate enough electricity in

2008 to power just over 1% (equivalent to 4.5 million households) of total electricity in U.S., up from less than 0.1% in 1999.

China had originally set a generating target of 30,000 MW by 2020 from renewable energy sources, but reached 22,500 MW by end of 2009 and could easily surpass 30,000 MW by end of 2010. Indigenous wind power could generate up to 253,000 MW. By 2008, wind power was growing faster in China than the government had planned, and indeed faster in percentage terms than in any other large country, having more than doubled each year since 2005. Policymakers doubled their wind power prediction for 2010, after the wind industry reached the original goal of 5 GW three years ahead of schedule. Current trends suggest an actual installed capacity near 20 GW by 2010, with China shortly thereafter pursuing the United States for the world wind power lead.

India ranks 5th in the world with a total wind power capacity of 9,587 MW in 2008, or 3% of all electricity produced in India.

Mexico recently opened La Vento II wind power project as an important step in reducing Mexico's consumption of fossil fuels. The 88 MW project is the first of its kind in Mexico, and will provide 13 percent of the electricity needs of the state of Oaxaca. By 2012 the project will have a capacity of 3500 MW.

Another growing market is Brazil, with a wind potential of 143 GW. The federal government has created an incentive program, called Proinfa, to build production capacity of 3300 MW of renewable energy for 2008, of which 1422 MW through wind energy. The program seeks to produce 10% of Brazilian electricity through renewable sources.

South Africa has a proposed station situated on the West Coast north of the Olifants River mouth near the town of Koekenaap, east of Vredendal in the Western Cape Province. The station is proposed to have a total output of 100 MW although there are negotiations to double this capacity. The plant could be operational by 2010.

France has announced a target of 12,500 MW installed by 2010, though their installation trends over the past few years suggest they'll fall well short of their goal.

Canada experienced rapid growth of wind capacity between 2000 and 2006, with total installed capacity increasing from 137 MW to 1,451 MW, and showing an annual growth rate of 38%. Particularly rapid growth was seen in 2006, with total capacity doubling from the 684 MW at end-2005. By 2025, Canada will reach its capacity of 55,000 MW of wind energy, or 20% of the country's energy needs.

1.10 Prospects of Wind Energy in Bangladesh

Wind can be a vital source of energy if properly utilized and exploited. But before high-end projects are implemented, adequate research should be done to study the feasibility and determine a suitable type of project to implement. The primary parameter needed is wind speed and direction. Bangladesh is situated between 20.30 – 26.38 degrees North latitude and 88.04 – 92.44 degrees East.

In Bangladesh, some early studies on wind energy prospects were made by Professor Muhtasham Hussain of Dhaka University and his colleagues [Hussain et. al 1986], as well as some enthusiasts from Bangladesh University of Engineering and Technologies (BUET). The Bangladesh Meteorological department has wind speed measuring stations in towns and cities. Data from earlier measurements and analysis of upper air data by CWET India show that wind energy resource of Bangladesh is not good enough (>7 m/s) for grid connected wind parks [GEF 2001].

Over the past years, many organizations have made many attempts to collect data on wind resources in Bangladesh. Wind speed has been measured in Patenga, Cox's Bazar, Kuakata, Moheshkhali, and Noakhali by the computerized anemometers. The wind computers have been installed at 20 meters height. According to this study annual average wind speeds in the coastal regions of Bangladesh are greater than 6.5 m/s at the height of 20 meters. It has been observed that during day times (8 a.m. to 7 p.m.) wind speeds are about 30 to 40% higher than the average values. The value of the power exponent α has been determined in the above sites and it is 0,139. So, at 40 meters height the annual average wind speed is about 7.15 m/s. So, wind speeds in the coastal regions of Bangladesh are suitable for both water pumping and electricity generation.

Based on this collected data, many small wind energy projects have been undertaken. At present, several wind resource assessment program (WERM, SWERA, WRAP OF BPDB) is ongoing in the country.

The first-ever generation of electricity from wind at the 0.9 Mw (900 kilowatt) plant near the Muhuri Dam in Sonagazi upazila under Feni district has ushered in new hopes for generation of power with minimum cost in the country, report BSS. The power plant having separate wind turbines of 225 kw each, established at a cost of Tk 90 million including Tk 19.3 million for feasibility study, is now ready to generate electricity from wind and supply to the Muhuri Irrigation Project and the national grid.

1.11 Objectives with specific aims and possible outcome

The objectives of the present study are as follows:

- To determine the aerodynamic characteristics of four/five/six blade Vertical Axis Vane Type rotor in dynamic condition i.e. power coefficient, torque coefficient at different tip speed ratio will be determined.

- To study the effect of number of blades of Vertical Axis Vane type rotor.

- To study the effect of change of reynolds number on its dynamic characteristics.

- A comparison will be made between the present dynamic method (for four/ five/six bladed Vertical Axis Vane Type Rotor) with the static[2] one

- A comparison will be made between the present dynamic method (for four/ five/six bladed Vertical Axis Vane Type Rotor) with other existing experimental and theoretical works on Vertical Axis Wind Turbines for different tip speed ratios.

1.12 Scope of the Thesis

The study covers only the experimental investigation of multi bladed vane type rotor.

The prime objective of the investigation is to compare the results of four, five and six bladed vane type rotor in dynamic condition to that of the predicted one. And also to determine the dynamic characteristics at different loading condition for different free stream velocity ranging from 5m/s to 9m/s. The several phases of the entire investigation are described in the thesis.

The brief description of the work which have been done in regard to the theoretical and experimental investigation of vertical axis wind turbine is provided in this section. The prime objectives of the investigation is to determine the dynamic characteristics of a vane type rotor of a vertical axis wind turbine.

Literature Survey containing historical background and review of the existing prediction methods are described in **Chapter 2**. In historical background, a short description of the history of wind power research and development from ancient period up to modern age is given. The papers related to the present study, which have been published so far by different authors, are provided in this chapter.

The existing theories i.e. the momentum theory and the blade element theory are described in **Chapter 3**. Only the theories that are directly related to the present work have been taken into consideration.

Chapter 4 presents detailed description of design and fabrication of vertical axis multi-bladed vane type rotor, choice of rotor blade material and selection of blade design parameters etc.

In **Chapter 5** mainly an account of the experimental arrangement and procedure adopted for the investigation are presented. It includes the description of wind tunnel, the constructional details of the test section. The experiment was conducted in the wind tunnel for two dimensional uniform cross flow with different wind speeds.

Chapter 6 presents the analysis concerning the result and discussions of the present experimental results which are printed in the graphical form. In few cases the existing experimental results of different researchers are correlated with the present one.

Finally, the conclusions which are drawn from the present work are given in **Chapter 7.** This chapter includes an outline regarding further research work in this field as well.

2 REVIEW OF LITERATURE

2.1 Introduction

Arising from the increasing practical importance of wind turbine aerodynamics, there have been, over the past few decades, an enormous increase in research works concerning laboratory simulations, full-scale measurements and more recently, numerical calculations and theoretical predications for flows over a wide variety of Savonius rotors. Researches in different countries have contributed greatly to the knowledge of analytical prediction methods of wind turbines, but the major part of the reported works is of fundamental nature involving the flow over horizontal axis wind turbine and vertical axis Darrieus rotor. Most of the researchers have conducted research works on either two/three semi cylindrical bladed Savonius rotor or S-shaped rotor with various flow parameters. A brief description of some of the papers related to the present work is given in this chapter.

2.2 Historical Background

The history of wind power shows a general evolution from the use of simple, light devices driven by aerodynamic drag forces; to heavy, material-intensive drag devices; to the increased use of light, material-efficient aerodynamic lift devices in the modern era. However aerodynamic lift (the force that makes airplanes fly) is not a modern concept as it was known to the ancients. The earliest known use of wind power is the sail boat, and this technology had an important impact on the later development of sail-type windmills. Ancient sailors understood lift and used it every day, even though they didn't have the physics to explain how or why it worked.

From the ancient period people have been working on various classes of wind contrivances to extract energy from the wind. Works on windmills have probably been started from 2000 B.C. The period from the ancient time up to the end of the 19^{th} century may be categorized as the ancient development period while that from the end of 19^{th} century up to date may be termed as the modern development period.

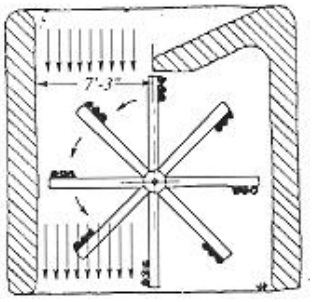

Figure 2. 1: Persian windmill of vertical-axis type

In the ancient development period, in the middle of 7th century, Persian vertical-axis windmill circa (Figure 2.1) was constructed which was used to grind grain. That kind of windmill was working up to about 12th century, when simultaneously in France and England Dutch type of windmills were made whose purpose were to grind grain and pump water. These windmills were of horizontal-axis types. Up to the end of 19th century people were working with these classes of windmills only.

Figure 2. 2: Windmill for water pumping

At the end of 19th century, the first modern windmill of horizontal-axis type with multi-blade was built in Denmark to produce electricity. It was the beginning of the modern development period. Starting from that time people in different countries especially in rural America has been constructing a large number of multi-bladed wind turbines for pumping water and generating electricity. Afterwards as a consequence of development works for several years, two or three bladed propeller type of windmills with airfoil shape blades were built in near about 1925. In 1931, 100 kW Russian horizontal-axis wind turbine was constructed while in 1934; the large 1250 kW Smith-Putnam horizontal-axis wind turbine was built.

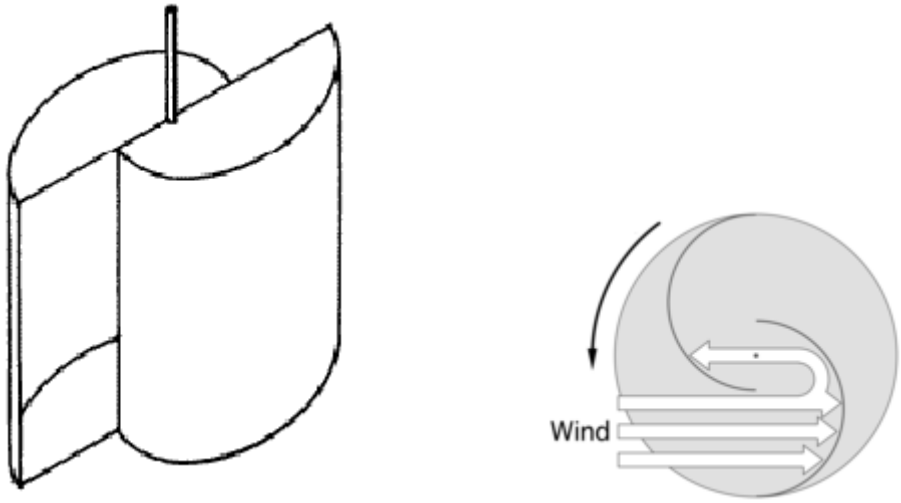

Side View Sectional view

Figure 2. 3: Savonius rotor

Modern development period have really begun with the development of horizontal-axis wind turbines. In 1924 Finnish Engineer S.J. Savonius constructed the first Savonius rotor of vertical-axis type (Figure 2.3) and he conceived the idea from the Flattener's Rotor. In 1925 G. J. M. Darrieus of France, proposed for United State patent a new type of wind turbine designed for the generation of power. The patent issued in 1931 as number 1,835,018 was for a "turbine having its rotating shaft transverse to the flow of the current". The straight-bladed configuration was also covered in the original Darrieus patent. This kind of wind machine is called Darrieus turbine (Figure 2.4) after the name of G. J. M. Darrieus.

Figure 2. 4: Darrieus wind turbine

Since the beginning of the twentieth century, researchers in the various part of the world had been giving much effort in the development works of the wind turbines but from about the middle of this century, it began to loose its momentum for further development. In about 1970's people took renewed interest in this field. Especially in 1973 with oil embargo, people were thinking regarding the alternate sources of energy. As a result in many developed and underdeveloped countries, a lot of new projects concerning the development of wind turbines have been taken.

Only during the last decade in the different countries enormous attention has been paid in the field of performance prediction method applicable to wind turbines. As an outcome, a number of analytical prediction methods have been developed. Works have also been extended to both the static and dynamic analyses of wind turbines. Different type of design methods has been worked out in many places. Still there exists no good and reasonable analytical performance prediction method especially for a high solidity Darrieus wind turbine.

2.3 Literature Concerning S-Shaped Savonius Rotor

Islam et al. [7] investigated the aerodynamic forces acting on a stationary S-shaped rotor and made an attempt to predict the dynamic performance from these forces. The work was done by measuring the pressure distribution over the surface of the blades. The measurements were carried out in a uniform flow jet produced by an open circuit wind tunnel and at a constant wind speed of 8.9 m/s, which corresponds, to a Reynolds ($R_e = \rho UoD/\mu$) of $1.1x10^5$. The results indicate that flow separates over the front and back surfaces of the blades and the point of separation depends on the rotor angle. The pressure difference was observed between the two surfaces of each blade, which in turn, gives drag coefficients. The drag and hence, the torque of each blade varies with rotor angle and becomes maximum at $\alpha = 45°$ for the advancing blade and at $\alpha = 105°$ for the returning blade. The net torque is maximum at $\alpha = 45°$ and becomes negative in the range of rotor angle between 135° to 165°.

Huda et al. [10] analyzed the performance of S-shaped rotor by placing a flat plate in front of the returning blade. They found that the power coefficient of an S-rotor is dependent on the Reynolds number and the value of Cp (power coefficient) is increased with Reynolds number (in the range of the Reynolds number studied). Maximum 20% of power coefficient can be increased by using the deflecting plate which occurs at a deflecting angle of 35° for b = 0.5D, where b = distance between plate and rotor center and D = diameter of the rotor.

Bowden, G.J. and McAleese, S.A [13] made some measurements on the Queensland optimum S-shaped rotor to examine the properties of isolated and coupled S-shaped rotor. In particular it is shown that the efficiency of the turbine is around 18%, which is lower than the figure of 23% given by earlier workers. In the experimental setup the UNSW open jet air-stream, diameter 0.76 m, was used to produce wind speeds in the range 0 to 30 m/s. The turbulence ($\sqrt{u^2}/V_\alpha$) in the jet stream was low. Wind flow measurement was investigated using 'tell-tales' (light pieces of cotton attached to a probe) and a stroboscope. In this way, it was possible to detect the direction of the airflow relative to the angular position of the rotor blades. Many photographs were taken and later used to construct a visual airflow pattern around the rotor. The linearized hot-wire anemometer, on the other hand, enabled measurements to be made of velocity magnitudes and fluctuations to an upper frequency limit of 5 kHz. It cannot however be used to measure direction. The hot-wire anemometer linearizer was based on a design due to the Institute of Sound and Vibration Research (ISVR), Southampton University, U.K. In general, a storage oscilloscope was used to record the data, particularly from the more structured turbulent regions. However, measurements of turbulence intensity were also made by connecting an rms voltmeter to the output of the hot-wire linearizer. The results of this research were subsequently used to suggest that some form of active coupling between Savonius rotors might be possible. In particular, it has been shown that if two counter-rotating rotor are placed side by side, a natural phase locking occurs between the two turbines.

Islam et al. [33] made an investigation on variation of static torque and drag coefficient of an S-Shaped Savonius rotor for different number of rotor blades. This has been done by measuring the pressure distribution on the blade surfaces for different rotor angles. All the experiments have been carried out at Reynolds number 1.07×10^5 in a uniform flow jet produced by an open circuit wind tunnel. Experimental results indicate that both of the drag force and hence the torque change frequently with rotor angle. It is also found that as the number of rotor blade increases, the starting torque of rotor increases but there is no significant increase in net torque output. It is observed that, torque distribution becomes more uniform as the number of blade of rotor increases.

Saha et al. [34] aimed at exploring the feasibility of S-shaped bladed Savonius rotor for power generation. The S-shaped blade in a three-bladed rotor system has been tested in a low speed wind tunnel, and its performance has been compared with conventional semicircular blades (with twist angle of 01). Performance analysis has been made on the basis of starting characteristics, static torque and rotational speed. Experimental evidence shows the potential of the S-shaped bladed rotor in terms of smooth running, higher efficiency and self-starting capability as compared to that of the conventional bladed rotor. Further experiments have been conducted in the same setup to optimize the twist angle.

Saha and Maity [41] experimented for augmenting the energy-harnessing effectiveness. The proposal given by them was to employ a V-shaped deflector mounted upstream of the rotor, apex into the wind, so that the air-flow resistance encountered by the half of the wind-turbine blade

advancing (i.e. moving) into the wind was reduced. By (i) carrying out experimental tests with the deflector in different positions relative to the rotor, and (ii) varying the wedge angle between the deflector blades, an optimal configuration for the particular system tested was determined. With the optimally pitched deflector set at its optimal location, the rotor harnessed about 20% more power, compared with the unblocked (i.e. standard) rotor both for an approximate wind speed of 4 m/s. Such a significant improvement, achieved by this simple cheap means, suggests that the use of the partially blocking wedge is highly desirable.

2.4 Literature Concerning Vertical Axis Darrieus Wind Turbine

The most simple prediction method for the calculation of the performance characteristics of a Darrieus wind turbine is the single stream tube model. It has been introduced first by Dr. Templin [14] in 1974. In this model the whole turbine is assumed to be enclosed within the single stream tube. Dr. Templin first incorporated the concept of the windmill actuator disc theories into the analytical model of a Darrieus wind turbine. In the actuator disc theory the induced velocity (rotor axial flow velocity) is assumed to be constant through the "disc" and is obtained by equating the stream-wise drag with the change in axial momentum. In the assumption of Templin, the actuator disc is considered as the surface of the imaginary body of revolution. It is assumed that the flow velocity is constant although the upstream and the downstream faces of the swept volume. This theory presented by Templin is the first approach to permit numerical design calculations for a vertical-axis Darrieus wind turbine.

An analytical method using single stream tube model is presented by Noll and Ham [15] for the performance prediction of a vertical-axis wind turbine with straight blades, which are cyclically pitched. They added the effect of strut drag, turbulent wake state and dynamic stall to their analytical method.

An improvement to the above method is the multiple stream tube model introduced by Wilson and Lissaman [16]. In this model the swept volume of the turbine is divided into a series of adjacent, aerodynamically independent stream tube. Blade element and momentum theories are then employed for each stream tube. In their method, they consider the flow as inviscid and incompressible for the calculation of the induced velocity through the stream tube. As a result, there appears only the lift force in the calculation of induced velocity. Wilson et al considered the theoretical lift for their calculation. This induced velocity varies over the frontal disc area both in the vertical and the horizontal directions. Atmospheric wind shear can be included in the

multiple stream tube models. Multiple stream tube model is still inadequate in its description of the flow field. Wilson's model can be applied only for a fast running lightly loaded wind turbine.

Strickland [17] in his paper presents a multiple stream tube model for a vertical axis Darrieus turbine. He finds the induced velocity by equating the blade element forces (including airfoil drag) and the change in the momentum along each stream tube. The basic difference between Wilson's and Strickland's model is that Wilson used the lift force (theoretical) only in the calculation of induced velocity while Strickland added the effect of drag force as well for the similar calculation. Wilson's model gives first convergence while Strickland's model gives slow convergence.

An improved version of multiple streamtube method is presented by Read and Sharpe [18] for vertical-axis Darrieus wind turbines. In their model, the parallel streamtube concept is dispensed with and expansion of the streamtube is included. It is strictly applicable to low solidity lightly loaded wind turbines with large aspect ratio. It can predict the instantaneous aerodynamic blade forces and the induced velocities better than that by the conventional multiple streamtube model. But prediction of overall power coefficients cannot be made with reasonable accuracy. It usually gives lower power than that obtained experimentally.

In their paper, Paraschivoiu and Delcalaux [19], presented improvements in the double multiple streamtube model. They considered the induced velocity variation as a function of the azimuthal angle for each streamtube. They have added a new formulation for an approximate Troposkien shape by considering the effect of gravitational field and a semi-empirical dynamic stall model.

Paraschivoiu, Fraunie and Beguier [20] introduce in their paper the expansion effects of the streamtube through the rotor and these are included with the double multiple model. With the measured and the predicted data they observe that streamtube expansion effects are relatively significant at high tip speed ratios.

Fanacci and Walters [21] presented a two-dimensional vortex model applicable to a straight-bladed wind turbine. In their analysis they consider the angle of attack very small thereby eliminating the stall effect.

Holme [22] presents a vortex model for a fast running vertical-axis wind turbine having a large number of straight, very narrow blades and a high height-diameter ratio (in order to make a two dimensional flow assumption). The analysis is valid for lightly loaded wind turbines only.

Wilson [23] also introduces a two-dimensional vortex analysis to predict the performance of a giromill. In his method he does not take into account the stall effect, because the angle of attack is assumed to be small.

Kamal et al. [35] investigated the drag and torque coefficients of a stationary five bladed vane type rotor by measuring the pressure distribution on the blade surfaces at various rotor angles. The experimental investigation has been performed at Reynolds number 1.65×10^5 in a uniform flow jet produced by an open circuit wind tunnel. It has been observed that the total static torque coefficient increases from 0^0 to 10^0, and reaches its maximum value and then decreases up to 300. From this point, the total static torque increases up to 72°. Total static torque coefficient at different rotor angles curve repeats from 72^0 to 144^0, 144^0 to 216^0, 216^0 to 288^0, and 288^0 to 360^0 angle of rotation. A quasi steady approach has been applied for the prediction of dynamic performance of the rotor using the static drag and torque coefficients. This method results in a fair agreement with the measured power coefficient.

Swamy and Fritzsche [36] investigated with the objective to improve the Darrieus type of motor. The conventional cross section of the blade for the Darrieus motor is that of a symmetrical airfoil section. Mathematical relations describing the blade geometry were presented and the behavior of the blade in a centrifugal force field was investigated, taking into account a comparison of the actual shape of the rotor blades with a quadratic parabola and catenaries for different rotor height-diameter ratios. The contribution to the torque provided by the various segments of the rotor was determined. There appeared to be a distinct advantage in using a straight cylindrical section instead of curved blades. This hypothesis is to be investigated with the aid of a small model.

Akiyoshi et al. [39] simulated flow around a vertical axis wind turbine and estimated its aerodynamic performance. The sub-grid scale turbulence model was developed to simulate the separated flow from the turbine blades. A sliding mesh technique was introduced to simulate flow through the rotational blades. Numerical results were compared with predictions based on momentum theory.

Ajedegba, J.O. [40] in this thesis analyzed the performance of a vertical axis wind turbine for applications in urban areas. Numerical simulations with FLUENT software are presented to predict the fluid flow through a novel Zephyr vertical axis wind turbine (VAWT). Simulations of air flow through the turbine rotor were performed to analyze the performance characteristics of the device. Major blade geometries were examined. A multiple reference frame (MRF) model capability of FLUENT was used to express the dimensionless form of power output of the wind turbine as a function of the wind free stream velocity and the rotor's rotational speed. A sliding mesh model was used to examine the transient effects arising from flow interaction between the

stationary components and the rotating blades. The simulation results exhibit close agreement with a stream-tube momentum model.

2.5 Literature Concerning Semi-cylindrical Bladed Savonius Rotor

F. Diaz et al [18] analyzed the drag and lift coefficient of Savonius wind machine, in order to obtain quantitative information about the aerodynamic performance of the Savonius rotor. The experiments were carried out in a low turbulence open jet of 30x50 cm section outlet, which provides an air speed adjustable between 0 and 30 m/s. The results of this work showed that for e/d=1/6, at which the rotor generates the optimum power, the drag and lift coefficients are little dependent on the operating conditions (Reynolds number, tip speed ratio λ) if λ is near the optimum value λ≈1. The re are three findings of this work: (a) the maximum efficiency of the Savonius rotor, it terms of power coefficient, takes place for λ≈1 and that c_d decreases sharply when λ increases or decreases from this value, (b) for a given Reynolds number, as the tip speed ratio increases from zero, the drag values are maintained practically constant, $C_D \approx 1.5$ in the interval ranging from λ = 0 to λ = 1.25. The most interesting zone for power extraction is located near λ≈ 1, where C_D shows minimal values. For tip speed ratios greater than 1.25, the drag coefficient increases, (c) in a wide interval around λ =1 (the most important region of operation of the Savonius rotor) the lift coefficient remains practically constant at $C_L \approx 0.5$.

Sawada, T., Nakamura, M. and Kamada, S., [24] experimentally studied the mechanism of rotation of Savonius rotor which have two semi-cylindrical blades. The force acting on a blade is measured in a water tank while a rotor is at rest condition and also while it is rotating. A flow around the rotor is observed by using aluminum powder floating on the water surface. The researchers concluded that (a) when the rotor is at rest, the rotor with overlap ratio 0.21 produces a positive torque at any attitude angle, (b) the lift around α = 240°~330° contributes a lot to the torque occurring when the rotor is rotated. Although the Savonius rotor is classified as a resistance type, the lift produce a torque in a pretty wide range of angles relative to the flow, (c) when the rotor is related, the effect of the pressure recovery by the flow through the overlap portion on the lift is little for the rotor with overlap ratio 0.21. For the rotor of a/d=0.51, the existence of a flow through the center of the rotor contributes to the production of a negative torque opposing the clockwise rotation.

Taha K. Aldos and Khalid M. Obeidat [25] analyzed the performance of two Savonius rotor running side by side at different separations using the discrete vortex method. Two configurations were considered. The torque and power coefficients were computed and

compared with the available experimental results presented by Aldoss and Najjar in an earlier paper.

R.D. Littler et al [26] made comparative tests of the Savonius rotor at constant Reynolds number. They suggested that a plain S-rotor may be good as or better than the conventional Savonius rotor with an inter-vane gap. A single S-rotor gives a Cp>0.15 (0.225 uncorrected wind-tunnel value); although duplex rotors have given Cp> 0.18 (0.32 uncorrected value). Comparative particle flow visualization studies within these rotors (Savonius rotor with conventional gap, S-rotor with no gap) and a rotor with separated vanes ('negative' gap) in a water-channel suggest the importance of attached flow round the convex surfaces of the vanes, the doubtful value of the conventional gap, and the importance of vane shape.

Sivasegaram, S. and Sivapalan, S. [27] made an experiment in improving the sectional geometry of slow-running vertical-axis wind rotors of the Savonius type has resulted in considerable improvement in rotor performance. They suggested that further improvement in power output from a rotor of given overall dimension demands the use of power augmenting systems. The influence of important design parameters of the augmenting system and that of wind direction has been determined. They showed that an eighty percent increase in power output could be achieved using a pair of vanes of moderate size.

Islam et al [4] investigated Aerodynamic characteristics of a Stationary Savonius rotor of two semi-cylindrical blades. The tests were carried out in a uniform flow jet produced by an open circuit wind tunnel. The exit of the wind tunnel consists of a square section nozzle with side length of 500m. The rotor was placed at the jet axis and 750 mm downstream of the nozzle exit. This study was carried out at a constant wind speed of U_0 = 13.3 m/s i.e., at Reynolds number, R_e= 2 x 10^5. The results of this work showed that flow separates over the convex surface of the blades and the separation point moves towards the leading and trailing edges of the advancing and returning blades respectively as the rotor angle increases from 0° to 90°. Beyond α = 90°, flow separates over the convex surface of the returning blade only. They also found that the difference in pressure on the convex and concave surfaces produces drag coefficients, C_n and C_t in the normal and tangential directions of the chord. Drag coefficients, C_n and C_t are a function of rotor angle and their resultant reaches maximum value at α = 120° and minimum value at α = 0°.

Gupta et al. [38] made a comparative study of a three-bucket Savonius rotor with a combined three-bucket Savonius–three-bladed Darrieus rotor. A combined Savonius–Darrieus type vertical axis wind rotor has got many advantages over individual Savonius or individual Darrieus wind rotor, such as better efficiency than Savonius rotor and high starting torque than Darrieus rotor. But works on the combined Savonius–Darrieus wind rotor are very scare. In view of the above,

two types of models, one simple Savonius and the other combined Savonius–Darrieus wind rotors were designed and fabricated. The Savonius rotor was a three-bucket system having provisions for overlap variations. The Savonius–Darrieus rotor was a combination of three-bucket Savonius and three-bladed Darrieus rotors with the Savonius placed on top of the Darrieus rotor. The overlap variation was made in the upper part, i.e. the Savonius rotor only. These were tested in a subsonic wind tunnel available in the department. The various parameters namely, power coefficients and torque coefficients were calculated for both overlap and without overlap conditions. From the present investigation, it is seen that with the increase of overlap, the power coefficients start decreasing. The maximum power coefficient of 51% is obtained at no overlap condition. However, while comparing the power coefficients (C_p) for simple Savonius-rotor with that of the combined configuration of Savonius–Darrieus rotor, it is observed that there is a definite improvement in the power coefficient for the combined Savonius–Darrieus rotor without overlap condition. Combined rotor without overlap condition provided an efficiency of 0.51, which is higher than the efficiency of the Savonius rotor at any overlap positions under the same test conditions.

Ammara, Leclerc and Masson [37] for the aerodynamic analysis of wind farms used various CFD techniques to simulate turbine performance, such as the viscous three dimensional differential/actuator disk method. In order to improve vertical axis wind turbine performance, CFD can be used to predict flow fields around a vertical axis wind turbine. The flow field around a vertical axis wind turbine is complicated, because of interactions between the large separated flow and wake itself.

Fujisawa [42] analyzed the power mechanism of a Savonius rotor by pressure measurements on the blade surface and by a flow visualization experiment. It was found that a low pressure region was formed on the convex side of the advancing blade contributing to the power production of the rotating rotor. This phenomenon was observed as a Coanda-like flow pattern in the flow visualization experiment, which controlled the flow separation on the convex side. It was also noticed that the flow field near the rotor was effectively two-dimensional as the torque and the power coefficients evaluated from the pressure measurements at the middle plane agreed closely with the results by total torque measurement.

3 THEORIES OF WIND TURBINES

3.1 Introduction

For predicting the performance of Wind Turbines, different theories are being used at present by different designers. Among them the classical theory is most commonly used. This theory is often called the strip theory or modified blade element theory. It is the combination of the momentum theory and the blade element theory. As the number of blades increases classical theory cannot satisfactorily predict the performance of the wind turbine. Cascade theory may be used for the turbine with multiple blades. This theory can predict the induced velocity reasonably whereas the classical theory cannot do this for the multi - bladed wind turbine.

The vortex theory may be used for predicting the performance of the wind turbine but it takes excessive computation time. On the other hand, it cannot always give reasonable results. Hence, in the present investigation only the classical theory has been used for prediction of the performance of wind turbines.

3.2 Vertical Axis Vane Type Rotor

Vane type wind turbines are drag based vertical axis wind turbine that operate on the theory and principle of a paddle propelling a boat through water. If no slip exists between the paddle and water, the maximum speed attained will be the same as the tangential speed of the paddle. Similarly, in a drag based vertical axis wind turbine, the speed at the tip of the blade can seldom exceed the speed of the wind. In other words, the drag can also be described as the pressure force or the thrust on the blades created by the wind as it passes through it.

The Vane type rotor is predominantly drag based, but also uses a certain amount of aerodynamic lift. Drag based vertical axis wind turbines have relatively higher starting torque and less rotational speed than their lift based counterparts. Furthermore, their power output to weight ratio is also less. Because of the low speed, these are generally considered unsuitable for producing electricity, although it is possible by selecting proper gear trains. Drag based windmills are useful for other applications such as grinding grain, pumping water and a small output of electricity. A major advantage of drag based vertical axis wind turbines lies in their self–starting capacity, unlike the Darrieus lift–based vertical axis wind turbines.

3.3 Computational Fluid Dynamic Technique

Computational Fluid Dynamics is an important tool for the analysis, development, and optimization of wind power systems. Various CFD techniques have been used to simulate turbine performance, such as the viscous three-dimensional differential/actuator disk method, adapted by Ammara, Leclerc and Masson [37] for the aerodynamic analysis of wind farms. In order to improve vertical axis wind turbine performance, CFD can be used to predict flow fields

around a vertical axis wind turbine. The flow field around a vertical axis wind turbine is complicated, because of interactions between the large separated flow and wake itself. The flow field through a vertical axis wind turbine is essentially unsteady, turbulent and separated flow. Akiyoshi et al. [39] simulated flow around a vertical axis wind turbine and estimated its aerodynamic performance. The sub-grid scale turbulence model was developed to simulate the separated flow from the turbine blades. A sliding mesh technique was introduced to simulate flow through the rotational blades. Numerical results were compared with predictions based on momentum theory.

CFD numerical techniques are useful in various flow aspects of turbine performance. The viscous three-dimensional differential/actuator disk method has been used for the aerodynamic analysis of wind turbine. In this approach, the rotor is modeled as a permeable surface from which the time-averaged mechanical work is extracted by the rotor from the air.

The torque and pressure on the rotors of a vertical axis wind turbine are important parameters for a design. With many vertical axis wind turbines, especially designs with high rotor-stator interaction, the power output of the turbine can be rapidly changing and diverse throughout each rotation. For such applications, an unsteady time-dependant CFD simulation can offer a useful and straightforward method for determining a turbine's power output throughout each cycle. This technique is effective even for power curves with a high level of fluctuation. This is an important benefit of the moving mesh model, as it is the only method available to produce reliable time-dependent results.

3.4 Aerodynamics Theory and Performance Characteristics

The aerodynamic analysis of vertical axis wind turbines is complicated due to their orientation in the oncoming wind. The vertical axis wind turbines have a rotational axis perpendicular to the oncoming airflow. This accounts for aerodynamics that is more complicated than a conventional horizontal axis wind turbine. However, the configuration has an independence of wind direction. The main shortfalls are the high local angles of attack and the wake coming from the blades in the upwind part and axis. Understanding the aerodynamics of the pure drag type of vertical axis wind turbine will give important insight for improving the lift coefficient, and designing this turbine for better and more efficient harnessing of the wind energy.

3.4.1 Lift Force

The lift force, L, is one of the major force components exerted on an airfoil section inserted in a moving fluid. It acts normal to the fluid flow direction. This force is a consequence of the uneven pressure distribution between the upper and lower blade surfaces (fig. 3.1), and can be expressed as follows:

$$L = 0.5 C_l \rho V^2 A \qquad (3.4.1)$$

where ρ is the air density, C_l is the lift coefficient and A is the blade airfoil area.

3.4.2 Drag Force

The drag force, D acts in the direction of the fluid flow. Drag occurs due to the viscous friction forces on the airfoil surfaces, and the unequal pressure on surfaces of the airfoil. Drag is a function of the relative wind velocity at the rotor surface, which is the difference between the wind speed and the speed of the surface, and can be expressed as

$$D = 0.5 C_d \rho (U - \Omega r)^2 A \qquad (3.4.2)$$

where Ωr is the speed of the surface at the blade, C_d is drag coefficient and U is the wind speed.

The lift and drag coefficient values are usually obtained experimentally and correlated against the Reynolds number. A section of a blade at radius r is illustrated in Fig. 3.1, with the associated velocities, forces and angles shown. The relative wind vector at radius r, is denoted by V_{rel}, and the angle of the relative wind speed to the plane of rotation, by φ. The resultant lift and drag forces are represented by L and D, which are directly perpendicular and parallel to the relative wind as shown

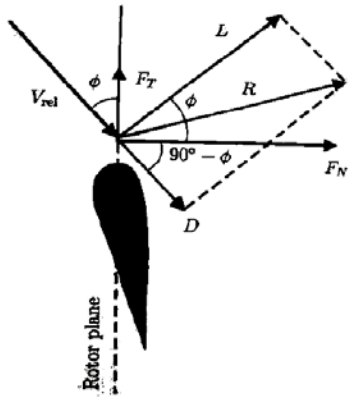

Figure 3. 1: Local forcesrces on a blade [43]

A careful choice of the rotor blades geometry and shape modification is crucial for maximum efficiency. Wind turbines have typically used airfoils based on the wings of airplanes, although new airfoils are specially designed for use on rotors. Airfoils use the concept of lift, as opposed to drag, to harness the wind's energy. Blades that operate with lift (forces perpendicular to the direction of flow) are more efficient than a drag machine. Certain curved and rounded shapes have resulted most efficient in employing lift. When the edge of the airfoil is angled slightly out of the direction of the wind, the air moves more quickly on the downstream (upper) side creating a low pressure. On the upstream side of airfoil, the pressure is high. Essentially, this pressure differential lifts the airfoil upward. (Fig.3.2). In the case of a wind turbine, the lift creates a turning effect. An operating conditions with a low blade angle of attack, α, thus favors the lift force.

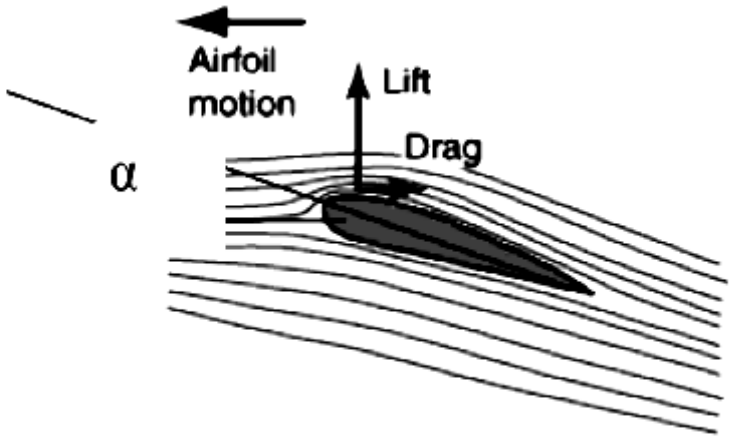

Figure 3. 2: Airflow around an airfoil

Bernoulli's principle indicates how faster flow implies lower pressure on the airfoil:

$$P + \frac{1}{2}\rho v = \text{constant} \tag{3.4.3}$$

The first term in equation (3.4.3) is the static pressure and the second term is the dynamic pressure. An increase in velocity leads to a corresponding decrease in the static pressure to maintain a constant, and vice versa. The equation can be understood through a conservation of energy as pressure work is converted to / from kinetic energy in the flow field.

3.4.3 Reynolds number

The Reynolds number Re is the ratio of the inertia forces to the viscous forces. It is a non-dimensional parameter that defines the characteristics of the fluid flow conditions. It is used when calibrating the lift and drag coefficients of an airfoil. For a high speed rotor,

$$\mathrm{Re} = \frac{UL}{\nu} = \frac{\rho UL}{\mu} = \frac{\rho V_\theta c}{\mu} \quad , \tag{3.4.4}$$

where μ is the fluid viscosity, $\upsilon = \frac{\rho}{\mu}$ is the kinematic viscosity, L is the characteristics length scale, c is the blade chord length and V_θ is the blade tip velocity.

3.4.4 Blade Solidity

Solidity is usually defined as the percentage of the circumference of the rotor which contains material rather than air. Savonius is a high solidity machine. It generates much higher starting

torque than low-solidity machines, like Darrieus for example, but is inherently less efficient than low-solidity machines.

Another advantage of high-solidity machines is that they do not need to be made with as much precision as low-solidity ones. This type of turbine is self-starting and provides high torque at low speeds.

The blade solidity,δ , is the ratio of the blade area compared with the swept area. For a vertical axis wind turbine, the solidity is defined as

$$\delta = \frac{Bc}{2\pi r} \tag{3.4.5}$$

where B is the number of blades. Changing the number of blades or the blade chord dimensions will alter the vertical axis wind turbine solidity. An increase in the chord results in a large aerodynamics force and consequently in high power.

3.4.5 Tip Speed Ratio

The tip speed ratio λ, is defined as the velocity at the tip of the blade, to the free stream velocity. It is given by

$$\lambda = \frac{R\omega}{V} \tag{3.4.6}$$

3.4.6 Betz number

The Betz number or Betz limit is a useful performance indicator of wind turbines. It is the maximum amount of power that can be extracted by a wind generator from the available wind kinetic energy. This maximum turbine power is the difference between the upstream and downstream wind powers.

$$P_t = \frac{1}{2} * \frac{dm}{dt} * (V^2 - V_0^2) \tag{3.4.7}$$

where

P_t = turbine output power (watts),

V = upstream wind velocity (m/s) and

V_0 = downstream wind velocity (m/s)

The mass of air flowing through the turbine rotor area is a function of the air density and velocity (upstream and downstream average),

$$\frac{dm}{dt} = \rho_{air} A * \frac{1}{2}(V + V_0) \tag{3.4.8}$$

Substituting equation (3.4.8) into equation (3.4.7), the turbine power becomes

$$P_t = \frac{1}{2}\left[\rho_{air} * A * \frac{(V + V_0)}{2}\right] * \{V^2 - V_0^2\} \qquad (3.4.9)$$

Equation (3.2.9) is rearranged to give the following expression:

$$P_t = \frac{1}{2} * \rho_{air} * A * V^3 * \frac{\left(1 + \frac{V_0}{V}\right) * \left[1 - \left(\frac{V_0}{V}\right)^2\right]}{2} \qquad (3.4.10)$$

This power from the turbine rotor can be expressed as a fraction of the upstream wind power, i.e.,

$$P_t = \frac{1}{2} * \rho_{air} * A * V^3 * C_p \qquad (3.4.11)$$

where Cp is the fraction of power captured by the rotor blades also called power coefficient or rotor efficienc

Re-arranging t $\left(1 + \frac{V_0}{V}\right) * \left[1 - \left(\frac{V_0}{V}\right)^2\right]$ that

$$C_p = \frac{\left(1 + \frac{V_0}{V}\right) * \left[1 - \left(\frac{V_0}{V}\right)^2\right]}{2} \qquad (3.4.12)$$

Figure 3.4.3 shows the variation of C_p with downstream to upstream wind speed ratio, V_0/V. The theoretical maximum rotor power coefficient is C_p = 16/27 (= 0.59), when the downstream to upstream wind speed ratio is V_0/V = 0.33, called the *Betz limit* after the first analysis carried out by Betz (1926). However, the practical limits for C_p are typically 0.46 for high speed two-blade system and 0.50 for three-blade turbines. The drag turbine operates at about 1/3 of the 0.59 Betz limit.

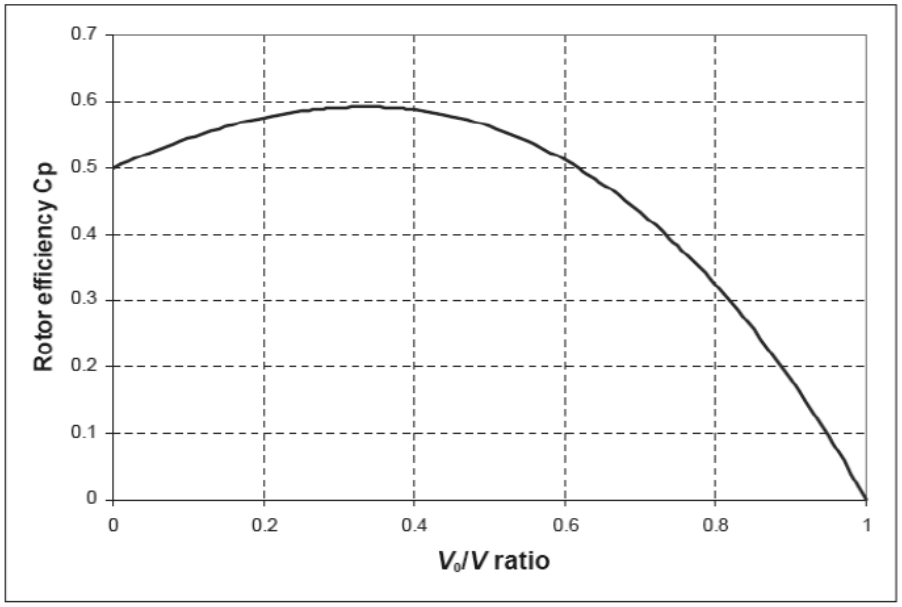

Figure 3. 3: Rotor efficiency vs. downstream / upstream wind speed ratio [44]

As with all turbines, only a part of the energy shown in fig. 3.4.4 can be extracted. If too much kinetic energy were removed, the exiting air flow would stagnate and thus cause blockage. When the air flow approaches the inlet of the turbine, it meets a blockage imposed by the rotor-stator blades. This causes a decrease in kinetic energy, while the static pressure increases to a maximum at the turbine blade. As the air continues through the turbine, energy in the fluid is transferred to the turbine rotor blades, while the static pressure drops below the atmospheric pressure as fluid flows away from the rotor. This will eventually further reduce the kinetic energy. Then kinetic energy from the surrounding wind is entrained to bring it back to the original state.

A “disk actuator” model of a horizontal axis wind turbine gives further insight into the process.

This model can be used in explaining the Betz limit.

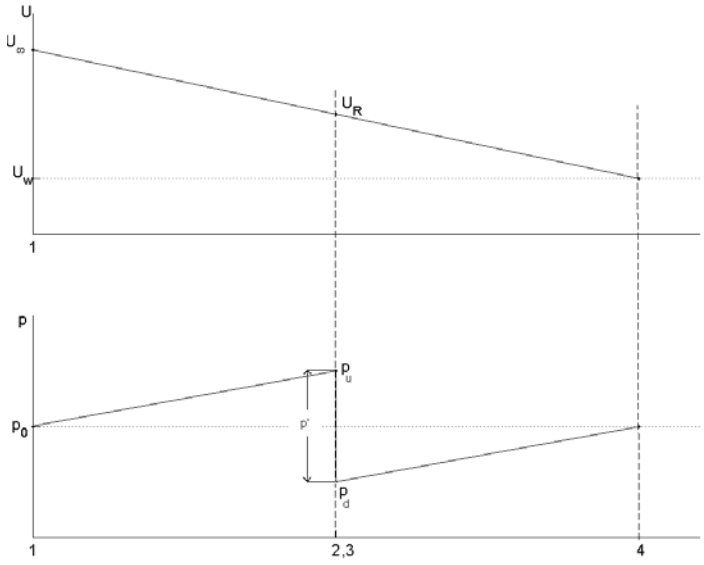

Figure 3. 4: Velocity and pressure distribution in a stream tube

Typical velocity and pressure distributions are illustrated in Figure 3.4.4, using the disk actuator model and Betz limit theory. If the stream tube model is applied to a vertical axis wind turbine, it gives insight into the velocity and pressure distributions for a multi-bladed S-shaped vane type wind turbine. Because of the continuity principle for the stream tube, the diameter of the flow field must experience an increase as the velocity decreases giving rise to a sudden pressure drop, $\{p' = (p^u - p_d)\}$,at the rotor plane. This pressure drop contributes to the torque for rotating turbine blades.

The actuator disk theory also provides a rational basis for illustrating the flow velocity at the rotor that is different from the free-stream velocity. The Betz limit from the actuator disk theory shows the maximum theoretically possible rotor power coefficient (0.59) for a wind turbine. In reality, three major effects account for a power coefficient:

• rotation of wake behind the rotor;

• finite number of blades and associated tip losses;

• non-zero aerodynamic drag.

3.5 Rotor Performance Parameters

A wind turbine designed for a particular application should have its performance characteristics tested before proceeding to prototype fabrication. A dimensionally similar and scaled down prototype of the design model is normally tested in a wind tunnel for this purpose.

The power performance of a wind turbine is normally expressed in dimensionless form. For a given wind speed, the power coefficient, torque coefficient and the tip speed ratio are good indicators to use as a performance measure. For a particular configuration of vertical axis vane type wind turbine, these parameters are

$$C_p = \frac{P_t}{\frac{1}{2}\rho V^3 A} \tag{3.5.1}$$

where

P_t = Power developed by the turbine

A = Rotor cross-sectional area = hd ,

d = Rotor diameter,

h = Height of turbine,

ρ = Air density and

V = Free stream wind speed.

$$Cq = \frac{T_t}{\frac{1}{2}\rho V^2 AR} \tag{3.5.2}$$

where

T_t = Actual torque the shaft can develop

R = Radius of the turbine rotor

Also, λ (tip speed ratio) of equation 3.4.6 is dimensionless value that can be used in predicting the performance of the turbine. Figure 3.5 shows typical sample predictions for different wind turbine types.

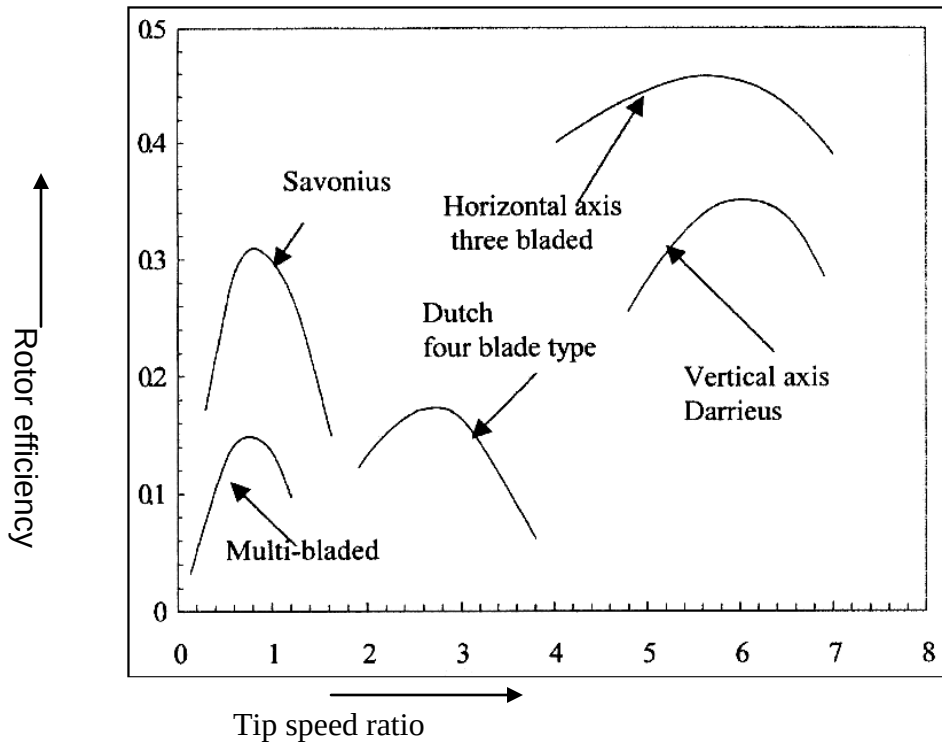

Figure 3. 5: Rotor efficiency vs. tip speed ratio [10]

Figure 3.5 is a sample extract [28]. It is an illustration of modern turbine C_p –λ curves where C_p and λ are represented on the plot as y-axis and x-axis respectively.

3.6 Axial Momentum Theory

For a conventional wind turbine operating under steady state condition in a free flowing wind stream of constant velocity, the velocity of a unit volume of air will decrease monotonically as it approaches the turbine, passes through it and starts to recede from it. As the air recede farther from the turbine, it will receive kinetic energy from the surrounding wind and its velocity will increase until it again reaches its free stream velocity. The density of the air cannot be controlled except within the limits of altitude string.

By use of axial momentum theory alone, it is possible to determine the forces acting on a rotor, which are responsible for the motion of the fluid and resulting power output from the windmill.

3.6.1 Non-Rotating Wake

The starting point in wind turbine analysis lies in the ‘Control Volume’ approach contained in the ‘Actuator Disc’ concept originated by Rankine [51] and extended it for marine propellers. This theory is useful in the derivation of ideal efficiency of a rotor of wind turbines.

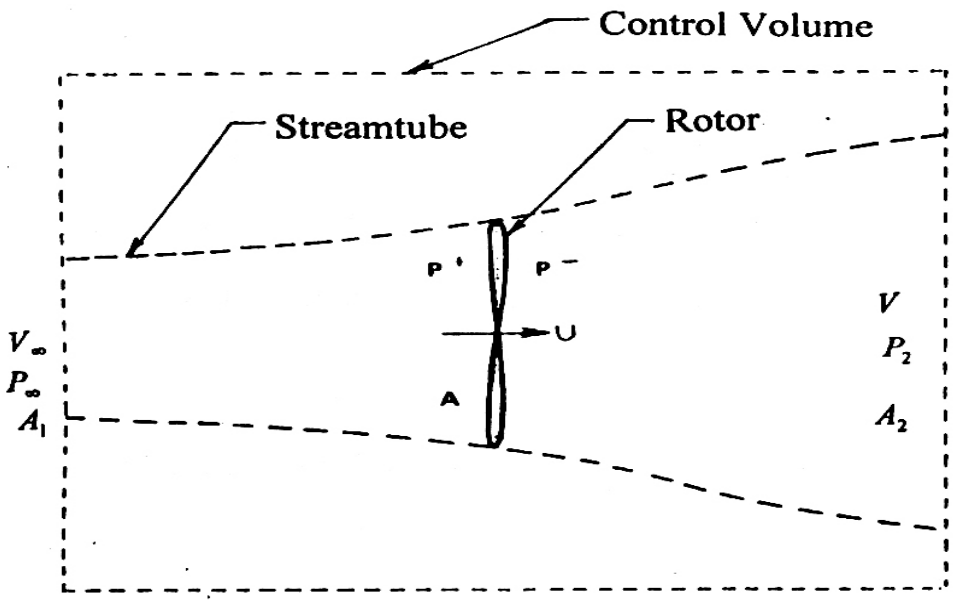

Figure 3. 6: Control Volume of a Wind Turbine

Assumptions in axial momentum theory (for maximum possible output of a wind turbine) are:

a. The fluid is incompressible and inviscid
b. The number of blades is infinite
c. The thrust loading is uniform
d. The static pressure far ahead and far behind the rotor are equal to the undisturbed ambient static pressure
e. The flow is homogeneous and
f. No frictional drag

Let us assume, the control volume as shown in Figure 3.6, where the upstream and downstream control volume planes are infinitely far removed from the turbine plane. The conservation of mass may be expressed as:

$$\rho A_1 V_\infty = \rho AU = \rho A_2 V \qquad (3.6.1)$$

The notations used are,

V_∞ = Undisturbed wind velocity far from the upstream, m/s

U = Wind velocity when it flows through the rotor, m/s

V = Wind velocity far behind the rotor, m/s

A = Turbine disc area, m^2

A_1 = Cross sectional area of incoming wind, m^2

A_2 = Wake cross sectional area, m^2

and

ρ = Air density, kg/m^3

The thrust T on the rotor is given by the change of momentum of the flow:

$T = m (V_\infty - V) = \rho A_1 V^2_\infty - \rho A_2 V^2$ (3.6.2)

Introducing equation (3.6.1), leads to the expression

$$T = \rho A U (V_\infty - V) \quad (3.6.3)$$

The thrust on the rotor can also be expressed from the pressure difference over the rotor area as,

$$T = A(P^+ - P^-) \quad (3.6.4)$$

Where

P^+ = pressure immediately in front of the rotor

P^- = Pressure immediately behind the rotor

Now applying Bernoulli's equation:

For upstream of the rotor: $P_\infty + \frac{1}{2}\rho V_\infty^2 = P^+ + \frac{1}{2}\rho U^2$ (3.6.5)

For downstream of the rotor: $P_\infty + \frac{1}{2}\rho V^2 = P^- + \frac{1}{2}\rho U^2$ (3.6.6)

Subtracting equation (3.6.6) from equation (3.6.5), one obtains

$$P^+ - P^- = \frac{1}{2}\rho(V^2_\infty - V^2) \quad (3.6.7)$$

The expression for the thrust from equation (3.6.4) becomes,

$$T = \frac{1}{2}\rho A(V_\infty^2 - V^2) \quad (3.6.8)$$

Equating the equation (3.6.8) with equation (3.6.3),

$$\frac{1}{2}\rho A(V_\infty^2 - V^2) = \rho A U (V_\infty - V)$$

or, $$U = \frac{V_\infty + V}{2} \quad (3.6.9)$$

The velocity at the rotor U so often defined in terms of an axial interference factor 'a' as,

$$U = V_\infty(1 - a) \quad (3.6.10)$$

Balancing equations (3.6.9) and (3.6.10), the wake velocity can be expressed as,

$$V = V_\infty (1 - 2a) \tag{3.6.11}$$

The change in kinetic energy of the mass flowing through the rotor area is the power absorbed by the rotor:

$$P = m\Delta KE = \frac{1}{2}\rho AU(V_\infty^2 - V^2) \tag{3.6.12}$$

With equations (3.6.10) and (3.6.11), the expressions for power becomes,

$$P = 2\rho AV_\infty^2 a(1-a)^2 \tag{3.6.13}$$

Maximum power occurs when, $\frac{dP}{da} = 0$

Therefore, $\frac{dP}{da} = 2\rho AV_\infty^2(1 - 4a + 3a^2) = 0$

Which leads to an optimum interference factor,

$$a = \frac{1}{3}$$

Putting this value in equation (3.6.13), maximum power becomes,

$$P_{\max} = \frac{16}{27}(\frac{1}{2}\rho AV_\infty^3) \tag{3.6.14}$$

The factor 16/27 is called the Betz-coefficient and represents theoretical maximum fraction, an ideal rotor can extract from the wind. This fraction is related to the power of an undisturbed flow arriving at an area A, where, in reality the volume flow rate through A is not AV_∞ but AU. Hence, the maximum efficiency for maximum power can be written as,

$$\eta_{eff} = \frac{P_{\max}}{\frac{1}{2}\rho AUV_\infty^2} = \frac{16}{27}\frac{V_\infty}{U} = \frac{16}{27}\frac{1}{(1-a)} = \frac{16}{27}\frac{1}{(1-\frac{1}{3})} = \frac{8}{9} \tag{3.6.15}$$

This model does not take into account additional effects of wake rotation. As the initial stream is not rotational, interaction with a rotating windmill will cause the wake to rotate in opposite direction. If there is rotational kinetic energy in the wake in addition to translational kinetic energy, then from the thermodynamic considerations we may expect lower power extraction than in the case of the wake having only translation. In the following article, this wake rotational will be taken into account.

3.6.2 Effect of Wake Rotation on Momentum Theory

Considering this effect the assumption is made that at the upstream of the rotor, the flow is entirely axial and the downstream flow rotates with an angular velocity ω but remains irrotational. This angular velocity is considered to be small in comparison to the angular velocity Ω of the wind turbine. This assumption maintains the approximation of axial momentum theory that the pressure in the wake is equal to the free stream pressure.

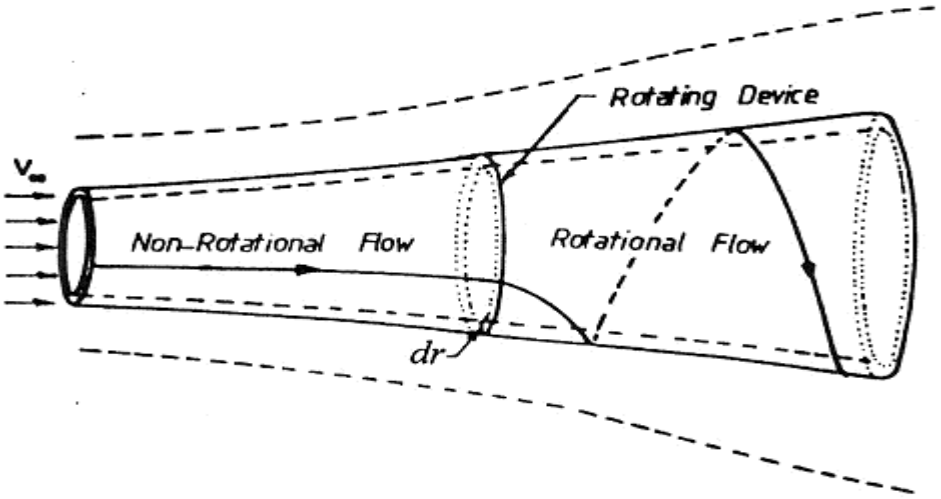

Figure 3. 7: Stream Tube Model Showing the Rotation of Wake

The wake rotation is opposite in direction of the rotor and represents an additional loss of kinetic energy for the wind rotor as shown in Figure 3.2.2. Power is equal to the product of the torque Q acting on the rotor and the angular velocity Ω of the rotor. In order to obtain the maximum power, it is necessary to have a high angular velocity and low torque because high torque will result in large wake rotational energy. The angular velocity ω of the wake and the angular velocity Ω of the rotor are related by an angular interference factor a' as,

$$a' = \frac{\omega}{2\Omega} \tag{3.6.16}$$

The annular ring through which a blade element will pass is illustrated in Figure

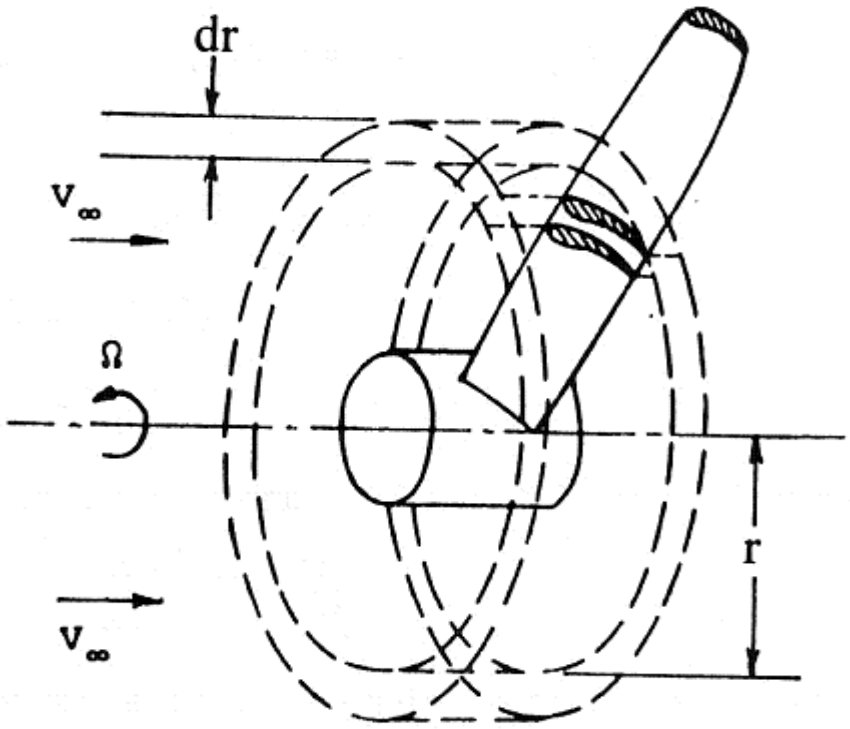

Figure 3. 8: Blade Element Annular Ring

Using the relation for momentum flux through the ring the axial thrust force dT can be expressed as,

$$dT = dm(V_\infty - V) = \rho dAU(V_\infty - V) \quad (3.6.17)$$

Inserting equations (3.2.10) and (3.2.11),

$$U = V_\infty(1-a) \quad (3.6.10)$$

$$V = V_\infty(1-2a) \quad (3.6.11)$$

and expressing the area of the annular ring dA as,

$$dA = 2\pi r dR \quad (3.6.18)$$

The expression for the thrust becomes,

$$dT = 4\pi r \rho V_\infty^2 a(1-a)dr \quad (3.6.19)$$

The thrust force may also be calculated from the pressure difference over the blades by applying Bernoulli's equation. Since the relative angular velocity changes from Ω to (ω+Ω), while the axial components of the velocity remain unchanged, Bernoulli's equation gives,

$$P^+ - P^- = \frac{1}{2}\rho(\Omega+\omega)^2 r^2 - \frac{1}{2}\rho\Omega^2 r^2$$

or, $P^+ - P^- = \rho(\Omega + \frac{1}{2}\omega)\omega r^2$

The resulting thrust on the annular element is given by,

$$dT = (P^+ - P^-)dA$$

or, $dT = \rho(\Omega + \frac{1}{2}\omega)\omega r^2 2\pi r dr$

Inserting equation (3.2.16),

$$dT = 4a'(1+a')\frac{1}{2}\rho\Omega^2 r^2 2\pi r dr \qquad (3.6.20)$$

balancing equation (3.6.20) and equation (3.6.19), leads to the expression,

$$\frac{a(1-a)}{a'(1+a')} = \frac{\Omega^2 r^2}{V_\infty^2} = \lambda_r^2 \qquad (3.6.21)$$

Where, λ_r is known as the local tip speed ratio which is given by,

$$\lambda_r = \frac{r\Omega}{V_\infty} \qquad (3.6.22)$$

To derive an expression for the torque acting on the rotor the change in angular momentum flux dQ through the annular ring is considered,

$$dQ = dmV_t r$$

or, $dQ = \omega r \rho dA U r$

Where, V_t is the wake tangential velocity.

Considering equations (3.6.10), (3.6.16) and (3.6.18), the expression for the torque acting on the annular ring is given by,

$$dQ = 4\pi r^3 \rho V_\infty (1-a)a'\Omega dr \qquad (3.6.23)$$

The generated power through the annular ring is equal to dP = ΩdQ, so the total power becomes,

$$P = \int_0^R \Omega dQ \qquad (3.6.24)$$

Introducing the tip speed ratio λ as,

$$\lambda = \frac{R\Omega}{V_\infty} \tag{3.6.25}$$

Equation for total power from equations (3.6.23) and (3.6.24) becomes,

$$P = \int_0^R 4\pi r^3 \rho V_\infty (1-a) a' \Omega^2 dr$$

This can be written as,

$$P = \frac{1}{2}\rho A V_\infty^3 \frac{8}{\lambda^2}\int_0^\lambda a'(1-a)\lambda_r^3 d\lambda_r \tag{3.6.26}$$

Where, A is the turbine swept area, which is given by $A = \pi R^2$

The power coefficient is defined as,

$$C_P = \frac{P}{\frac{1}{2}\rho A V_\infty^3}$$

Inserting equation (3.6.26) power co-efficient can be written as,

$$C_P = \frac{8}{\lambda^2}\int_0^\lambda a'(1-a)\lambda_r^3 d\lambda_r \tag{3.6.27}$$

Rearranging equation (3.6.21),

$$a' = -\frac{1}{2} + \frac{1}{2}\sqrt{1 + \frac{4}{\lambda_r^2}a(1-a)} \tag{3.6.28}$$

Substituting this value in equation (3.6.27) and taking the derivative equal to zero, the relation between λ_r and a for maximum power becomes,

$$\lambda_r = \frac{(1-a)(4a-1)^2}{(1-3a)} \tag{3.6.29}$$

Introducing equation (3.6.29) into equation (3.6.21), the relationships between a and a' becomes,

$$a' = \frac{1-3a}{4a-1}$$

This relation will be used later for design purposes.

3.7 Blade Element Theory

Forces acting on a differential element of the blade can be calculated with the help of "Blade Element Theory". In this theory, the performance of the entire rotor is determined by integrating the element characteristic over the length of the blade.

The blade element theory is based on the following assumption:

a. Along each blade there is no interference between the adjacent blades.
b. The forces acting on the blade element are determined from only the lift and drag characteristics of the sectional profile of the element.
c. The pressure in the far wake is equal to that of the free stream.

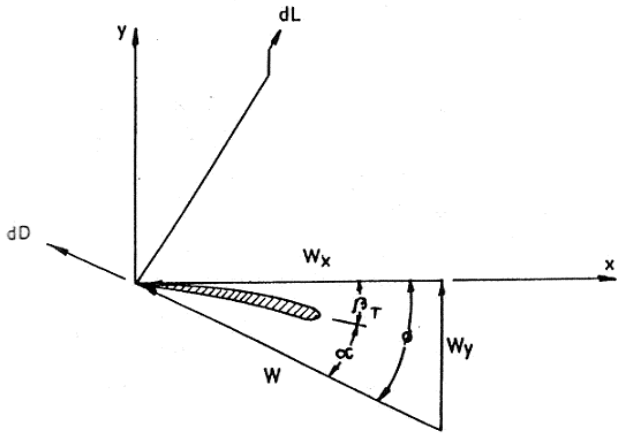

Figure 3. 9: Velocity Diagram of a Blade Element

The aerodynamic force components acting on the blade element are shown in Figure 3.3.1 where, x - y co-ordinate system is used. Among the forces the lift force component dL acts perpendicular to the resulting velocity vector W and the drag force component dD acts in the same direction of the resulting velocity. The sectional lift and drag forces may be defined as,

$$dL = C_L \frac{1}{2} \rho W^2 C dr \qquad (3.7.1)$$

$$dD = C_D \frac{1}{2} \rho W^2 C dr \qquad (3.7.2)$$

From the geometry of the figure, the thrust and torque experienced by the blade element are given by the following expression,

$$dT = dL \cos\phi + dD \sin\phi \qquad (3.7.3)$$

$$dQ = (dL \sin\phi - dD \cos\phi) r \qquad (3.7.4)$$

Assuming that 'B' is the number of blades of the rotor, the expressions for the thrust and torque can be written as,

$$dT = BC\frac{1}{2}\rho W^2(C_L\cos\phi + C_D\sin\phi)dr$$

or, $$dT = BC\frac{1}{2}\rho W^2 C_L\cos\phi(1+\frac{C_D}{C_L}\tan\phi)dr \qquad (3.3.5)$$

and $$dQ = BC\frac{1}{2}\rho W^2(C_L\sin\phi - C_D\cos\phi)rdr$$

or, $$dQ = BC\frac{1}{2}\rho W^2 C_L\sin\phi(1-\frac{C_D}{C_L}\frac{1}{\tan\phi})rdr \qquad (3.7.6)$$

From Figure 3.7.1, the relative velocity W can be expressed as,

$$W = \frac{(1-a)V_\infty}{\sin\phi} = \frac{(1+a')\Omega r}{\cos\phi} \qquad (3.7.7)$$

From the geometry of Figure 3.7.1, the following trigonometric relations can be obtained,

$$\tan\phi = \frac{(1-a)V_\infty}{(1+a')\Omega r} = \frac{(1-a)}{(1+a')\lambda_r} \qquad (3.7.8)$$

and $\beta_T = \phi - \alpha$ (3.7.9)

On the other hand, the local solidity ratio σ, can be expressed as,

$$\sigma = \frac{BC}{2\pi r} \qquad (3.7.10)$$

The equations of the blade element theory become,

$$dT = (1-a)^2\frac{\sigma C_L\cos\phi}{\sin^2\phi}(1+\frac{C_D}{C_L}\tan\phi)\frac{1}{2}\rho V_\infty^2 2\pi r dr \qquad (3.7.11)$$

$$dQ = (1+a')^2\frac{\sigma C_L\sin\phi}{\cos^2\phi}(1-\frac{C_D}{C_L}\frac{1}{\tan\phi})\frac{1}{2}\rho\Omega^2 r^3 2\pi r dr \qquad (3.7.12)$$

3.8 Strip Theory

The performance of a wind turbine can be determined from the axial momentum theory and blade element theory by developing a couple of relationships. In order to do this, the thrust obtained from the momentum theory [equation (3.6.19)] is equated to the thrust obtained from the blade element theory for an annular element at radius r [equation (3.7.11)],

$$dT_{momentum} = dT_{bladeelement}$$

$$\text{or, } \frac{a}{1-a} = \frac{\sigma C_L \cos\phi}{4\sin^2\phi}\left(1+\frac{C_D}{C_L}\tan\phi\right) \qquad (3.8.1)$$

This is an important relation which relates axial interference factor 'a' with the solidity ratio σ together with the lift coefficient C_L and drag coefficient C_D.

On the other hand, equating the expression of angular momentum obtained from the momentum theory [equation (3.2.23)] with the expression of the same obtained from the blade element theory [equation (3.3.12)] one finds,

$$dQ_{momentum} = dQ_{blade\ element}$$

$$\text{or, } \frac{a'}{1+a'} = \frac{\sigma C_L}{4\cos\phi}\left(1-\frac{C_D}{C_L}\frac{1}{\tan\phi}\right) \qquad (3.8.2)$$

Equation (3.4.2), determines the annular interference factor, which contains the lift coefficient and the local solidity ratio.

The drag co-efficient C_D should be omitted in the calculations of axial interference factor 'a' and the tangential interference factor 'a'' because the retarded air due to drag is confined to thin helical sheets in the wake and have little effect on the induced flow as described by Wilson and Lissaman [63]. Thus inserting the drag coefficient $C_D = 0$, the expressions of the interference factors can be obtained as,

$$\frac{a}{1-a} = \frac{\sigma C_L \cos\phi}{4\sin^2\phi} \qquad (3.8.3)$$

$$\frac{a'}{1+a'} = \frac{\sigma C_L}{4\cos\phi} \qquad (3.8.4)$$

Considering the equations (3.4.4) and (3.3.12), the elemental torque can be obtained as,

$$dT = 4a(1-a)(1+\frac{C_D}{C_L}\tan\phi)\frac{1}{2}\rho V_\infty^2 2\pi r dr \qquad (3.8.5)$$

Also inserting equation (3.4.4) and (3.3.8) into equation (3.3.12), the expression of the elemental torque can be written as,

$$dQ = 4a'(1+a)(1-\frac{C_D}{C_L}\frac{1}{\tan\phi})\frac{1}{2}\rho\Omega 2\pi r^3 dr \qquad (3.8.6)$$

Elemental power is given by,

$$dp = dQ\Omega$$

or, $$dP = 4a'(1+a)(1-\frac{C_D}{C_L}\frac{1}{\tan\phi})\frac{1}{2}\rho\Omega^2 2\pi r^3 dr \qquad (3.8.7)$$

Introducing the local tip speed ratio λ_r from equation (3.6.22) with,

$$\lambda_r = \frac{r\Omega}{V_\infty}$$

Equations of total thrust, torque and power become,

$$T = \frac{1}{2}\rho A V_\infty^{\ 2}\frac{8}{\lambda^2}\int_0^\lambda a(1-a)(1+\frac{C_D}{C_L}\frac{1}{\tan\phi})\lambda_r d\lambda_r \qquad (3.8.8)$$

$$Q = \frac{1}{2}\rho A V_\infty^{\ 2}\frac{8}{\lambda^3}\int_0^\lambda a'(1-a)(1-\frac{C_D}{C_L}\frac{1}{\tan\phi})\lambda_r^{\ 3} d\lambda_r \qquad (3.8.9)$$

and

$$P = \frac{1}{2}\rho A V_\infty 3\frac{8}{\lambda^2}\int_0^\lambda a'(1-a)(1-\frac{C_D}{C_L}\frac{1}{\tan\phi})\lambda_r^{\ 3} d\lambda_r \qquad (3.8.10)$$

These equations are valid only for a wind turbine having infinite number of blades.

3.9 Tip and Hub Losses

In the preceding sections, the rotor was assumed to be possessed a finite number of blades with an infinitely small chord. In reality, however, the number of blades is finite. According to the theory discussed previously, the wind imparts a rotation to the rotor, thus dissipating some of its kinetic energy or velocity and creating a pressure difference between one side of the blade and

the other. At tip and hub, however, this pressure difference leads to secondary flow effects. The flow becomes three - dimensional and tries to equalize the pressure difference as shown in Figure 3.9.1. This effect is more pronounced as one approaches the tip. It results in a reduction of the torque on the rotor and thus in a reduction of the power out-put. The method suggested by Prandtl will be used here. The idea in Prandtl's method is to replace the system of vortices at the tip with a series of parallel planes for which the flow is more easily calculated. It should however be remembered that this approximation was developed for a lightly loaded propeller under optimum conditions which may differ somewhat from the conditions of a wind turbine.

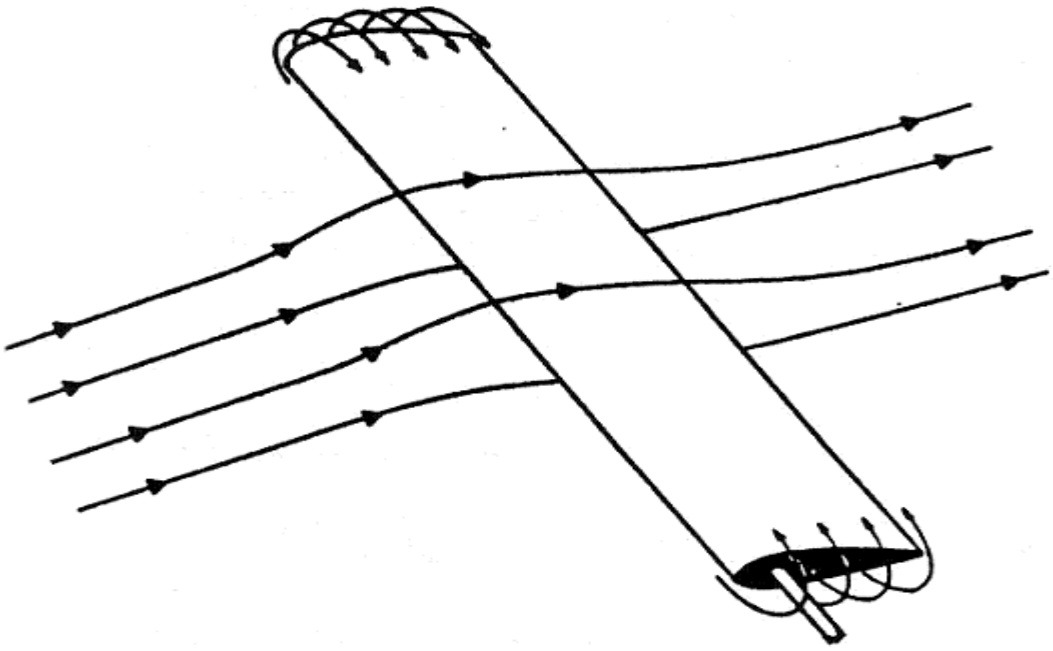

Figure 3. 10: Tip and Hub losses Flow Diagram

The correction factor suggested by Prandtl is,

$$F_{tip} = \frac{2}{\pi}\arccos e^{-f}$$

Where, $f = \frac{B}{2}\frac{R-r}{r\sin\phi}$

It may also be applied for hub region and f is then defined as,

$$f = \frac{B}{2}\frac{R-r_{hub}}{r_{hub}\sin\phi}$$

Hence, a correction factor F for total losses is applied as,

$F = F_{up}.F_{hub}$

The loss factor F may be introduced in several ways for the rotor performance calculation. In the method, adopted by Wilson and Lissaman [63], the induction factors 'a' and 'a'' are multiplied with F and thus the axial and tangential velocities in the rotor plane as seen by the blades are modified. It is further assumed that these corrections only involve the momentum formulas.

Thus the thrust and torque from [equation (3.2.19) and (3.2.23)] momentum theory becomes,

$$dT = 4\pi r\rho V_\infty^2 aF(1-aF)dr \tag{3.9.1}$$

$$dQ = 4\pi r^3 \rho V_a a'F(1-aF)\Omega dr \tag{3.9.2}$$

The results of the blade element theory remain unchanged.

$$dT = (1-a)^2 \frac{\sigma C_L \cos\phi}{\sin^2\phi}(1+\frac{C_D}{C_L}\tan\phi)\frac{1}{2}\rho V_\infty^2 2\pi dr$$

and $$dQ = (1+a')^2 \frac{\sigma C_L \sin\phi}{\cos^2\phi}(1-\frac{C_D}{C_L}\tan\phi)\frac{1}{2}\rho\Omega^2 r^4 2\pi dr$$

The equations can also be written as

$$dQ = (1-a)^2 \frac{\sigma C_L}{\sin\phi}(1-\frac{C_D}{C_L}\tan\phi)\frac{1}{2}\rho V_\infty{}^2 2\pi r^2 dr \tag{3.9.3}$$

Balancing the equation (3.5.2) with (3.3.11) one finds,

$$aF(1-aF) = \frac{\sigma C_L \cos\phi(1-a)^2}{4\sin^2\phi}(1+\frac{C_D}{C_L}\tan\phi) \tag{3.9.4}$$

and considering the equations (3.5.3) and (3.5.4),

$$a'F(1-aF) = (1-a)^2 \frac{\sigma C_L}{4\sin\phi}(1-\frac{C_D}{C_L}\tan\phi) \tag{3.9.5}$$

Omitting the drag terms the following expressions yield,

$$aF(1-aF) = \frac{\sigma C_L \cos\phi(1-a)^2}{4\sin^2\phi} \tag{3.9.6}$$

$$a'F(1-aF) = (1-a)^2 \frac{\sigma C_L}{4\sin\phi} \tag{3.9.7}$$

From the equations (3.5.7) and (3.5.8), the final expressions for the elemental thrust and torque become,

$$dT = 4aF(1-aF)(1+\frac{C_D}{C_L}\tan\phi)\rho V_\infty^2 \pi r dr \qquad (3.9.8)$$

and

$$dQ = 4a'F(1-aF)(1-\frac{C_D}{C_L}\tan\phi)\rho V_\infty^2 \pi r^2 dr \qquad (3.9.9)$$

3.10 Equations for Thrust, Torque and Power Coefficient

Elemental thrust, torque and power co-efficient are defined as,

$$dC_T - \frac{dT}{\frac{1}{2}\rho A V_\infty^{\ 2}} \qquad (3.10.1)$$

$$dC_Q - \frac{dQ}{\frac{1}{2}\rho A V_\infty^{\ 2} R} \qquad (3.10.2)$$

and $dC_P - \frac{dP}{\frac{1}{2}\rho A V_\infty^{\ 3}} = \frac{dQ\Omega}{\frac{1}{2}\rho A V_\infty^3}$

or, $dC_P - \frac{dQ\Omega R}{\frac{1}{2}\rho A V_\infty^{\ 2} R V_\infty} = dC_Q \lambda \qquad (3.10.3)$

Considering the equations (3.5.9) and (3.6.1), the elemental thrust co-efficient can be written as,

$$dC_T = \frac{8}{R^2} aF(1-aF)(1+\frac{C_D}{C_L}\tan\phi) r dr \qquad (3.10.4)$$

Again, from equations (3.5.10) and (3.6.2), the elemental torque co-efficient is given by,

$$dC_Q = \frac{8}{R^3} a'F(1-aF)(1-\frac{C_D}{C_L}\tan\phi) r^2 dr \qquad (3.10.5)$$

Elemental power co-efficient can be obtained from equation (3.10.3) as,

$$dC_P = \frac{8\Omega}{R^2 V_\infty} a'F(1-aF)(1-\frac{C_D}{C_L}\tan\phi) r^2 dr \qquad (3.10.6)$$

Finally, total thrust, torque and power co-efficient can be obtained by the following equations,

$$C_T = \frac{8}{R^2}\int_0^R aF(1-aF)(1+\frac{C_D}{C_L}\tan\phi)rdr \qquad (3.\ 10.7)$$

$$C_Q = \frac{8}{R^3}\int_0^R a'F(1-aF)(1-\frac{C_D}{C_L}\tan\phi)r^2 dr \qquad (3.10.8)$$

$$C_P = \frac{8\Omega}{R^2 V_\infty}\int_0^R a'F(1-aF)(1-\frac{C_D}{C_L}\tan\phi)r^2 dr \qquad (3.10.9)$$

3.11 Equations for Maximum Power

For maximum power output, the relation between 'a' and 'a'' may be expressed by the equation (3.2.29) as,

$$a' = \frac{1-3a}{4a-1}$$

Introducing the equations of induction factors as follows,

$$\frac{a}{1-a} = \frac{\sigma C_L \cos\phi}{4\sin^2\phi} \qquad (3.11.1)$$

$$\frac{a}{1+a'} = \frac{\sigma C_L}{4\cos\phi} \qquad (3.11.2)$$

From equations (3.2.29), (3.4.3) and (3.4.4), the following expression yields,

$$\sigma C_L = 4(1-\cos\phi) \qquad (3.\ 11.3)$$

Considering the local solidity σ as,

$$\sigma = \frac{BC}{2\pi r} \qquad (3.\ 11.4)$$

Equation (3.7.1) transforms into,

$$C = \frac{8\pi r}{BC_L}(1-\cos\phi) \qquad (3.\ 11.5)$$

Local tip speed ratio λ_r is given by,

$$\lambda_r = \frac{r\Omega}{V_\infty}$$

From equation (3.3.8),

$$\tan\phi = \frac{1-a}{1+a'}\frac{1}{\lambda_r} \qquad (3.\ 11.6)$$

Now replacing the values of (1-a) and $(1+a')$ from equations (3.4.3) and (3.4.4) and putting the value of σC_L from equation (3. 11.1), the following relation can be deduced,

$$\lambda_r = \frac{\sin\phi(2\cos\phi - 1)}{(1-\cos\phi)(2\cos\phi + 1)} \qquad (3.\ 11.7)$$

and this can be reduced to,

$$\phi = \frac{2}{3}\arctan\frac{1}{\lambda_r} \qquad (3.\ 11.8)$$

Equation of blade twist angle from the equation (3.11.6) can be written as,

$$\beta_T = \phi - \alpha$$

3.12 Effect of Number of Blades

Effect of number of blades on the performance of model wind turbine design, the question arises how many blades should be used. In general, as the number of blades increases so does the cost. The advantages of increasing the number of blades are improved performance and lower torque variations due to wind shear. The number of blades also affects the maximum power coefficient. A finite number of blades, instead of the ideal infinite blade number, causes an extra reduction in power, particularly at low tip of the blade: the higher pressure at the lower side of the blade and the lower pressure at the upper side are 'short circuited' at the tip of the blade. For lower tip speed ratios, in general, higher number of blades is chosen. This is done because the influence of number of blades on power coefficient is larger at lower tip speed ratio. For higher design tip speed ratios higher number of blades will lead to very small and thin blades which results in manufacturing problems and negative influence on the lift and drag properties of the blades. For a rotor with a given tip speed ratio, one can choose between many blades with a small chord width or less blades with a larger chord. For a given tip speed ratio, a rotor with less blades will have larger tip losses. Since the chords become smaller for high tip speed ratios, that effect is smaller for higher tip speed ratios. However, the maximum power coefficient is affected by changing the number of blades. Increase the number of blades shows that region of higher power coefficients move to the region of smaller values of tip speed ratios. So, as in the case of slow running load where the design tip speed ratio is generally low, large number of blades provides higher starting torque.

4 DESIGN AND FABRICATION

4.1 Introduction

Wind-driven power systems that can produce large amounts of power are relatively new technologies. Many earlier models failed catastrophically because blades struck their support structure or tore off the hubs, or towers collapsed. Such failures have diminished in recent years because of improved designs, but other failures such as unacceptable material fatigue and component malfunction are common. In general, failures occur because the effects of unanticipated loads and unknown load levels and load paths are substantial. To combat such effects, wind turbine designers rely heavily on time-tested safety factors that account for this lack of knowledge. Such a design methodology greatly limits the cost effectiveness of new wind turbine designs, which is critical if wind-generated electricity is to be economically competitive with traditional energy sources.

In many respects, design codes (also labeled as modeling tools) bridge the gap between theorized predictions and experimental or observable measurements. Design codes essentially perform virtual experiments that can yield load analysis results quickly and cheaply. In many situations, virtual experimentation offers the only practical method of research and testing.

Most wind turbines have three blades. Very small turbines may use two blades for ease of construction and installation. Vibration intensity decreases with larger numbers of blades. Noise and wear are generally lower, and efficiency higher, with three instead of two blades. Turbines with larger numbers of smaller blades operate at a lower Reynolds number and so are less efficient. Small turbines with 4 or more blades suffer further losses as each blade operates partly in the wake of the other blades. Also, the cost of the turbine usually increases with the number of blades.

4.2 Application of Vertical Axis Vane Type Rotor

Vertical axis vane type rotor blade can be made many different ways with buckets, paddles, sails, and oil drums. All of these designs turn relatively slowly, but yield a high torque. They can be useful for grinding grain, pumping water, and many other tasks; but are not good for generating large amounts of electricity. RPMs above 1000 are generally best for producing electricity; however, drag-based vertical axis wind turbines usually turn below 100 RPM. A gearbox can be used, but then efficiency suffers and the machine may not start at all easily.

4.3 Materials

One of the strongest construction materials available (in 2006) is graphite-fibre in epoxy, but it is very expensive and only used by some manufactures for special load-bearing parts of the rotor blades. Modern rotor blades (up to 126 m diameter) are made of lightweight pultruded glass-reinforced plastic (GRP), smaller ones also from aluminium. GRP is the most common material for modern wind turbines. Wood and canvas sails were originally used on early windmills. Unfortunately they require much maintenance over their service life. Also, they have a relatively high drag (low aerodynamic efficiency) for the force they capture. For these reasons they were superseded with solid airfoils.

4.3.1 Choice of Rotor Blade Material

The material of the turbine blade plays a vital role in the wind turbines. The material of the blade should possess the high stiffness, low density and long fatigue life. In selecting materials for an application, technological considerations of material properties and characteristics are important. The economic aspects of material selection, such as availability, cost of raw materials, and cost of manufacturing, are equally important.

The important factors affecting selection of materials for the rotor blades are mentioned below:

1) One of the most important factors affecting selection of materials for engineering design is the properties of the materials. The important properties of the materials are mechanical, thermal, chemical properties etc.

2) The material of which a part is composed must be capable of performing a part's function (always it must be possible or not) with out failure.

3) A material in a given application must also be reliable.

4) A material must safely perform its function.

5) Physical attributes such as configuration, size, weight, and appearance sometimes also serve as functional requirements.

6) The environment in which a product operates strongly influences service performance.

7) A material must be readily available, and available in large enough quantity, for the intended application.

8) The cost of the materials and the cost of processing the materials into the product or part.

And in any material selection, the following requirements are focused. They are

- High material stiffness is needed to maintain optimal shape of performance.

- Low density is needed to reduce gravity forces,
- Long-fatigue life is needed to reduce material degradation.

The optimal design of the rotor blades is today a complex and multifaceted task and requires optimization of properties, performance and economy.

Wind energy is captured by the rotation of the wind turbine's rotor blades. Different blade materials can be used for rotor construction. These have historically been made of wood, but because of its sensitivity to moisture and processing costs modern materials such as glass fiber reinforced plastic (GFRP), carbon fiber reinforced plastic (CFRP), steel and aluminum are replacing the traditional wooden units.

Wood is a composite of cellulose and lignin. Wood finds many engineering applications and has long been a common construction material. Woods are potentially interesting because of their low density, but their rather low stiffness makes it difficult to limit the (elastic) deflections for very large rotor blades. Even wood materials with cellulosed fibers all aligned in the major load-bearing directions are close to the maximum performance possible for wood. Furthermore, wood is a natural material and thus environmentally attractive, but at the same time difficult to obtain in reproducible and high quality, which is a requirement for stable and economical manufacturing of rotor blades and thus economically attractive wind energy.

Steel is an alloy of iron and carbon. Older style wind turbines were designed with heavier steel blades or nickel alloy steels which have higher inertia, and rotated at speeds governed by the AC frequency of the power lines. The high inertia buffered the changes in rotation speed and thus made power output more stable. The purpose of nickel alloy is lessens distortion in quenching and lowers the critical temperatures of steel and widens the range of successful heat treatment.

Nickel alloy possesses good corrosion and oxidation resistance. Alloy steel was once thought to be an optimum choice for blade fabrication, but was soon abandoned because of its high weight and low fatigue level.

Aluminium is a silvery white metal with a density about a third that of steel. Aluminum was only implemented in testing situations because it was found to have a lower fatigue level than steel. Aluminium is ductile and good heat conductor. Aluminium is a low price metal but it has good reliability and has a low tensile strength. Aluminum is lightweight, but weaker and less stiff than steel.

The fibers and the matrix materials like polyesters, vinyl esters, epoxies etc., are combined into the composites. These composites have good properties like mechanical, thermal and chemical properties.

Firstly, the glass fibers are amorphous with isotropic properties. Most glass-reinforced products are made with E-glass (electrical glass), which has good electrical and mechanical properties and high heat resistance. E-glass is available as chopped fiber, milled fiber, continuous roving, woven roving, woven fabric, and reinforcing mat. Glass fibers for composites have good properties like moderate stiffness, high strength, and moderate density.

Carbon fibers are composed of nearly pure carbon, which forms a crystallographic lattice with a hexagonal shape called graphite. In recent years carbon fibers have become of increasing interest because of the requirements presented by the ever-larger rotor blades and the decreasing price of carbon fibers. Carbon fibers for composites have an excellent combination of very high stiffness, high strength, light weight and low density.

Aramid fibers (aromatic polyamides) are characterized by excellent environmental and thermal stability, static and dynamic fatigue resistance, and impact resistance. These fibers have the highest specific tensile strength (strength/density ratio) of any commercially available continuous-filament yarn. Aramid reinforced thermoplastic composites have excellent wear resistance. Aramid fibers have low or very low densities.

One of the most important factors in decision making is the degree of uncertainty. Whenever the designer makes a decision, he is performing a prediction of the effect of future events in technical feasibility, economic viability and trade-off between them. To make a successful prediction, good information (previous experience, outcomes from the similar circumstance, design knowledge, expertise etc.), proper methods and sometime good intuition are needed. And all geometry information, material properties, manufacturing process parameters, market change, customers' preference, development and manufacturing cost etc. can be estimated exactly and the future events are perfectly predictable.

In this analysis the PVC type had been chosen because of its high stiffness, high strength, light weight and low density. Above all this material was economically viable and by far obtainable in market.

4.4 Effect of Number of Blades on the Performance of VAWT

In considering a wind turbine design, the question arises how many blades should be used. In general, as the number of blades increases so does the cost. The advantages of increasing the number of blades are improved performance and lower torque variations due to wind shear. The number of blades also affects the maximum power co-efficient. This is caused due to tip losses that occur at the tips of the blades. These losses depend on the number of blades and tip speed ratios. For lower tip speed ratios, in general, higher number of blades is chosen. This is done because the influence of number of blades on power co-efficient is larger at lower tip speed ratios. For higher design tip speed ratios higher number of blades will lead to very small and thin blades which results in manufacturing problems and a negative influence on the lift and drag properties of the blades.

5 EXPERIMENTAL SET-UP AND PROCEDURE

5.1 Introduction

The investigation on wind loading and aerodynamic effects on the four/five/six semi cylindrical bladed Vertical Axis vane rotor has been conducted essentially with the help of a subsonic wind tunnel together with the experimental set up of the Vane rotor. The following sections describe in detail set-up of the experiment and techniques adopted for the investigation.

5.2 Specification of the Wind Tunnel

The schematic diagram of the wind tunnel has been shown in Figure 5.2.1. An open circuit subsonic type wind tunnel was used to develop the required flow. The tunnel was 5.93 meter long with a test section of 490 mm x 490 mm in cross-section. The successive sections of the wind tunnel comprised of a converging entry, a Perspex section, a rectangular section, a fan section (two rotary axial flow fans), a butterfly valve section, a silencer with honey comb section, a diverging section, a converging section and an exit flow straightened section. The central longitudinal axis of the wind tunnel was maintained at a constant height from the floor. The converging mouth entry was incorporated into the system for easy entry of air into the tunnel and maintains uniform flow into the duct free from outside disturbances. In order to smooth the flow, the honeycomb was fixed near the outlet of the wind tunnel. The induced flow through the wind tunnel was produced by two-stage rotating axial flow fan of capacity 18.16 m^3/s at a head of 152.4 mm of water and 1475rpm with each of the fans connected to a motor of 2.25 kW capacity and 2900 rpm. A butterfly valve as shown in Figure 5.2.1 was used to control the wind speed. It was actuated by a screw thread mechanism placed behind the fan. A silencer was connected just after the butterfly valve for reduction of noise of the system. The converging and diverging section of the wind tunnel was 1550 mm long and made of 16 SWG black sheets. The angle of them was 7^0, which had been done with a view to minimizing expansion, contraction loss and reducing the possibility of flow separation. Other three outlet square (610 mm each) sections were used to make the flow straight and uniform.

Figure 5. 1: Schematic diagram of a wind tunnel

Figure 5. 2: Wind Tunnel

5.3 Description of the Experimental Set-up

The experiment was carried out in the open circuit subsonic wind tunnel with an outlet test section of (490 mm x 490 mm) cross-section and the rotor was positioned at the exit section of the wind tunnel. The central longitudinal axis of the wind tunnel was always kept at a constant height of 990 mm from the floor. The model turbine was placed at 0.5m – rotor diameter downstream from the wind tunnel exit end as shown in Figure 5.3.1. The axis of the model was also placed coinciding with the axis of the wind tunnel.

Each time after changing the speed of axial flow fan average wind tunnel air velocity was measured directly by an electrical anemometer. This velocity distribution was along the vertical direction passing through the axis of the wind tunnel. Similarly, velocity distribution along the horizontal direction was observed as well. The anemometer was placed in front of the wind tunnel behind the rotor at different vertical distances between 100 mm downstream and 100 mm upstream of wind tunnel and average velocity was calculated. The velocity was more or less uniform throughout that can be seen from the Figure 5.3.2. The flow velocities were varied from 5m/s to 9m/s covering the Reynolds numbers up to 1.35×10^5.

A non-contact digital tachometer was used to measure the rpm of the shaft at different loading condition.

Figure 5. 3: Set-up of the Experiment

Figure 5. 4: Set – up of the Experiment (4 Bladed Vane Type Rotor)

Figure 5. 5: Set – up of the Experiment (5 Bladed Vane Type Rotor)

Figure 5. 6: Set – up of the Experiment (6 Bladed Vane Type Rotor)

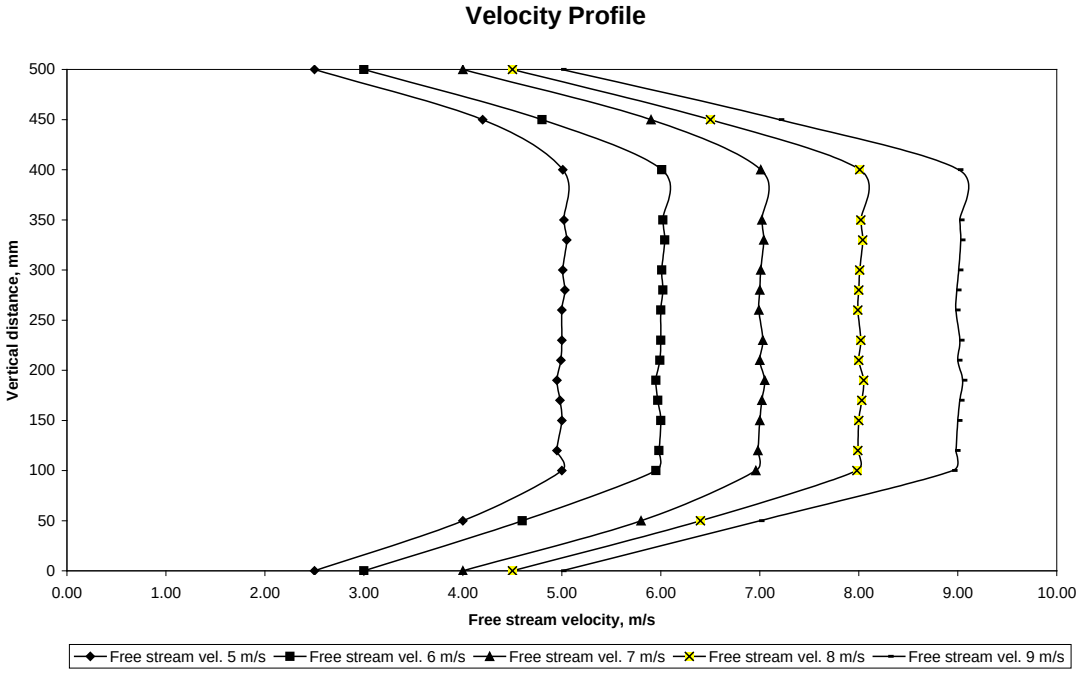

Figure 5. 7: Velocity distribution in upstream side of test section.

5.4 Constructional Detail of the Four/Five/six Bladed Vane Type Rotor

The constructional detail of the test section is shown in Figure 5.4.1. Four, Five and Six bladed vane type rotor were made up of respectively four, five and six half cylinders (blade) of diameter, d =65 mm and height, H = 340 mm. Rotor diameter, D was 200 mm. Optimum value of d/D ratio was taken as 1/3. The cylinders were made of PVC material. Both the top and bottom ends of the rotor were fitted with end caps. The whole rotor was fixed on an iron frame by using a shaft that was inserted into it and two ball bearings. A pulley was attached at one end of shaft. A strip whose one side was tied to a spring balance and other side to a load carrying plate was prepared for passing over that pulley. A radium sticker was attached to that side of shaft. The spring balance was attached to the iron frame. The whole experimental set-up is shown in Figure 5.3. The cross-sectional views of four, five and six bladed vane type rotor are shown respectively in Figure 5.8, Figure 5.9 and Figure 5.10. And their consttructional detail views are shown respectively in Figure 5.11, Figure 5.12 and Figure 5.13.

Figure 5. 8: Sectional view of 4 Bladed Rotor

Figure 5. 9: Sectional view of 5 Bladed Rotor

Figure 5. 10: Sectional view of 6 Bladed Rotor

Figure 5. 11: Constructional Details of 4 Bladed Vertical Axis Vane Type Rotor

Figure 5. 12: Constructional Details of 5 Bladed Vertical Axis Vane Type Rotor

Figure 5. 13: Constructional Details of 6 Bladed Vertical Axis Vane Type Rotor

Figure 5. 14: Forces acting on the blade (4 bladed rotor)

Figure 5. 15: Forces acting on the blade (5 bladed rotor)

Figure 5. 16: Forces acting on the blade (6 bladed rotor)

5.5 Experimental Procedure

The flow velocities in the test section were varied from 5m/s to 9m/s covering the Reynolds numbers up to 1.2×10^5. The effect of temperature was considered in this experiment and the experiment was carried out at atmospheric temperature i.e. at $T = 30^0C$ where kinematic viscosity of air was $\nu = 1.60 \times 10^{-5}$ m^2/s.

The experimental procedures are given below in brief:

a) The on button of one of the motor was pressed in order to rotate one axial flow fan for the purpose of generating free stream air of uniform velocity through the wind tunnel.

b) In front of the wind tunnel without placing the rotor model the wind velocity was measured by an anemometer at different vertical distances between 100mm upstream and 100mm downstream of wind tunnel.

c) The speed of the axial flow fan was adjusted to obtain a particular free steam velocity at the exit section of wind tunnel. The free stream velocity was first adjusted to 5 m/s.

d) The four bladed vane type rotor with structural frame was placed in front of the wind tunnel. It was placed 100 mm down stream of the tunnel exit section on a stand.

e) It was observed that the rotor with shaft was rotating because of the free stream velocity at the exit of the wind tunnel. At this condition, the light from digital non-contact tachometer was focused on the radium sticker attached to the shaft and the rpm reading at no load condition was taken.

f) At different loading condition the reading of rpm of the shaft using con-contact tachometer, the reading of weight from spring balance and the applied weight in the load carrying plate were noted down.

g) After taking all the readings up to maximum loading condition, the free stream velocity was further adjusted to 6 m/s. And the same procedures were followed.

h) Thus rapidly the free stream velocity was increased by 1 m/s and each time the same procedures were followed. The free stream velocity was raised rapidly up to 9 m/s.

i) The same procedures were followed for five and six bladed vane type rotor.

j) Output power was obtained from the above reading. Experimental values of the power coefficients were calculated from the ratio of the total output power to the theoretical available power.

k) Experimental values of the Torque coefficients were calculated from the ratio of power coefficient to the tip speed ratio.

Figure 5. 17: Velocity Triangles combining the effect of free stream velocity and blade rotation (4 bladed rotor).

Figure 5. 18: Velocity Triangles combining the effect of free stream velocity and blade rotation (5 bladed rotor).

Figure 5. 19: Velocity Triangles combining the effect of free stream velocity and blade rotation (6 Bladed rotor).

6 RESULTS AND DISCUSSION

6.1 Introduction

This chapter provides with the discussions of the results of experimental investigation conducted for the wind tunnel flow over three, four and five bladed Vertical Axis Vane Type Rotor. The results of the power coefficient as well as torque coefficient of the three rotors with different number of blades at different Reynolds number as well as at different loading conditions are analysed. In addition, a comparative study of the existing experimental results of the power coefficients as well as torque coefficients for Vertical Axis Vane Type Rotor with the predicted results of Vertical Axis Vane Type Rotor [2] is presented. At last a comparative study of the existing research works (predicted) and the present investigation of dynamic characteristics are also presented.

6.2 Dynamic Aerodynamic Characteristics

This topic includes the analysis of power coefficient (Cp) and torque coefficient (Cq) with respect to different tip speed ratio for multi bladed vane type rotor at different Reynolds number.

6.2.1 Power coefficient

6.2.1.1 Power Coefficient for Four Bladed Vane type Rotor

The effect of Reynolds number on power coefficient for Four Bladed Vane Type Rotor is shown in Figures 6. 2. 1 to 6. 2. 5. The variations of Reynolds number were made by varying the free stream velocity. Figure 6. 2. 1 shows the power coefficient vs. tip speed ratio for four bladed vane type rotor at Reynolds number $0.6375x10^5$, here the value of maximum power coefficient is 0.113, occurs at tip speed ratio of 0.438. For further loading step by step with the decrease in rotor r.p.m, tip speed ratio also decreases. However, the value of power coefficient starts falling as the tip speed ratio becomes lower than 0.438 although so far it was at increasing condition. From Figure 6. 2. 2, it is found that the value of maximum power coefficient is 0.121, occurs at tip speed ratio 0.53 at Reynolds number $0.80x10^5$. From these two figures, it is observed that the maximum power coefficient is slightly higher and it is shifted towards the higher values of tip speed ratios as the Reynolds number is increased. For Reynolds number of $0.9x10^5$, $1.02x10^5$ and $1.2x10^5$ the same repetition is observed. The maximum value of power coefficients are found as 0.122, 0.125 and 0.139 occur at tip speed ratios of 0.54, 0.65 and 0.73 at Reynolds numbers of $0.9x10^5$, $1.02x10^5$ and $1.2x10^5$ respectively.

In Figure 6. 2. 6, a comparison of power coefficient vs. tip speed ratio for Four Bladed Vane Type Rotor with different Reynolds number has been depicted. From the graph it is clearly visualized that the maximum value of power coefficient increases with increasing the Reynolds number and it is shifted towards the higher values of tip sped ratios. Here it is

observed that the maximum value of power coefficient increases by 23% as the Reynolds number increases from 0.6375 x 10^5 to 1.2 x 10^5. So it can be concluded that the increase in Reynolds number make the nature of curve slightly steeper.

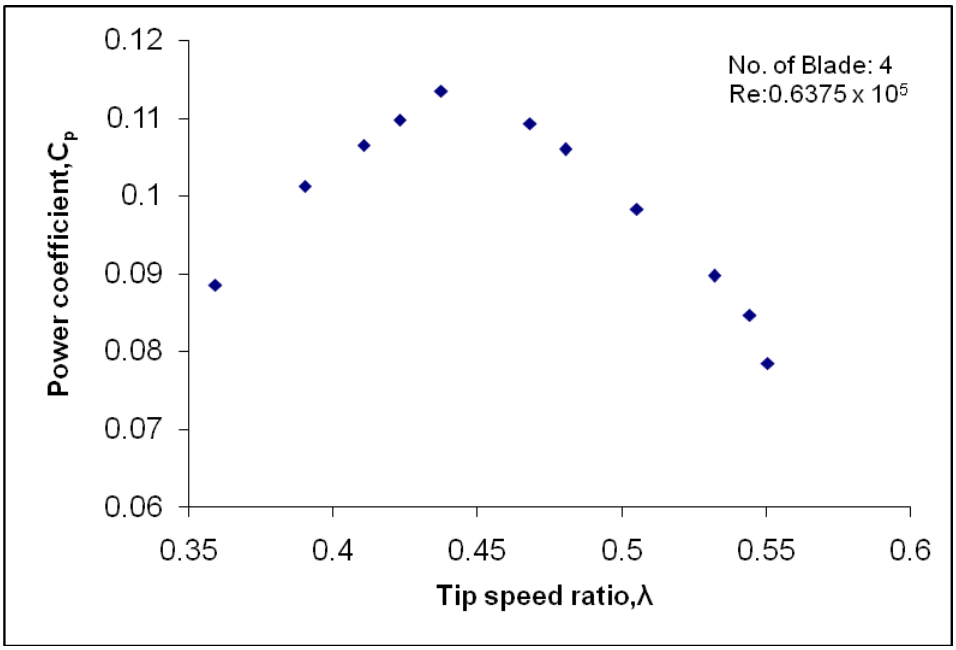

Figure 6. 2. 1: Variation of power coefficient with tip speed ratio at Reynolds number of 0.6375x10^5 for Four Bladed Vane Type Rotor.

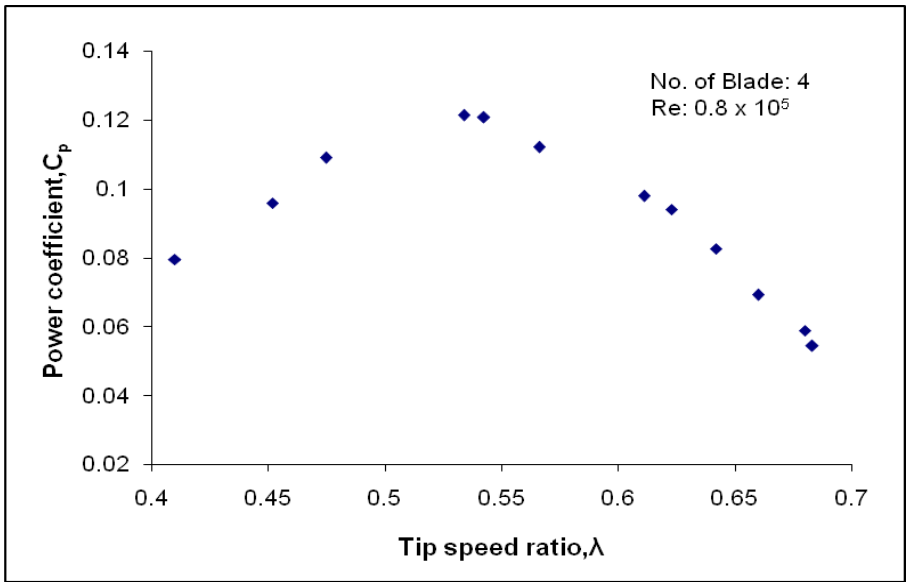

Figure 6. 2. 2: Variation of power coefficient with tip speed ratio at Reynolds number of 0.8x105 for Four Bladed Vane Type Rotor.

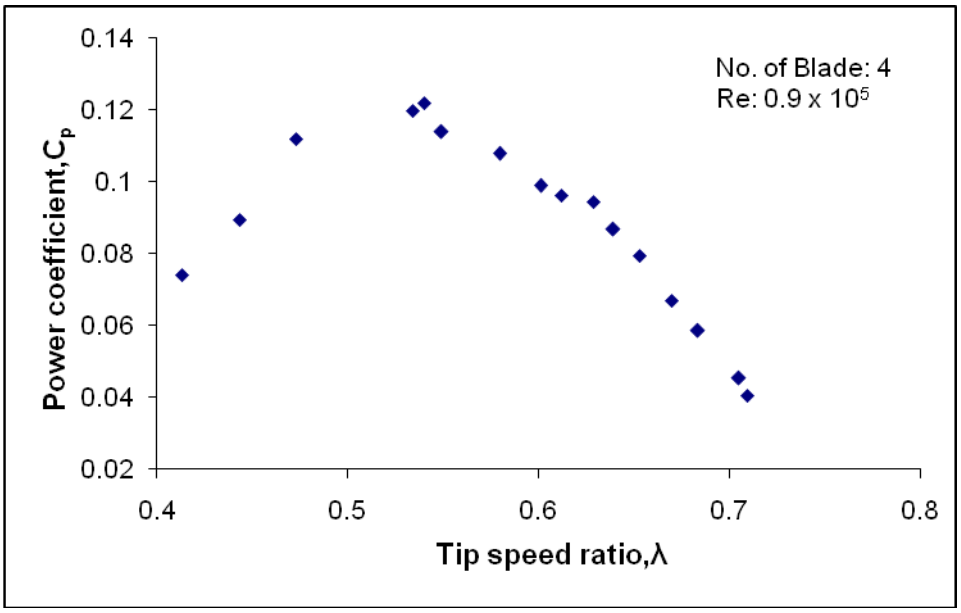

Figure 6. 2. 3: Variation of power coefficient with tip speed ratio at Reynolds number of 0.9x105 for Four Bladed Vane Type Rotor.

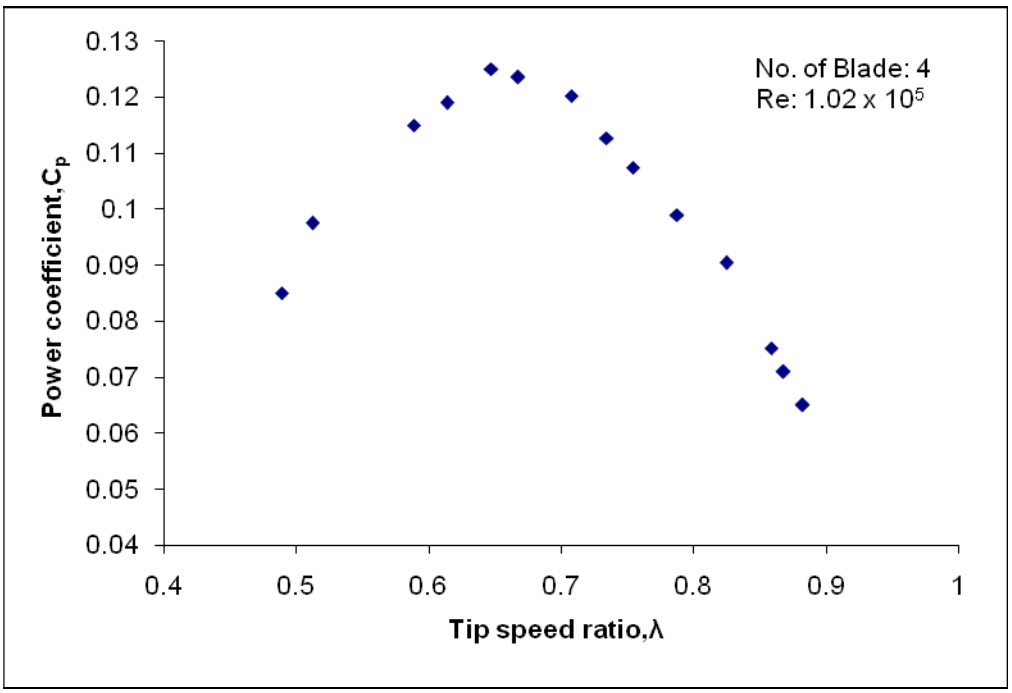

Figure 6. 2. 4: Variation of power coefficient with tip speed ratio at Reynolds number of $1.02x10^5$ for Four Bladed Vane Type Rotor.

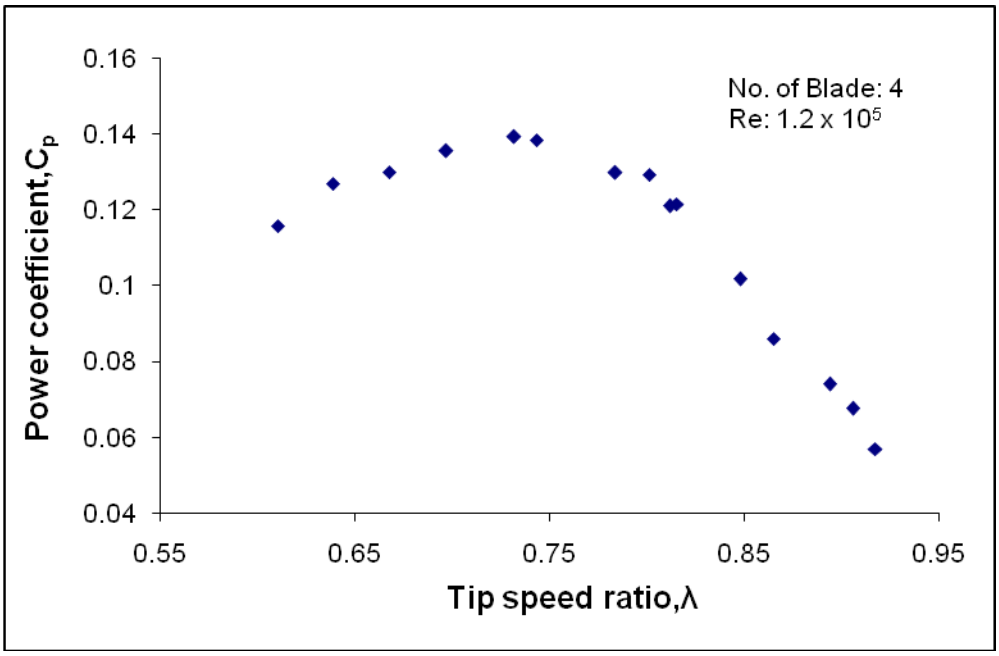

Figure 6. 2. 5: Variation of power coefficient with tip speed ratio at Reynolds number of $1.2x10^5$ for Four Bladed Vane Type Rotor.

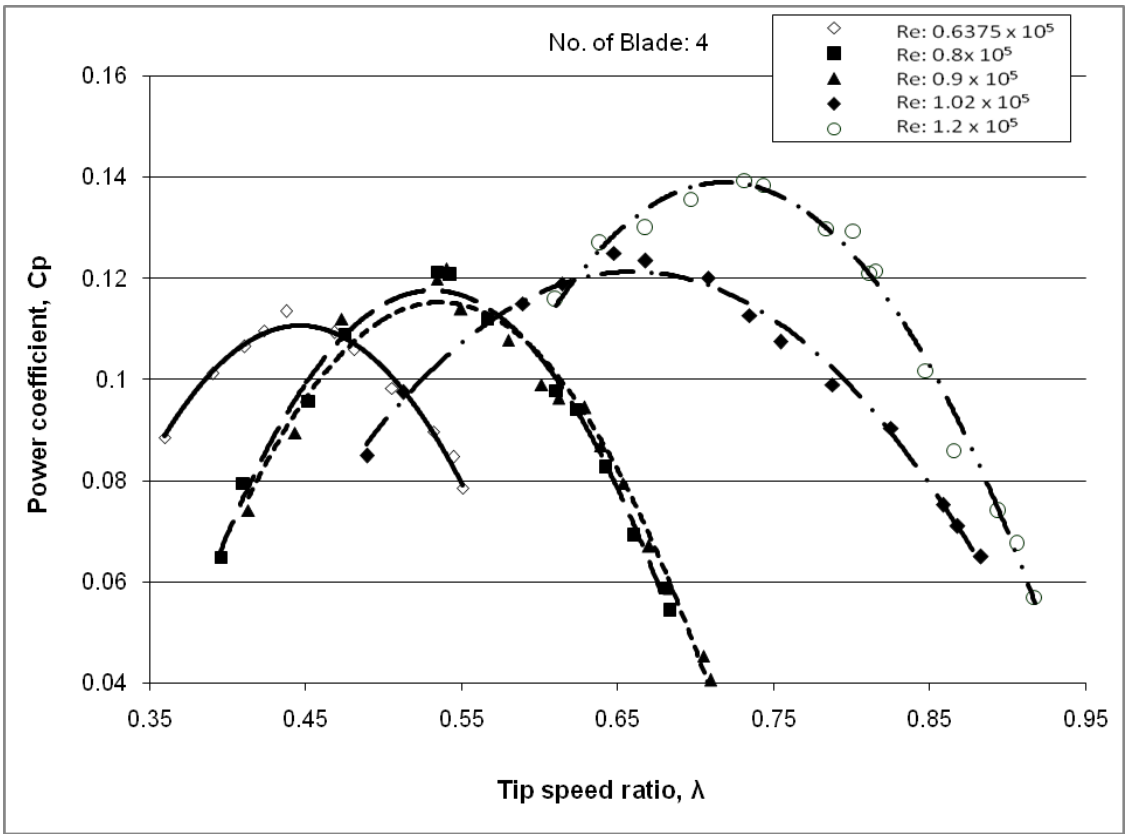

Figure 6. 2. 6: Comparison of power coefficient vs. tip speed ratio for Four Bladed Vane Type Rotor at Reynolds number.

6.2.1.2 Power Coefficient for Five Bladed Vane Type Rotor

The variations of results for Five Bladed Vane Type Rotor in terms of power coefficient vs. tip speed ratio are shown in Figures 6. 2. 7 to 6.11 for Reynolds number 0.6375 x 10^5, 0.8x10^5, 0.9 x 10^5, 1.02 x 10^5 and 1.2 x 10^5 respectively.

From Figure 6. 2. 7 it is observed that at Reynolds number 0.6375 x 10^5, the maximum value of power coefficient is 0.132 occurs at tip speed ratio 0.681. For further loading step by step with the decrease in tip speed ratio the power coefficient also decreases. At Reynolds number 0.8 x 10^5, from Figure 6. 2. 8 it is seen that the maximum power coefficient is 0.136 which is achieved at tip speed ratio 0.69. Here same repetition is observed as Four Bladed Vane Type Rotor, i.e. the maximum power coefficient is affected by the change in Reynolds number. Just as the curves of Four Bladed Rotor, the value of maximum power coefficient increases slightly with the increase in Reynolds number and the region of this higher power coefficient move to the region of larger values of tip speed ratios. For Reynolds number 0.9 x 10^5, 1.02 x 10^5 and 1.2 x 10^5 the maximum value of power coefficient is 0.143, 0.145 and 0.148 which is obtained at tip speed ratio of 0.73, 0.75 and 0.766 respectively.

In Figure 6. 2. 12 a comparison of power coefficient vs. tip speed ratio has been presented at different Reynolds number for five bladed vane type rotor. From this graph it is apparent that the value of maximum power coefficient increases with the increase in Reynolds number and it is shifted towards the higher values of tip speed ratios. Here it is also observed that the value of maximum power coefficient is increased by 11.4% as the Reynolds number has been changed from 0.6375 x 10^5, to 1.2 x 10^5. So, a conclusion can be drawn as, the increase in Reynolds number make the nature of power coefficient vs. tip speed ratio curve slightly steeper.

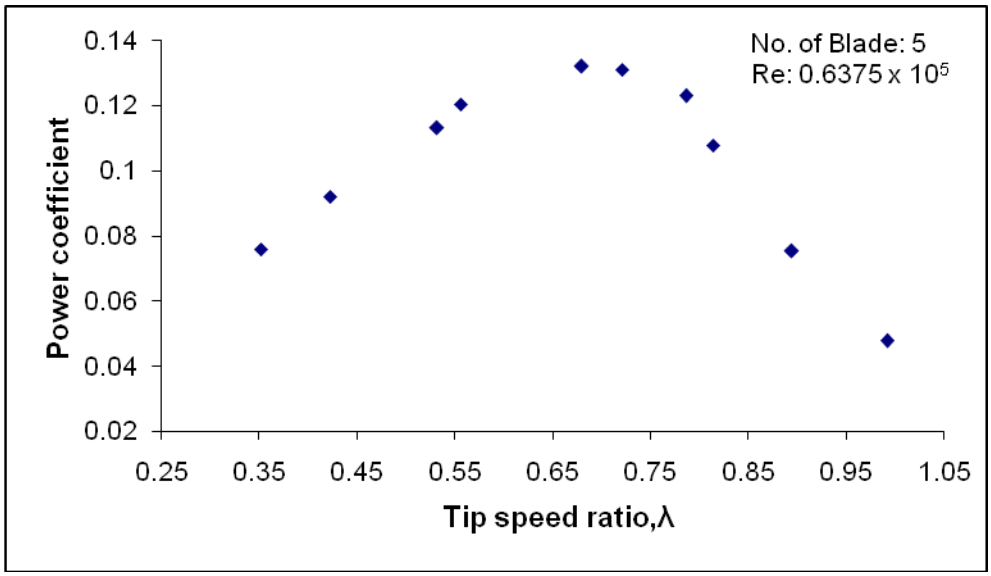

Figure 6. 2. 7: Variation of power coefficient with tip speed ratio at Reynolds number of 0.6375 x 10^5 for Five Bladed Vane Type Rotor.

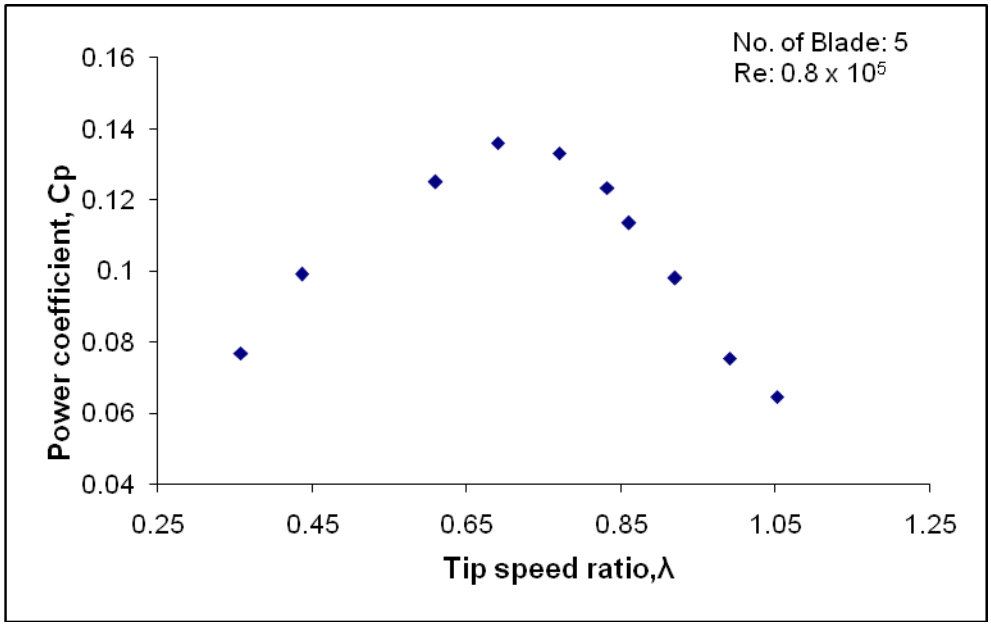

Figure 6. 2. 8: Variation of power coefficient with tip speed ratio at Reynolds number of 0.8 x 10^5 for Five Bladed Vane Type Rotor.

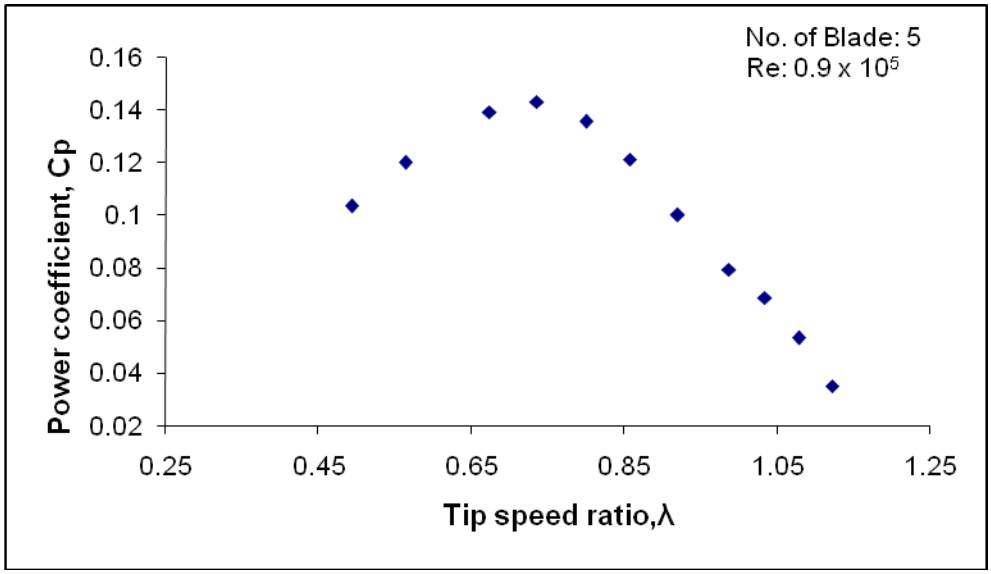

Figure 6. 2. 9: Variation of power coefficient with tip speed ratio at Reynolds number of 0.9 x 10^5 for Five Bladed Vane Type Rotor.

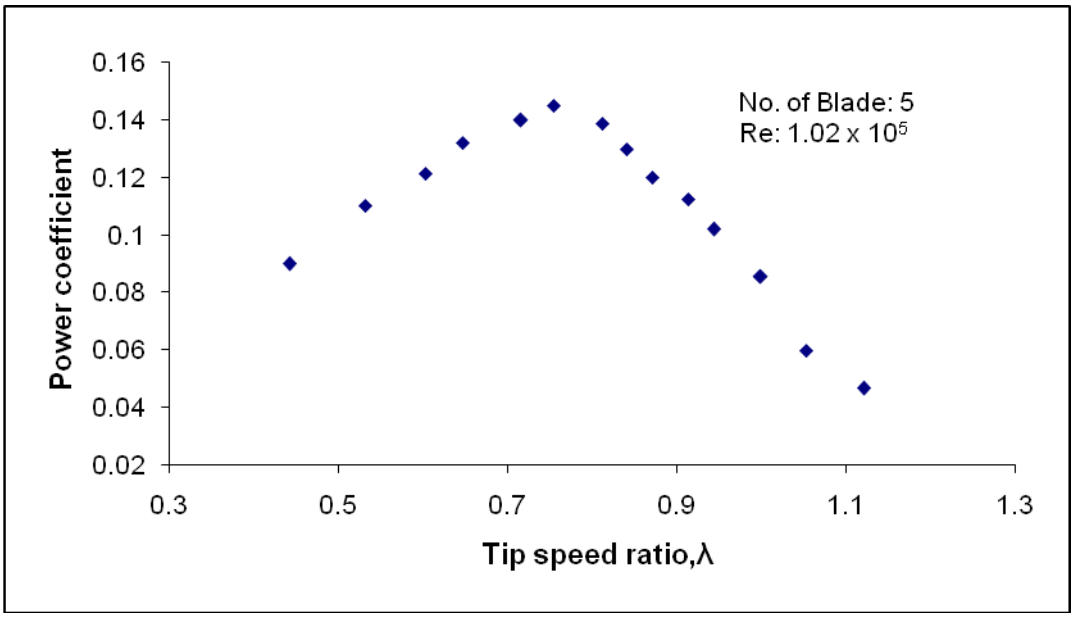

Figure 6. 2. 10: Variation of power coefficient with tip speed ratio at Reynolds number of 1.02 x 10^5 for Five Bladed Vane Type Rotor.

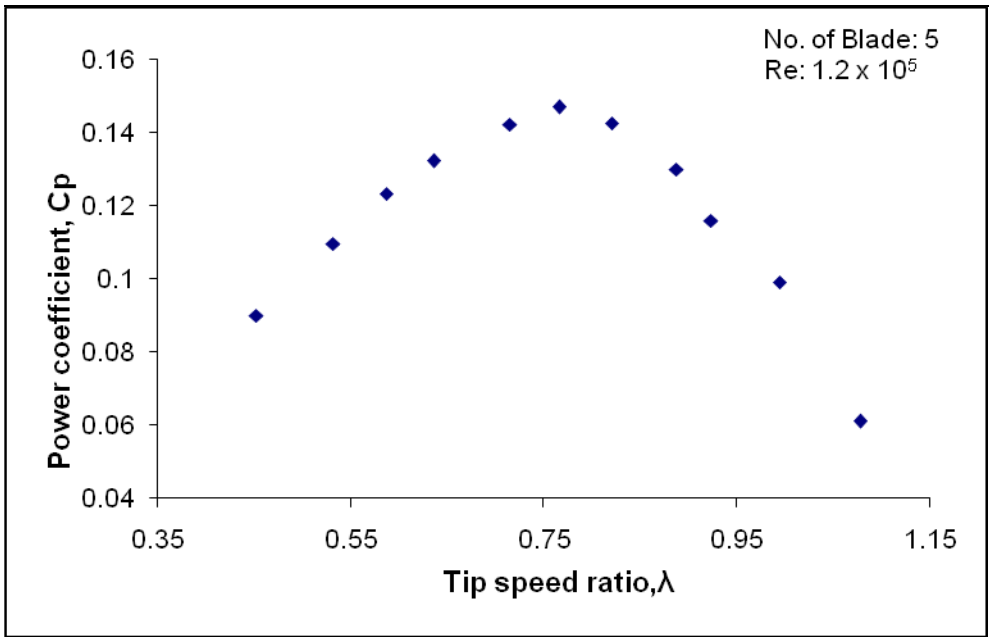

Figure 6. 2. 11: Variation of power coefficient with tip speed ratio at Reynolds number of 1.2 x 10^5 for Five Bladed Vane Type Rotor.

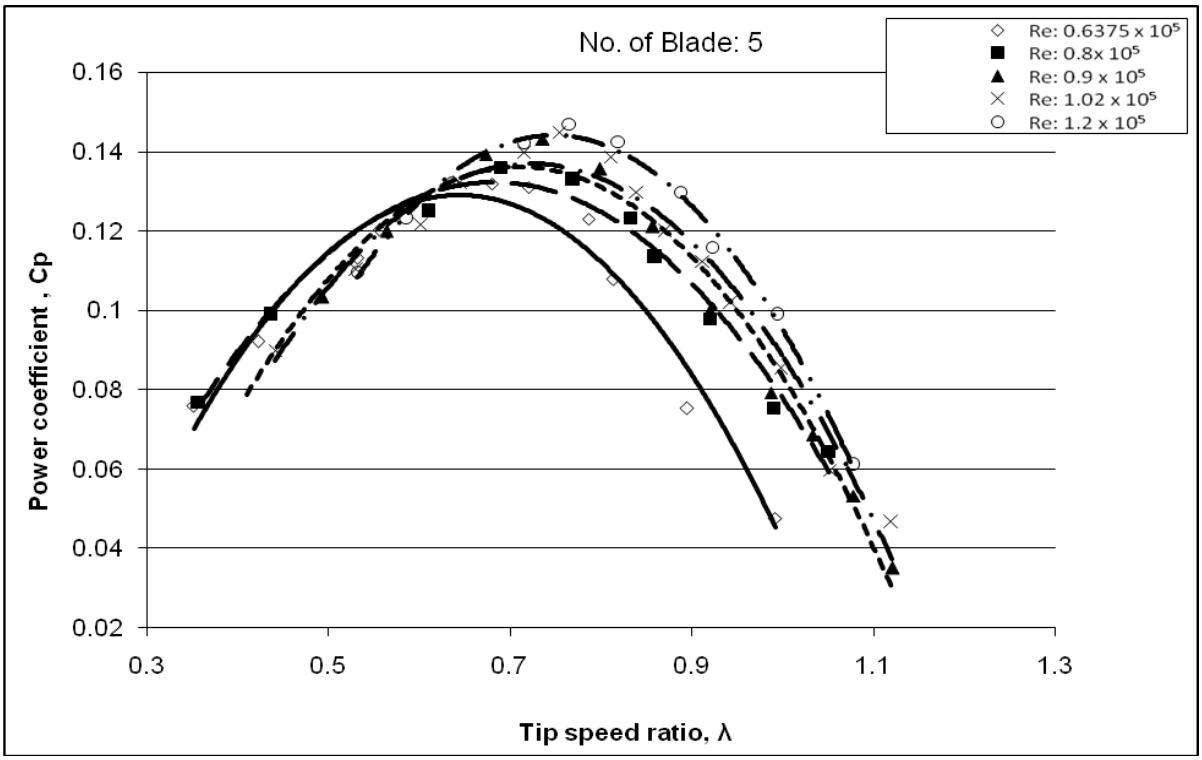

Figure 6. 2. 12: Comparison of power coefficient vs. tip speed ratio for Five Bladed Vane Type Rotor at different Reynolds number.

6.2.1.3 Power Coefficient for six bladed Vane Type Rotor

The variations of results of power coefficient vs. tip speed ratio for six bladed rotor are presented in Figures 6. 2. 13 to 6. 2. 17 for the Reynolds number of 0.6375 x 10^5, 0.8 x 10^5, 0.9 x1 0^5, 1.02 x 10^5 and 1.2 x 10^5 respectively.

From Figure 6. 2. 13 it is seen that the maximum power coefficient of six bladed rotor at Reynolds number of 0.6375 x 10^5 is 0.148 which is achieved at tip speed ratio 0.52. For further loading step by step as the value of tip speed ratio decreases, the power coefficient also decreases. For Reynolds number 0.8 x 10^5, 0.9 x 10^5, 1.02 x 10^5 and 1.2 x 10^5 the maximum values of power coefficients are found as 0.152, 0.157, 0.161 and 0.163 available at tip speed ratio of 0.56, 0.579. 0.67 and 0.69 respectively.

Just as the previous figures of four and five bladed rotor, the six bladed rotor also show the same phenomena i.e. maximum power coefficient increases with increasing the Reynolds number and this higher values of power coefficient move to the region of larger values of tip speed ratios.

Figure 6. 2. 18 represents a comparison of power coefficient vs tip speed ratio for six bladed vane type rotor at different Reynolds number. From this graph it is apparent that with the increase in Reynolds number the maximum value of power coefficient increases and it is shifted towards the higher values of tip speed ratios. Here it is also observed that the value of maximum power coefficient increases by 10.5% as the Reynolds number changes from 0.6375 x 10^5, to 1.2 x 10^5. So a conclusion can be drawn as the increase of Reynolds number make the nature of power coefficient vs. tip speed ratio curve slightly sharper.

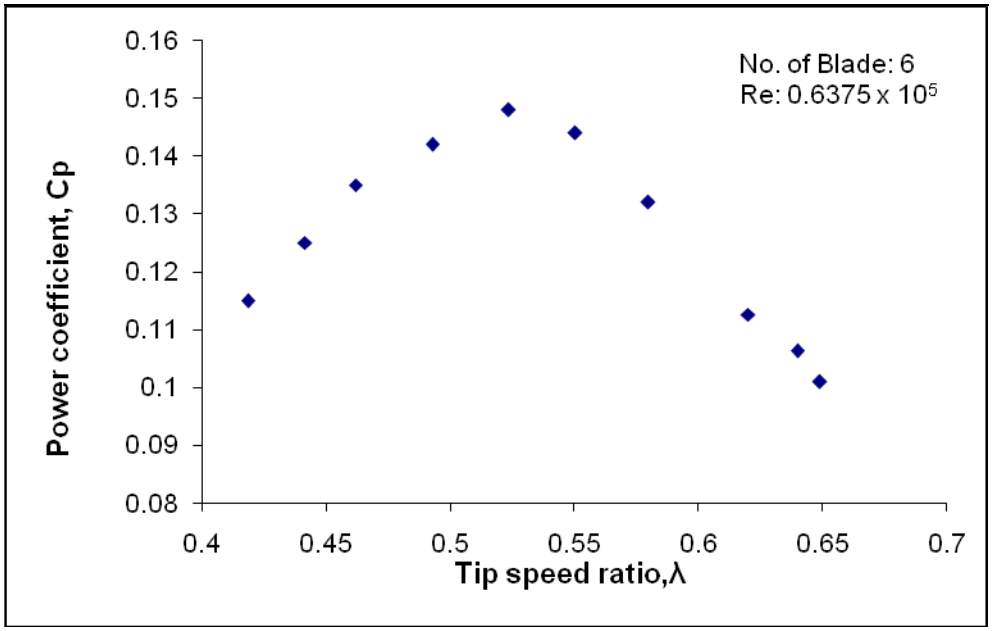

Figure 6. 2. 13: Variation of power coefficient with tip speed ratio at Reynolds number of 0.6375 x10^5 for Six Bladed Vane Type Rotor.

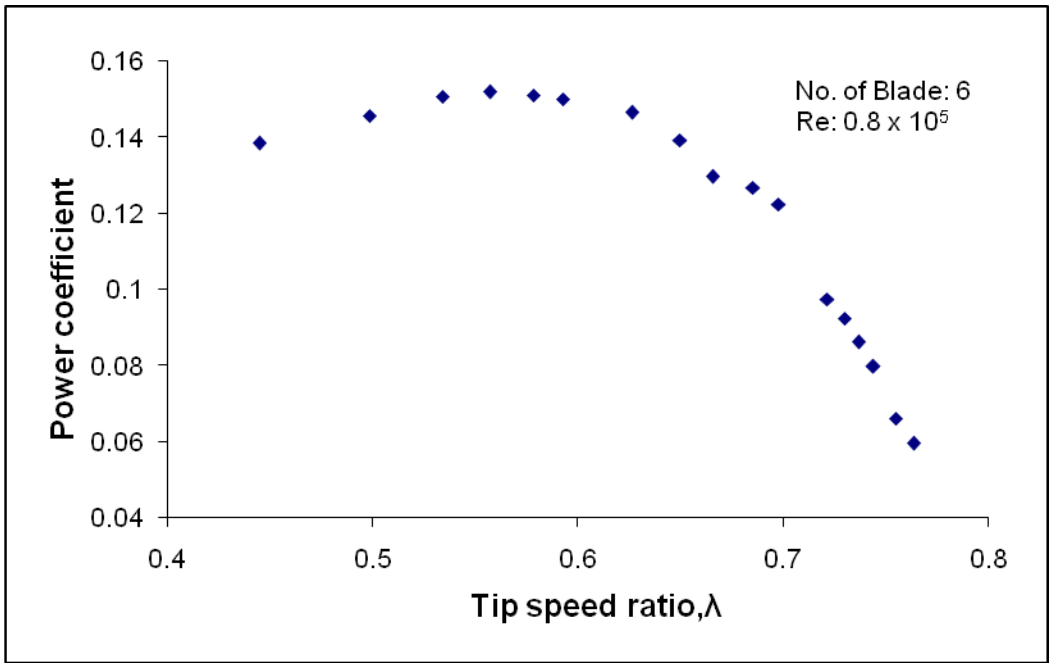

Figure 6. 2. 14: Variation of power coefficient with tip speed ratio at Reynolds number of 0.8 x 10^5 for Six Bladed Vane Type Rotor.

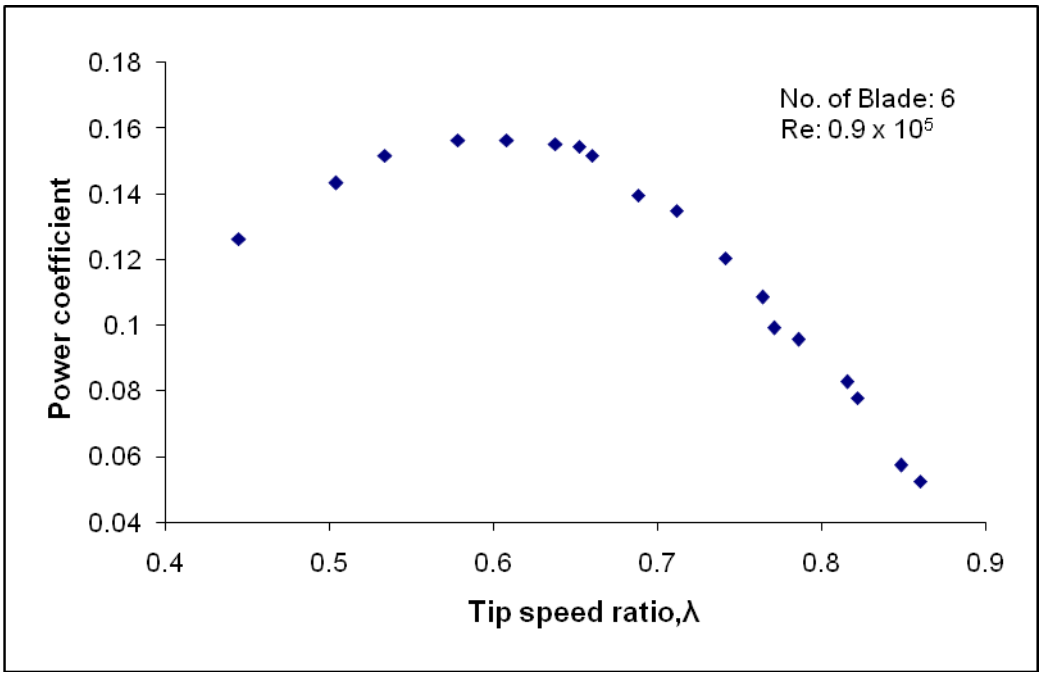

Figure 6. 2. 15: Variation of power coefficient with tip speed ratio at Reynolds number of 0.9 x 10^5 for Six Bladed Vane Type Rotor.

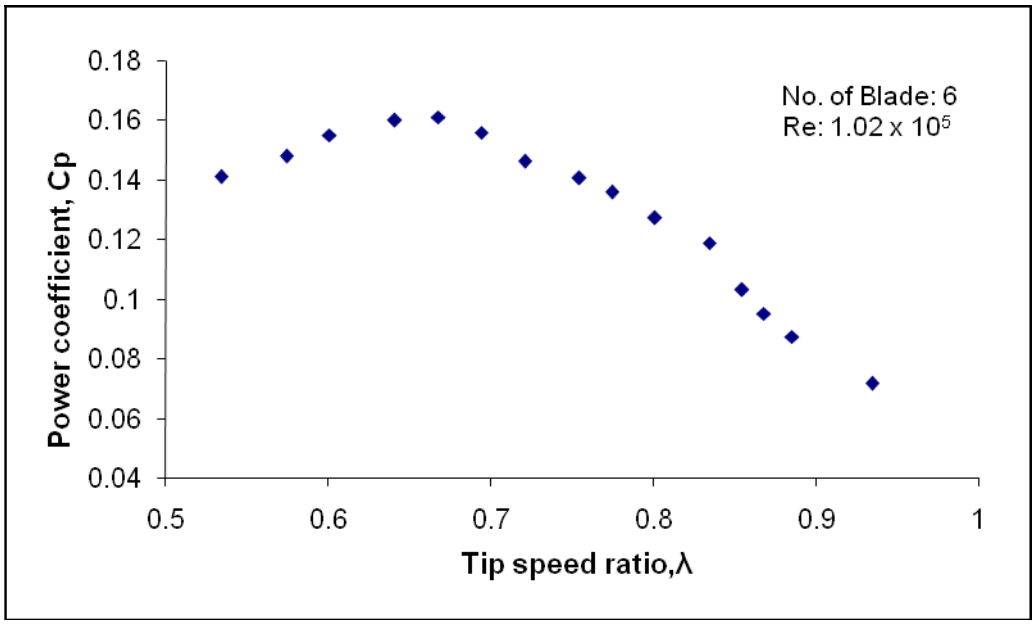

Figure 6. 2. 16: Variation of power coefficient with tip speed ratio at Reynolds number of 1.02 x 10^5 for Six Bladed Vane Type Rotor.

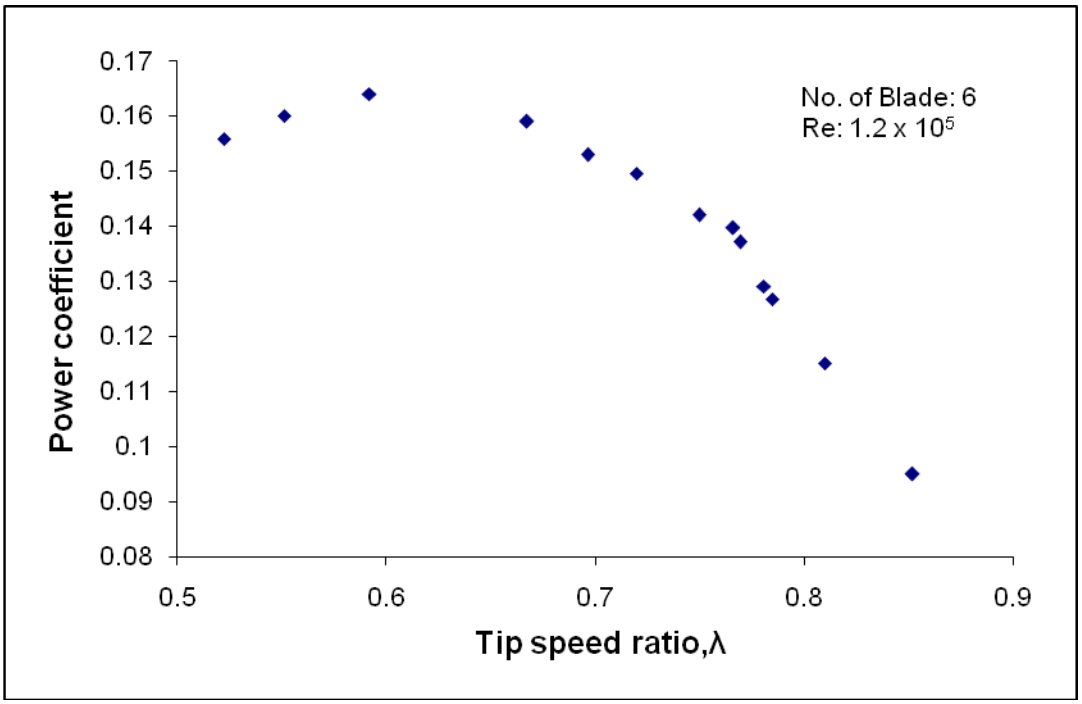

Figure 6. 2. 17: Variation of power coefficient with tip speed ratio at Reynolds number of 1.2 x 10^5 for Six Bladed Vane Type Rotor.

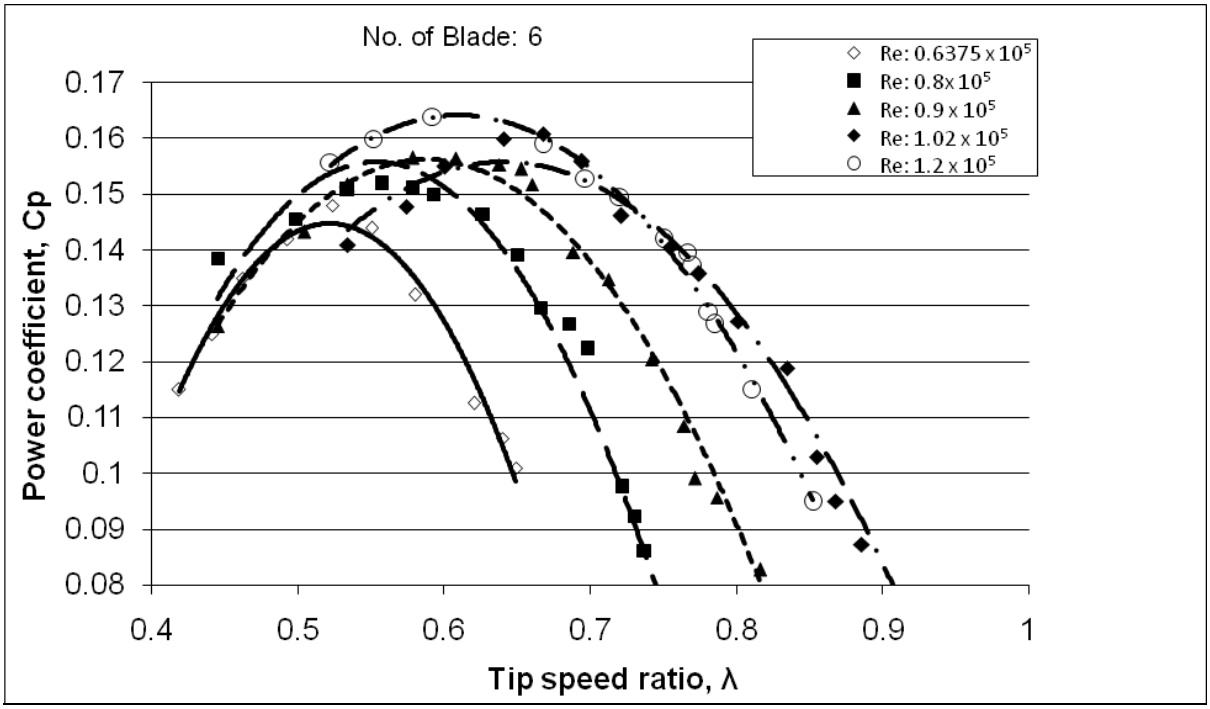

Figure 6. 2. 18: Comparison of power coefficient vs. tip speed ratio for Six Bladed Vane Type Rotor at different Reynolds number.

6.2.1.4 Power coefficient at different Reynolds number for 4,5 and 6 Bladed Vane Type Rotor

Figures 6.2.19 to 6.2.23 shows a comparison among the curves of power coefficient vs. tip speed ratio of multi bladed rotor at different Reynolds number. In each figure, a comparison have been made among different curves of power coefficient vs. tip speed ratio of 4, 5 and 6 bladed vane type rotor at a particular Reynolds number.

Figure 6. 2. 19 shows a comparison of power coefficient vs. tip speed ratio for four, five and six bladed vane type rotor at Reynolds number of 0.6375×10^5. From this figure it is found that the value of maximum power coefficient for 4, 5 and 6 bladed rotor are recorded as 0.113, 0.132 and 0.148, occurs at tip speed ratio of 0.438, 0.68 and 0.52 respectively. The figure implies that with the increase in number of blades power coefficient also increases and it is shifted toward the higher values of tip speed ratio. From this figure it is observed that the value of maximum power coefficient increases 30.97% as the number of blades increases from four to six for Reynolds number 0.6375×10^5.

In Figures 6. 2. 20 to 6. 2. 23 the same repitation is observed, that is power coefficient increases with increasing number of blades. The maximum values of power coefficient for 4, 5 and 6 bladed rotors are 0.121, 0.3136 and 0.152 occur at tip speed ratio of 0.53, 0.69 and 0.56 respectively at Reynolds number of 0.8×10^5. Here it is observed that the maximum value of power coefficient increases by 25% as the number of blades increases from four to six at Reynolds number 0.8×10^5. At Reynolds number 0.9×10^5 the values of maximum power coefficient are found as 0.123, 0.143 and 0.157 occur at tip speed ratio of 0.55, 0.73 and 0.58 respectively. At Reynolds number 0.9×10^5 the maximum value of power coefficient is increased by 27.6% as the number of blade increases from four to six. At Reynolds number of 1.02×10^5 the values of maximum power coefficient are recorded as 0.125, 0.145 and 0.161 occur at tip speed ratio of 0.65, 0.75 and 0.67 respectively. The value of maximum power coefficient is increased by 28.8% at Reynolds number of 1.02×10^5 as the number of blade is increased from four to six. At Reynolds number of 1.2×10^5 the values of power coefficient are 0.139, 0.147 and 0.164 occur at tip speed ratio of 0.73, 0.76 and 0.59 respectively. For this Reynolds number the value of maximum power coefficient is increased by 17.63% as the number of blades increases from four to six. All the graphs show the same trend, i.e. the value of maximum power coefficient is higher for the rotor of higher numbers of blades and it is shifted towards the higher values of tip speed ratio. It is also apparent that the number of blades is more significant for lower number of Reynolds number.

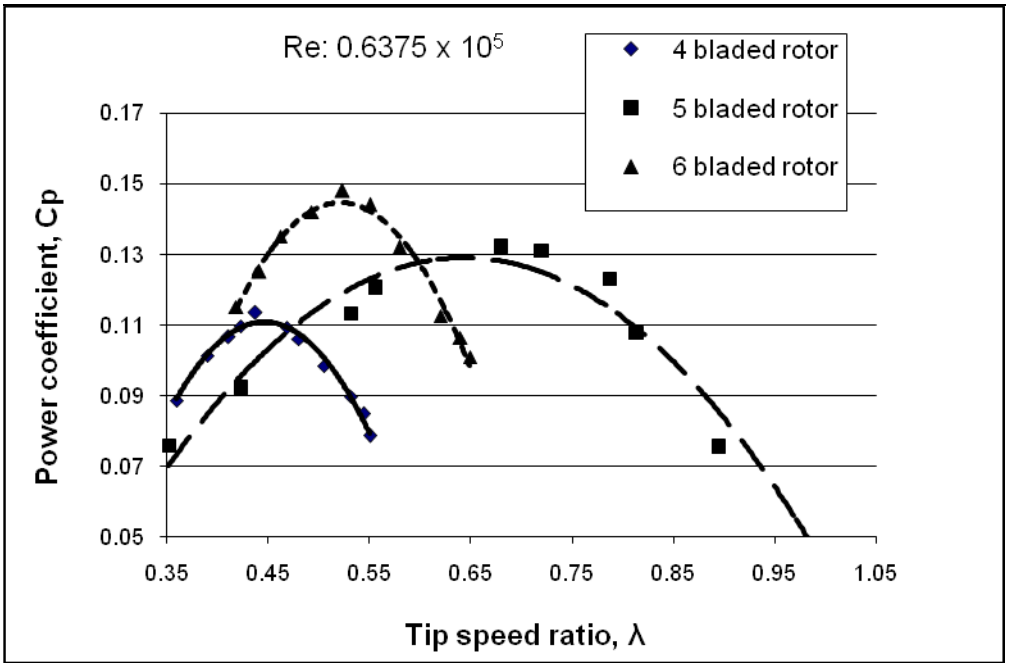

Figure 6. 2. 19: Comparison of power coefficient vs. tip speed ratio of 4, 5, and 6 Bladed Vane Type Rotor at Reynolds number of 0.6375×10^5.

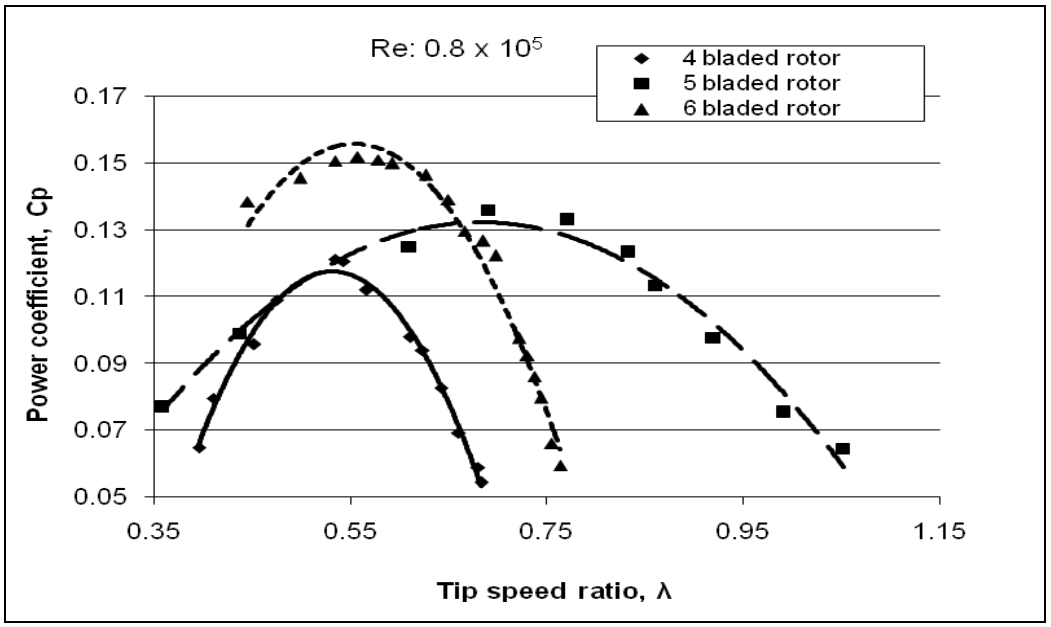

Figure 6. 2. 20: Comparison of power coefficient vs. tip speed ratio of 4, 5, and 6 Bladed Vane Type Rotor at Reynolds number of 0.8×10^5.

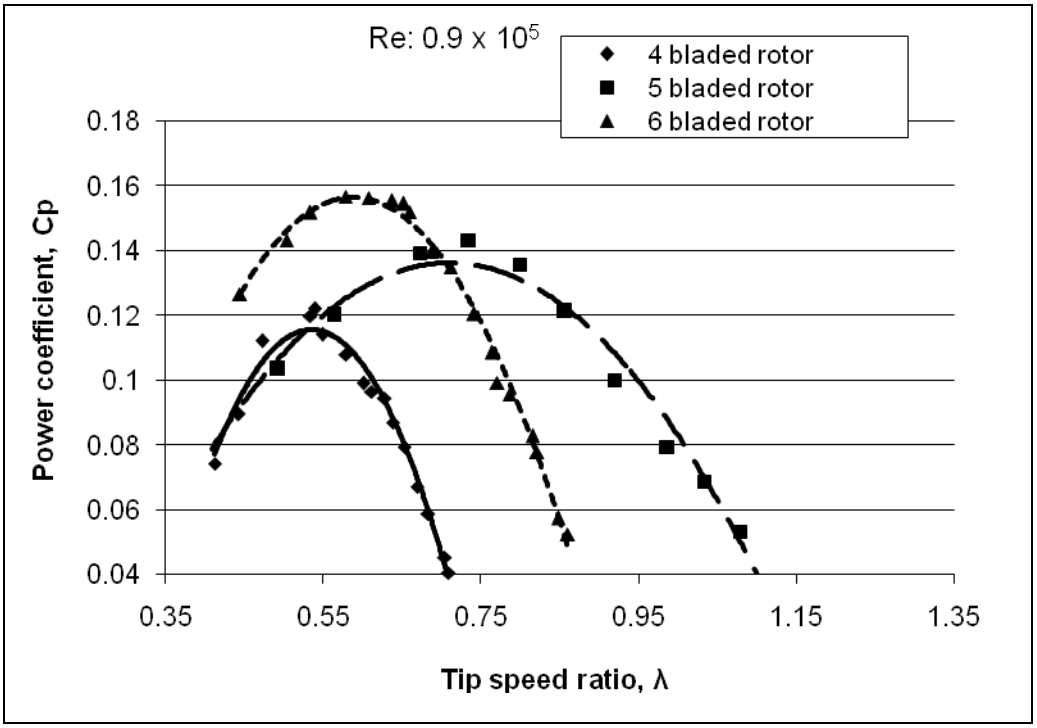

Figure 6. 2. 21: Comparison of power coefficient vs. tip speed ratio of 4, 5, and 6 Bladed Vane Type Rotor at Reynolds number of 0.9 x 10^5.

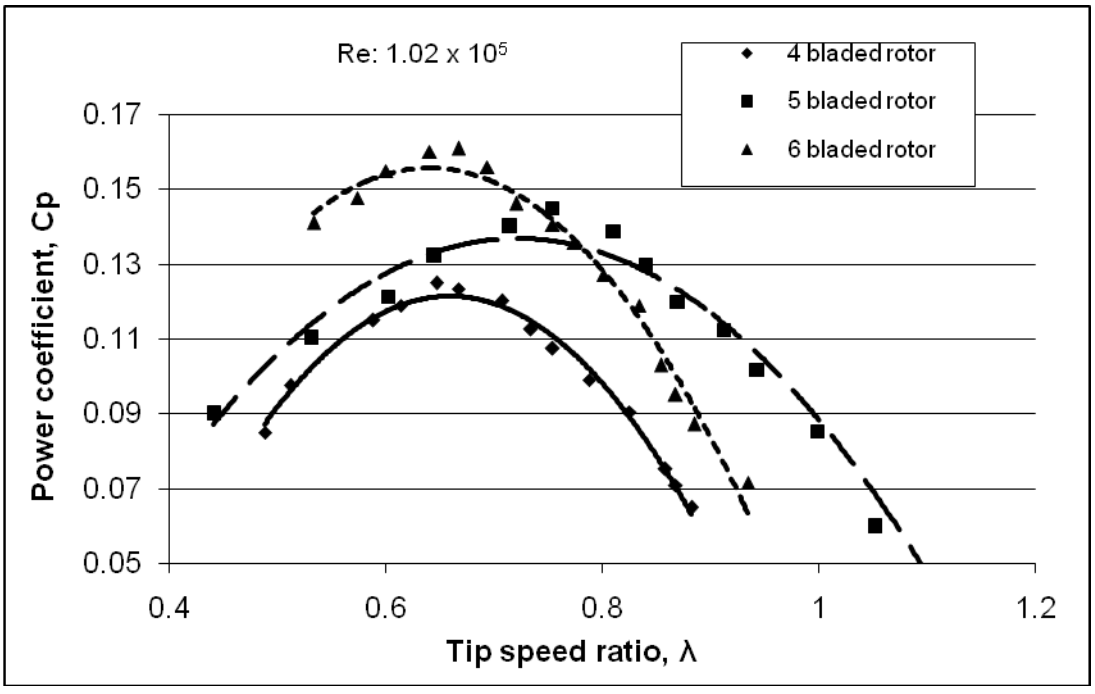

Figure 6. 2. 22: Comparison of power coefficient vs. tip speed ratio of 4, 5, and 6 Bladed Vane Type Rotor at Reynolds number of 1.02 x 10^5.

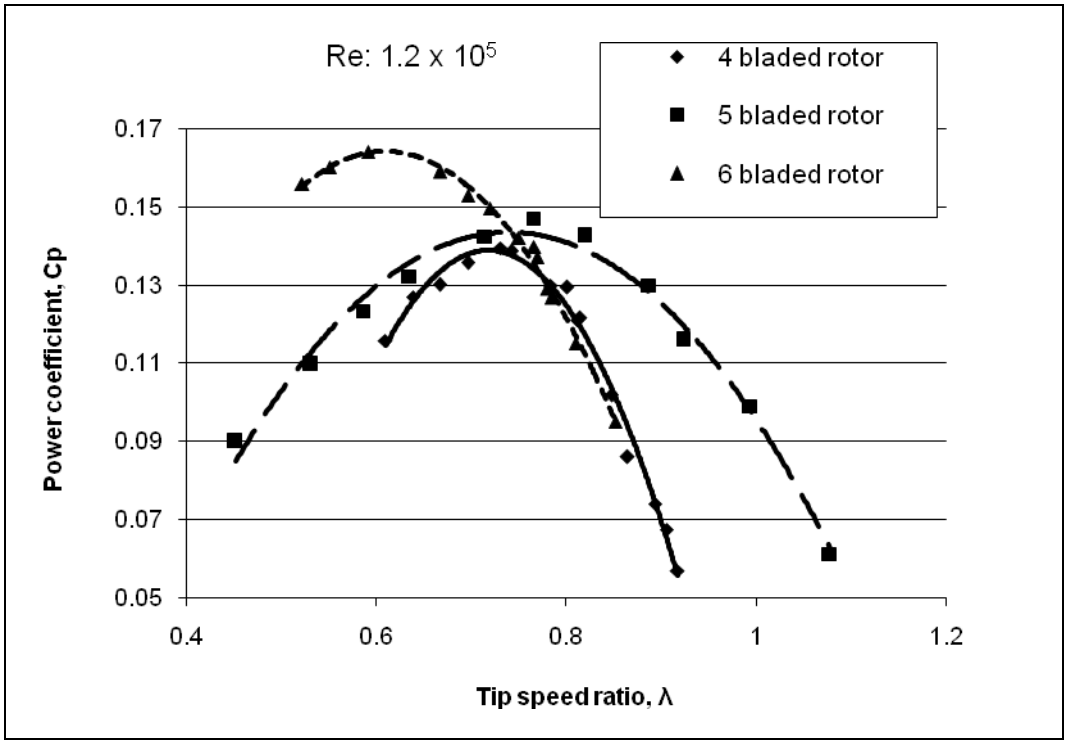

Figure 6. 2. 23: Comparison of power coefficient vs. tip speed ratio of 4, 5, and 6 Bladed Vane Type Rotor at Reynolds number of 1.2 x 10^5.

6.2.2 Torque Coefficient

6.2.2.1 Torque coefficient for Four Bladed Vane Type Rotor

The variations of results for Four Bladed Vane Type Rotor in terms of torque coefficient vs. tip speed ratio for increasing Reynolds number are shown in Figures 6. 2. 24 to 6. 2. 28 for Reynolds number of $0.6375x10^5$, $0.8x10^5$, $0.9x10^5$, $1.02x10^5$ and $1.2x10^5$ respectively.

From Figure 6. 2. 24 the value of maximum torque coefficient for four bladed rotor at Reynolds number 0.6375 x 10^5 is found as 0.259 at tip speed ratio 0.39. As the load is increased step by step rotor r.p.m. and tip speed ratio is decreased. However, the value of torque coefficient increases accordingly. So, for any particular Reynolds number the highest value of torque coefficient can be found at the lowest value of tip speed ratio. From Figure 6. 2. 25, at Reynolds number 0.8 x 10^5 maximum torque coefficient is recorded as 0.23 at tip speed ratio of 0.475. It seems that the maximum torque coefficient is affected by changing the Reynolds number. Increase in Reynolds number decreases the value of torque coefficient slightly, i.e. increase in Reynolds number make the nature of torque coefficient vs. tip speed ratio curve slightly blunt. For Reynolds number $0.9x10^5$, $1.02x10^5$ and $1.2x10^5$ same repetition is observed and the maximum torque coefficients

are recorded as 0.21, 0.195 and 0.191 at tip speed ratio of 0.53, 0.55 and 0.64 respectively.

In Figure 6. 2. 29 the torque coefficient vs. tip speed ratio has been presented at different Reynolds number for 4 Bladed Vane Type Rotor. From this graph, it is observed that for higher values of Reynolds number the maximum value of torque coefficient is lower and it is shifted towards the higher values of tip speed ratio. It is also apparent that the maximum value of torque coefficient is decreased by 35.6% as the Reynolds number is increased from 0.6375 x 10^5 to 1.2 x 10^5.

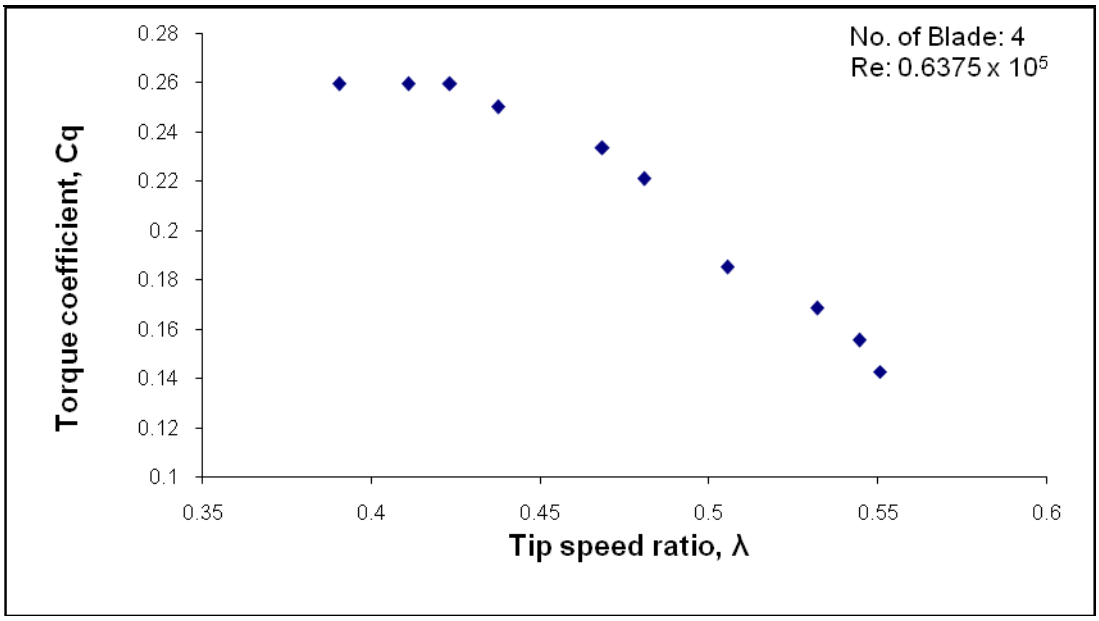

Figure 6. 2. 24: Variation of torque coefficient vs. tip speed ratio at Reynolds number of 0.6375x10^5 for Four Bladed Vane Type Rotor.

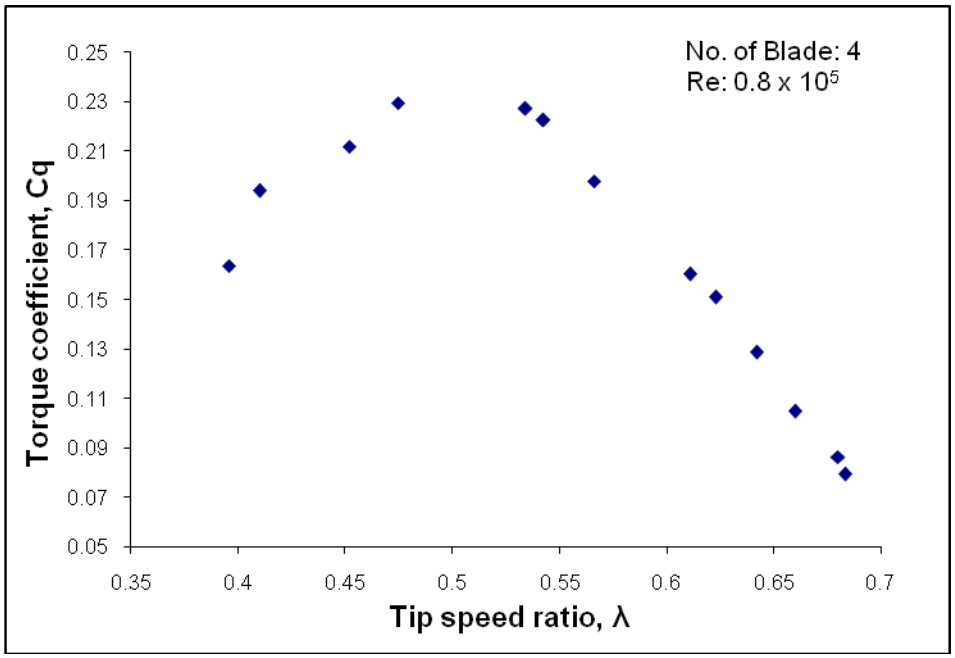

Figure 6. 2. 25: Variation of torque coefficient vs. tip speed ratio at Reynolds number of 0.8 x 10^5 for Four Bladed Vane Type Rotor.

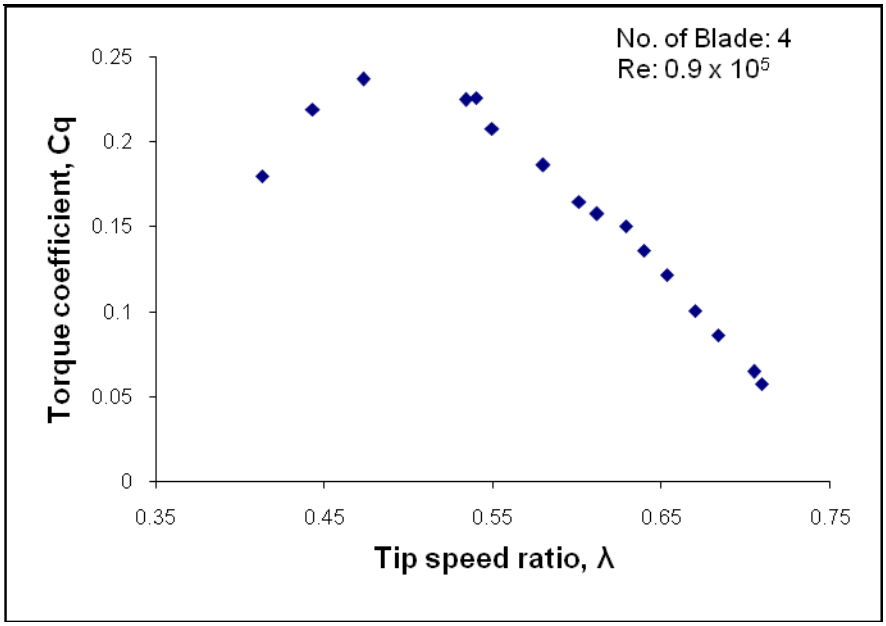

Figure 6. 2. 26: Variation of torque coefficient vs. tip speed ratio at Reynolds number of 0.9 x 10^5 for Four Bladed Vane Type Rotor.

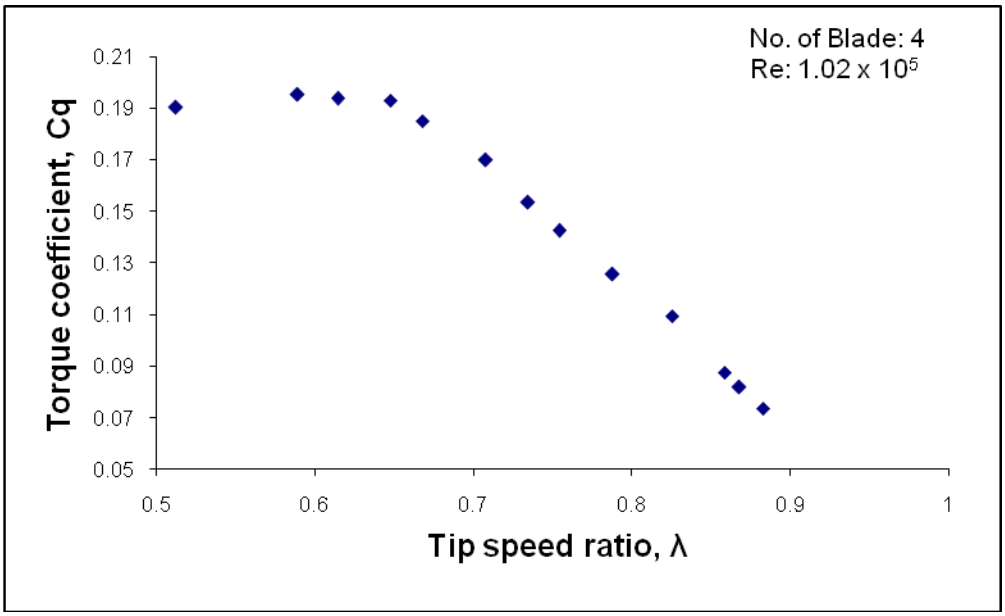

Figure 6. 2. 27: Variation of torque coefficient vs. tip speed ratio at Reynolds number of 1.02 x 10^5 for Four Bladed Vane Type Rotor.

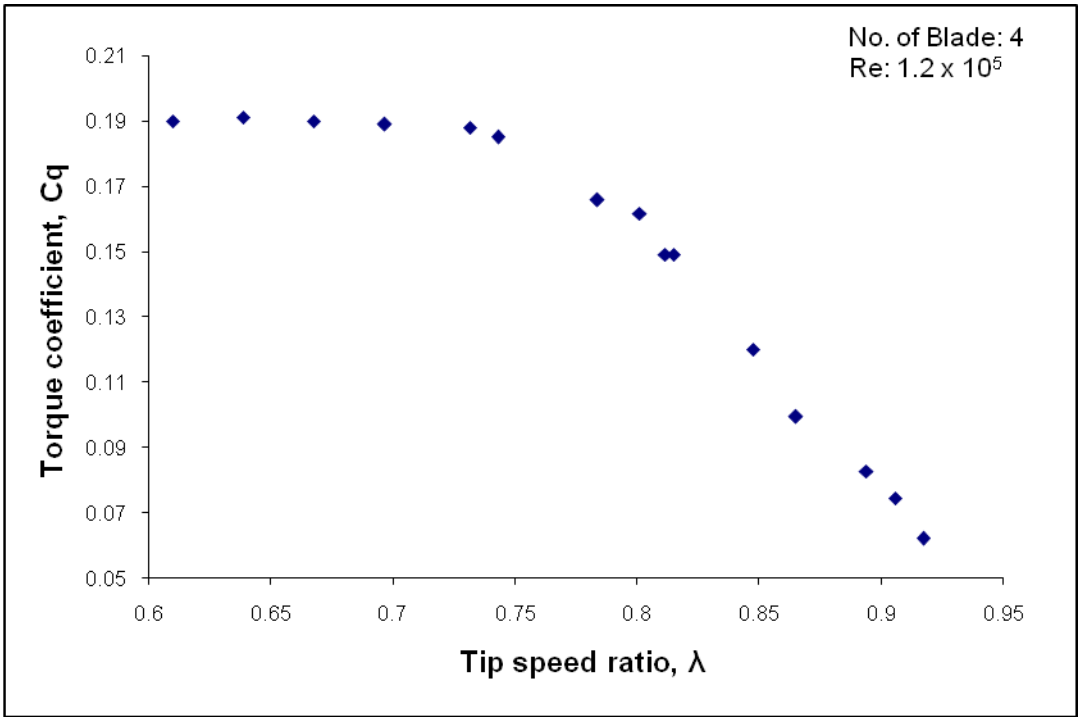

Figure 6. 2. 28: Variation of torque coefficient vs. tip speed ratio at Reynolds number of 1.2 x 10^5 for Four Bladed Vane Type Rotor.

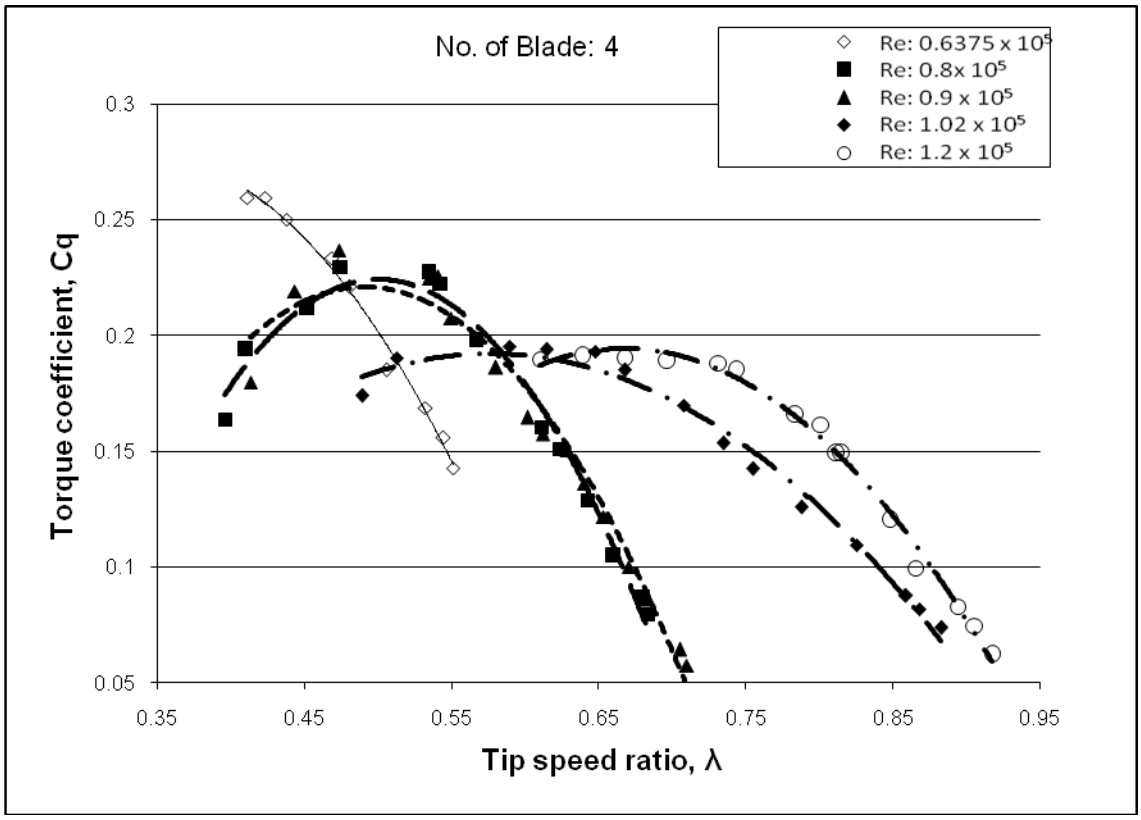

Figure 6. 2. 29: Comparison of torque coefficient vs. tip speed ratio for Four Bladed Vane Type Rotor at different Reynolds number.

6.2.2.2 Torque coefficient for Five Bladed Vane Type Rotor

The variations in results for increasing Reynolds number for Five Bladed Vane Type Rotor in terms of torque coefficient vs. tip speed ratio are shown in Figures 6. 2. 30 to 6. 2. 34 for Reynolds number of $0.6375x10^5$, $0.8x10^5$, $0.9x10^5$, $1.02x10^5$ and $1.2x10^5$ respectively.

From Figure 6. 2. 30, at Reynolds number 0.6375×10^5 the value of maximum torque coefficient is found as 0.28 at tip speed ratio 0.35. At Reynolds number 0.8×10^5 ,in Figure 6. 2. 31 the value of maximum torque coefficient is recorded as 0.27 at tip speed ratio 0.36. Just as four bladed rotor, the value of maximum torque coefficient is also affected by changing the Reynolds number for five bladed rotor. From these two curves it is found that for comparatively higher Reynolds number the value of maximum torque coefficient is lower. So, also for five bladed rotor it can be said that increase in Reynolds number make the nature of torque coefficient vs. tip speed ratio curve slightly blunt. For Reynolds number of $0.9x10^5$, $1.02x10^5$ and $1.2x10^5$ maximum torque coefficients are recorded as 0.26, 0.24 and 0.23 at tip speed ratio of 0.41, 0.44 and 0.48 respectively.

In Figure 6. 2. 35 the torque coefficient vs. tip speed ratio has been presented at different Reynolds number for Five Bladed Vane Type Rotor. From this graph it is once again apparent that for higher Reynolds number the value of maximum torque coefficient is lower and it is shifted towards the higher values of tip speed ratio. Here the value of maximum torque coefficient is decreased by 21.74% as the Reynolds number increases from 0.6375 x 10^5 to 1.2 x 10^5.

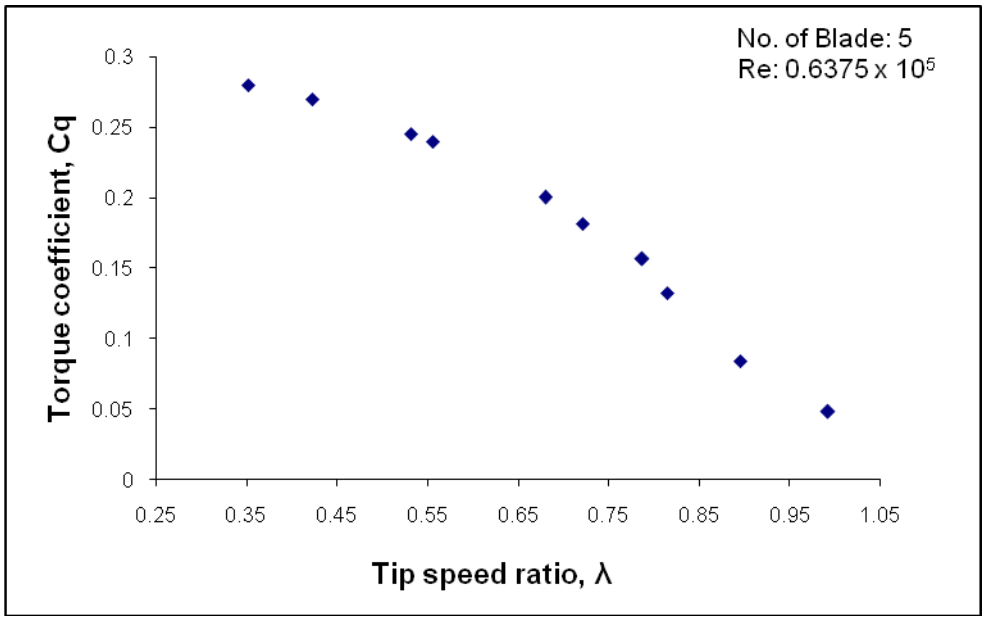

Figure 6. 2. 30: Variation of torque coefficient vs. tip speed ratio at Reynolds number of 0.6375 x 10^5 for Five Bladed Vane Type Rotor.

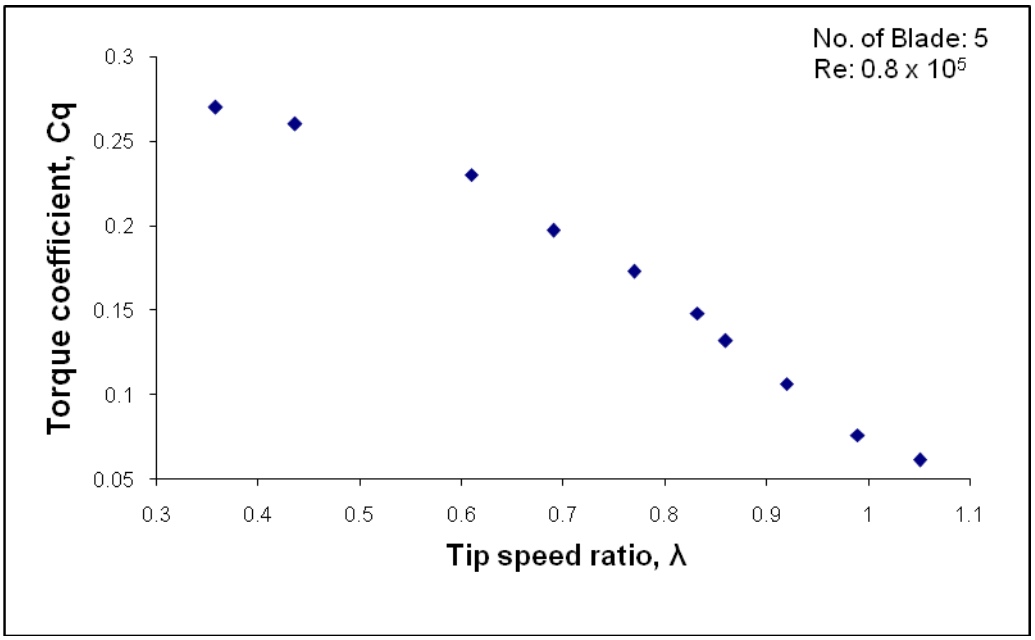

Figure 6. 2. 31: Variation of torque coefficient vs. tip speed ratio at Reynolds number of 0.8 x 10^5 for Five Bladed Vane Type Rotor.

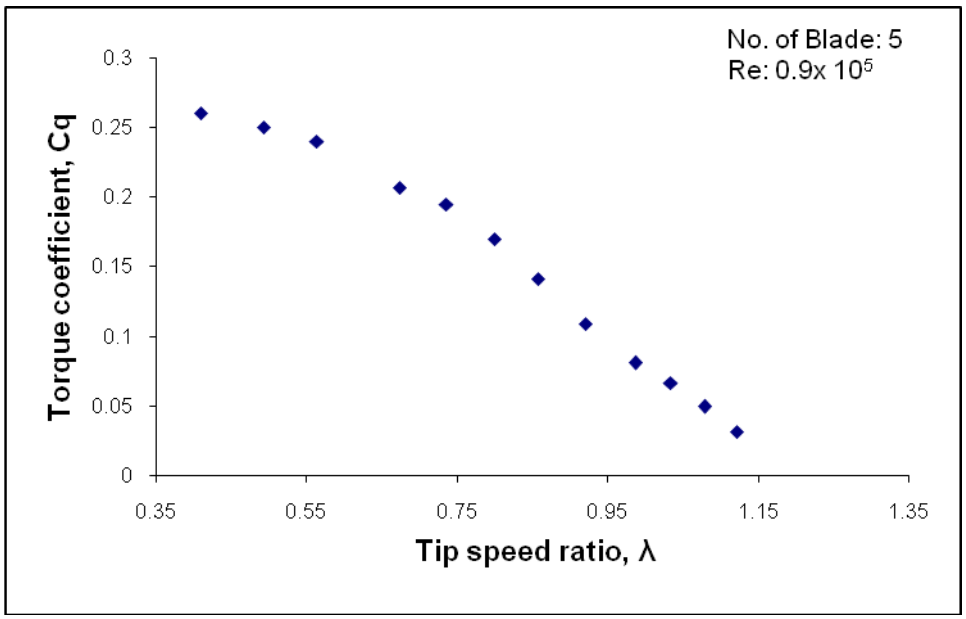

Figure 6. 2. 32: Variation of torque coefficient vs. tip speed ratio at Reynolds number of 0.9 x 10^5 for Five Bladed Vane Type Rotor

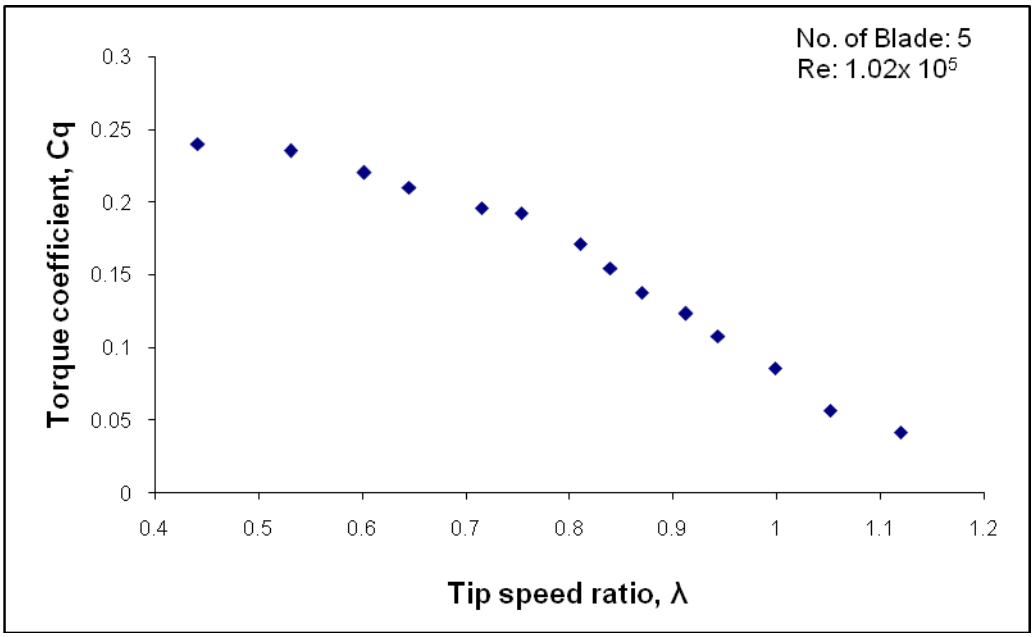

Figure 6. 2. 33: Variation of torque coefficient vs. tip speed ratio at Reynolds number of 1.02 x 10^5 for Five Bladed Vane Type Rotor

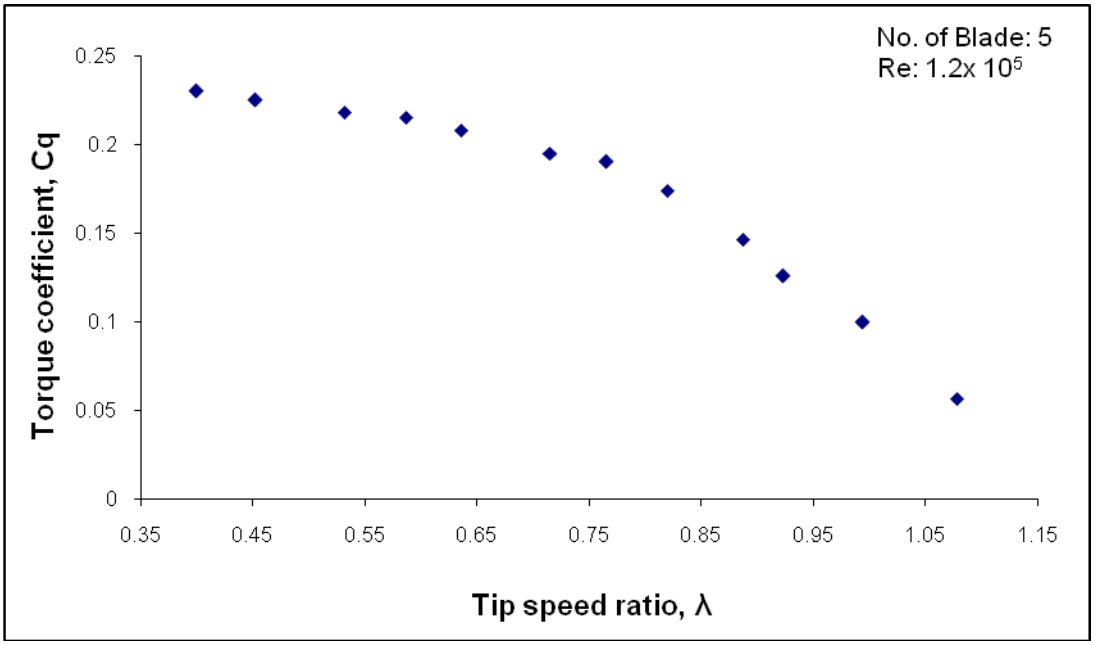

Figure 6. 2. 34: Variation of torque coefficient vs. tip speed ratio at Reynolds number of 1.2 x 10^5 for Five Bladed Vane Type Rotor

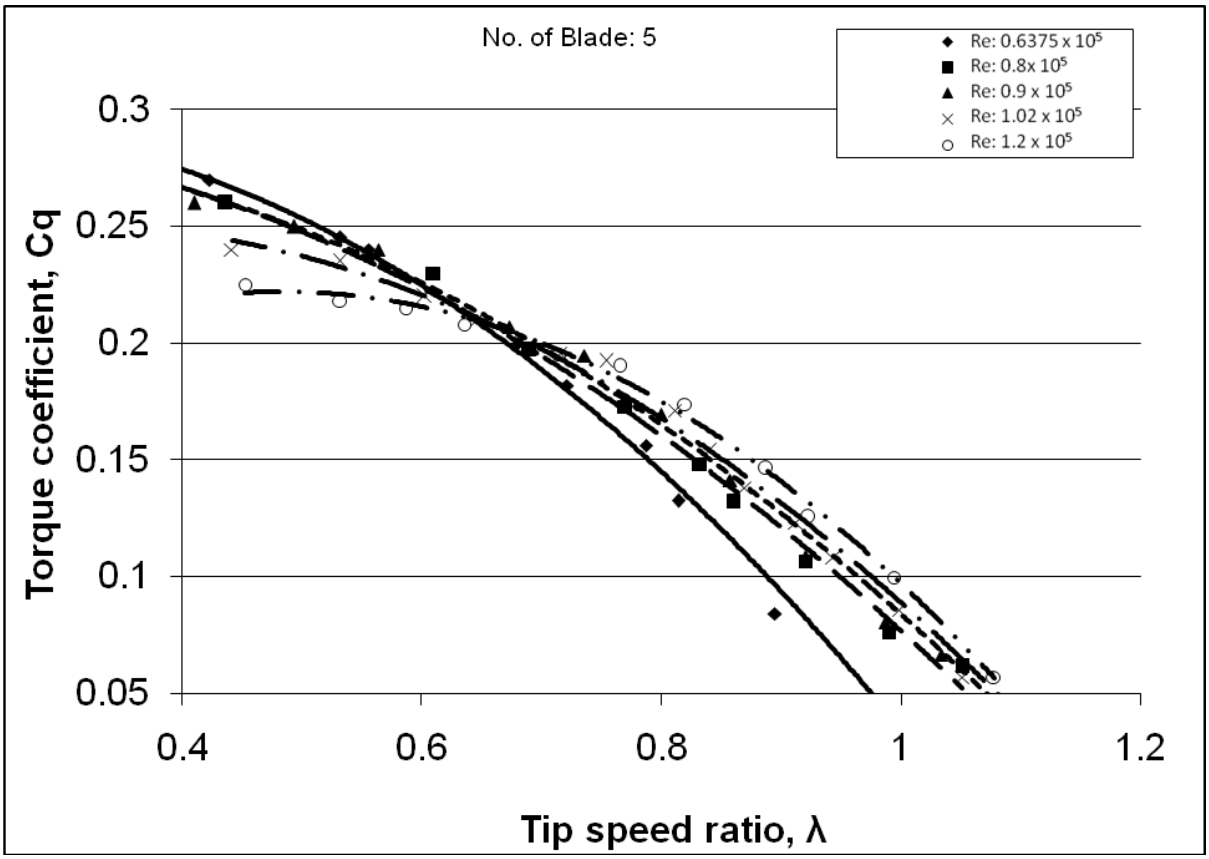

Figure 6. 2. 35: Comparisons of torque coefficient vs. tip speed ratio for Five Bladed Vane Type Rotor at different Reynolds number.

6.2.2.3 Torque coefficient for Six Bladed Vane Type Rotor

The variations of results for increasing Reynolds number for Six Bladed Vane Type Rotor in terms of torque coefficient vs. tip speed ratio are presented in Figures 6. 2. 36 to 6. 2. 40 for the Reynolds number of 0.6375 x 10^5, 0.8 x 10^5, 0.9 x 10^5, 1.02 x 10^5 and 1.2 x 10^5 respectively.

From Figure 6. 2. 36, it is observed that at Reynolds number 0.6375 x 10^5 maximum value of torque coefficient is recorded as 0.3 at tip speed ratio 0.4. Just as four and five bladed rotors, in case of six bladed rotor the same observation is found i.e. with the decrease in tip speed ratio the value of torque coefficient increases. As a result, for any particular Reynolds number at the lowest value of tip speed ratio highest value of torque coefficient is found. At Reynolds number 0.8 x 10^5, the value of maximum torque coefficient is found 0.295 at tip speed ratio 0.445. From these two curves it is seen that the torque coefficient is lower for higher values of Reynolds number. That means the increase in Reynolds number make the nature of torque coefficient vs. tip speed ratio curve slightly blunt. For Reynolds number 0.9 x 10^5, 1.02 x 10^5 and 1.2 x 10^5 the same

event is repeated. At Reynolds number 0.9 x 10^5, 1.02 x 10^5 and 1.2 x 10^5 the value of maximum torque coefficients are recorded as 0.284, 0.264 and 0.255 at tip speed ratio 0.5, 0.53 and 0.54 respectively.

Figure 6. 2. 41 shows the comparison of torque coefficient vs. tip speed ratio for six bladed rotor at different Reynolds number. From this graph, again it is apparent that for comparatively higher values of Reynolds number the maximum value of torque coefficient is comparatively lower and it is shifted towards the higher values of tip speed ratio. Here the value of torque coefficient is decreased by 17.65% as the Reynolds number increases from 0.6375 x 10^5 to 1.2 x 10^5.

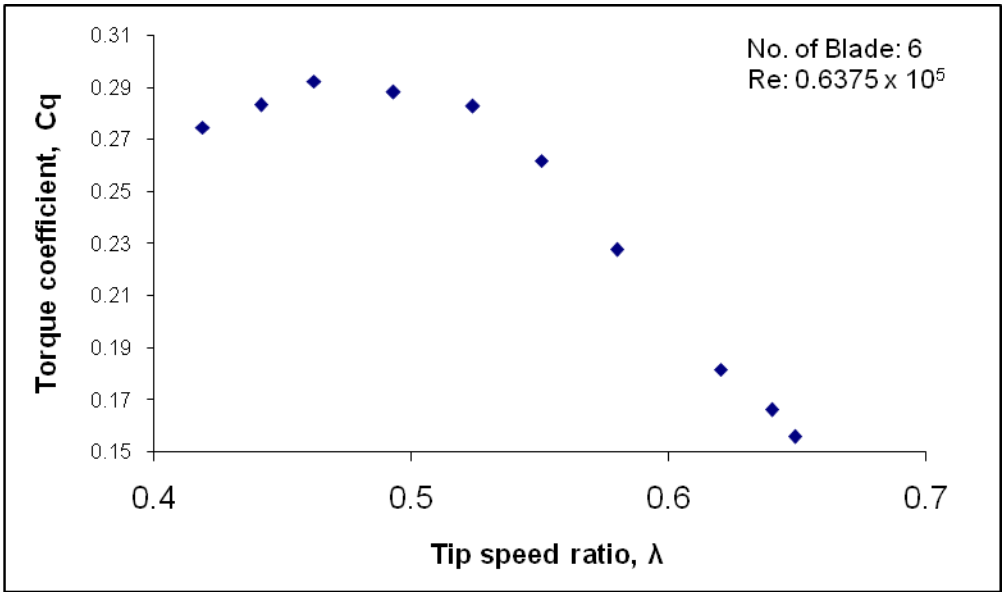

Figure 6. 2. 36: Variation of torque coefficient vs. tip speed ratio at Reynolds number of 0.6375 x 10^5 for Six Bladed Vane Type Rotor.

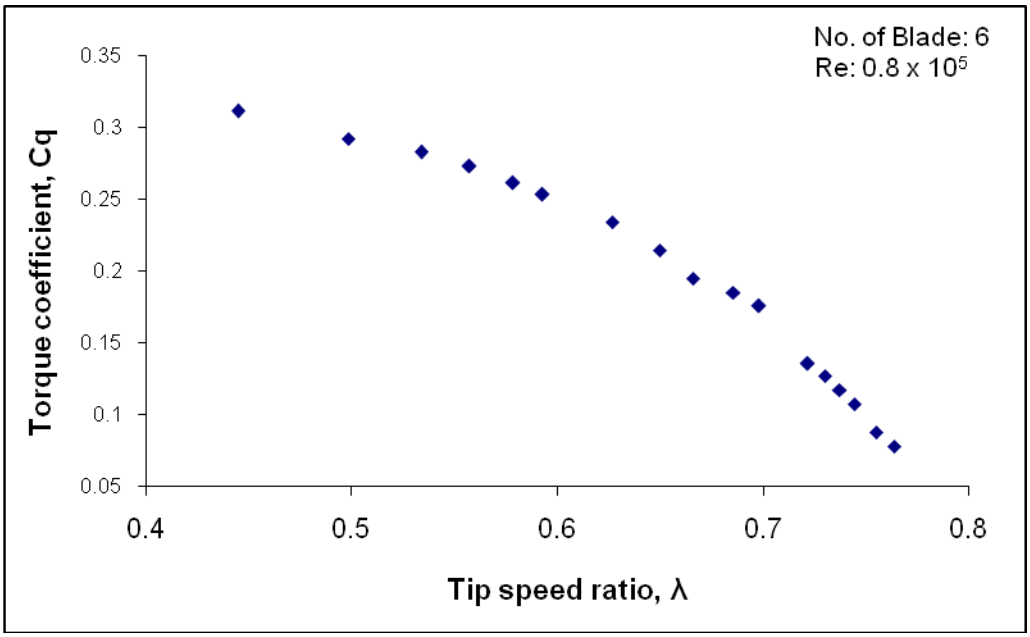

Figure 6. 2. 37: Variation of torque coefficient vs. tip speed ratio at Reynolds number of 0.8 x 10^5 for Six Bladed Vane Type Rotor.

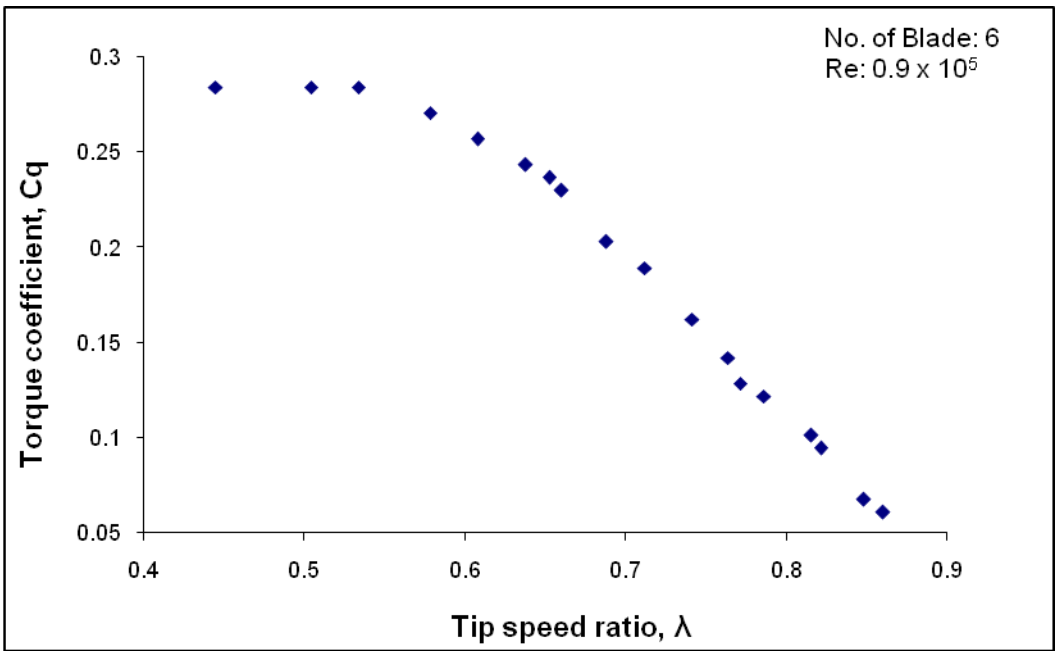

Figure 6. 2. 38: Variation of torque coefficient vs. tip speed ratio at Reynolds number of 0.9x10^5 for Six Bladed Vane Type Rotor

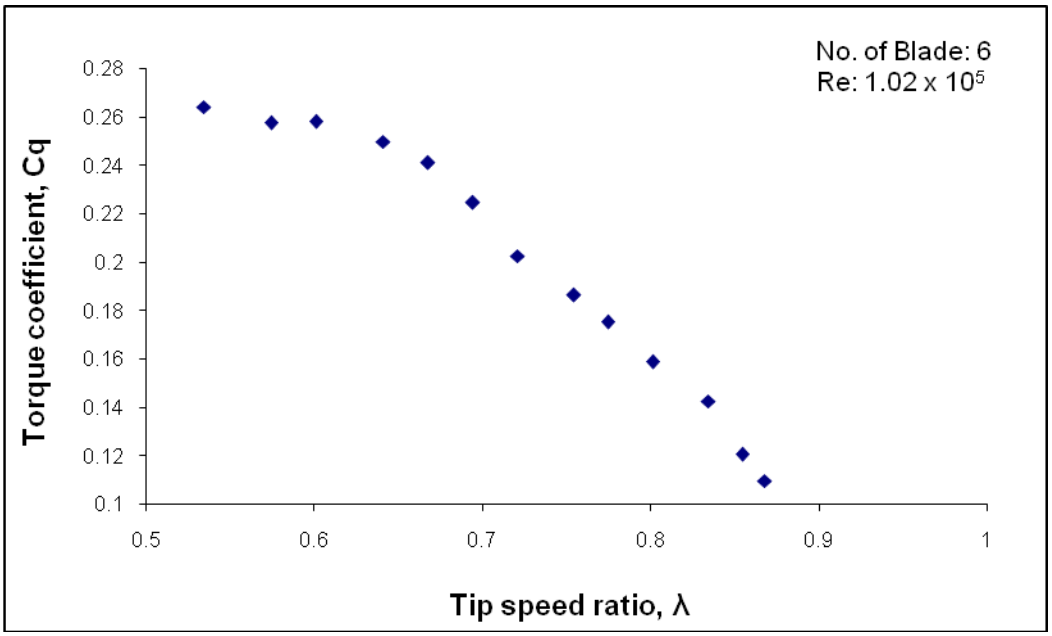

Figure 6. 2. 39: Variation of torque coefficient vs. tip speed ratio at Reynolds number of 1.02 x 10^5 for Six Bladed Vane Type Rotor.

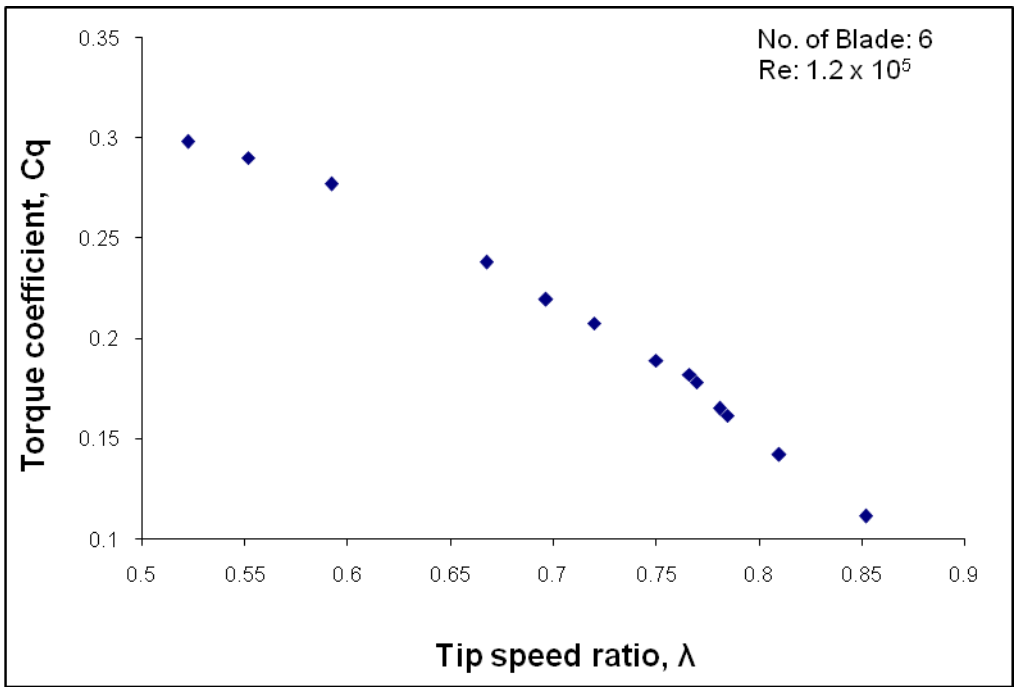

Figure 6. 2. 40: Variation of torque coefficient vs. tip speed ratio at Reynolds number of 1.2 x 10^5 for Six Bladed Vane Type Rotor.

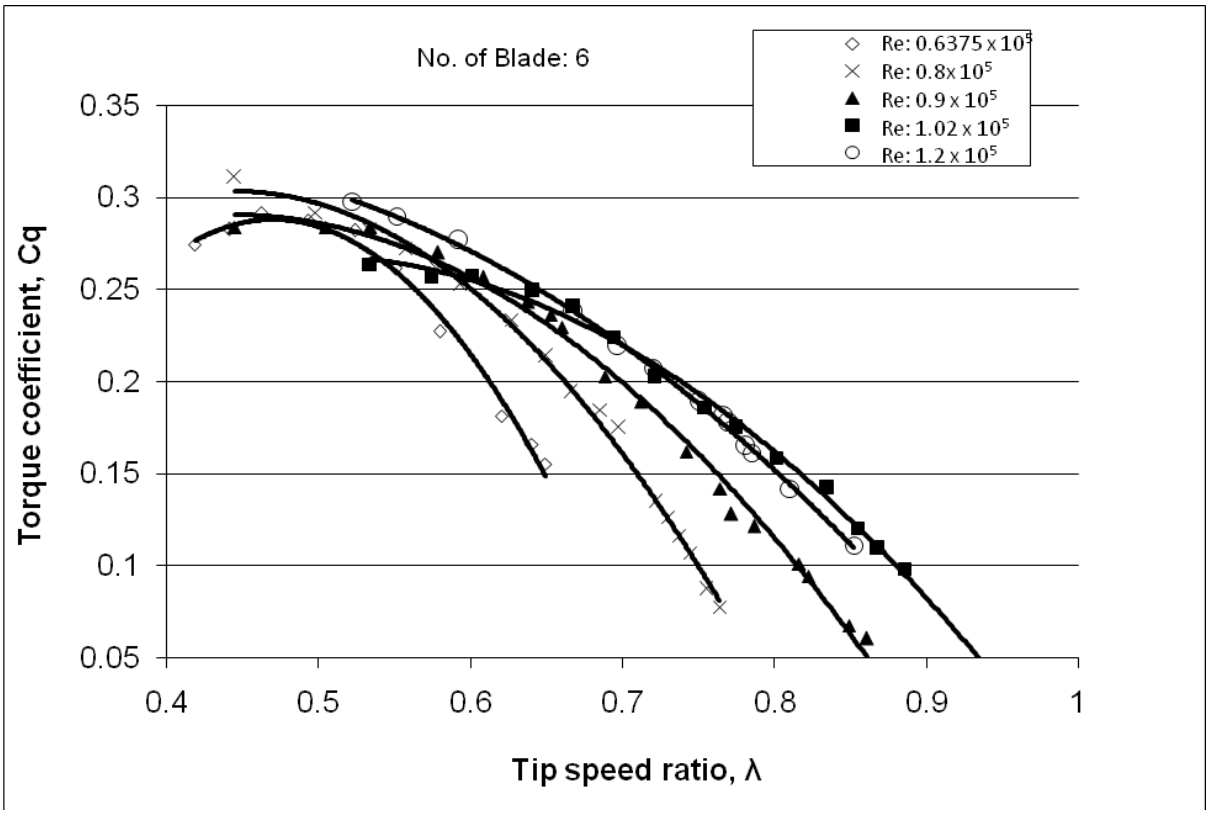

Figure 6. 2. 41: Comparison of torque coefficient vs. tip speed ratio for Six Bladed Vane Type Rotor at different Reynolds number.

6.2.2.4 Torque coefficient at different Reynolds number for 4,5 and 6 Bladed Vane Type Rotor

A comparison have been made among the curves of torque coefficient vs. tip speed ratio of four, five and six bladed rotor at a particular Reynolds number in Figures 6. 2. 42 to 6. 2. 46. From Figure 6. 2. 42 it is observed that the value of maximum torque coefficient at Reynolds number 0.6375×10^5 is 0.26 occurs at tip speed ratio 0.39 whereas for 5 and 6 bladed rotor the maximum torque coefficients are recorded as 0.28 and 0.3 at tip speed ratios of 0.35 and 0.4 respectively for the same Reynolds number. From this graph, it is clear that rotor with higher number of blades have higher value of maximum torque coefficient and it is shifted towards the lower values of tip speed ratio. Here it is also found that the maximum value of torque coefficient increases by 15.8% as the number of blades increases from four to six at Reynolds number 0.6375×10^5. That is, the increases in number of blades make the nature of torque coefficient versus tip speed ratio curve sharper.

In Figures 6. 2. 43 to 6. 2. 46 the same phenomena is repeated. At Reynolds number 0.8 x 10^5 , the maximum value of torque coefficients are recorded as 0.229, 0.27 and 0.295 for 4, 5 and 6 bladed rotors, at tip speed ratio of 0.475, 0.36 and 0.445 respectively. It is seen that the value of maximum torque coefficient is increased by 28.8% as the number of blades increase from four to six at Reynolds number 0.8 x 10^5. At Reynolds number of 0.9 x 10^5 the maximum value of torque coefficients are recorded as 0.226, 0.26 and 0.284 at tip speed ratios of 0.54, 0.41 and 0.5 respectively, which indicate that the value of maximum torque coefficient increases by 25.7% as the number of blades increases from four to six at the Reynolds number of 0.9 x 10^5. At Reynolds number of 1.02 x 10^5, the values of maximum torque coefficients are recorded as 0.193, 0.24 and 0.264 at tip speed ratio of 0.65, 0.44 and 0.53 respectively. It indicates that the value of maximum torque coefficient is increased by 36.8% as the number of blades increase from four to six at Reynolds number 1.02 x 10^5. At Reynolds number of 1.2 x 10^5 the values of maximum torque coefficients are recorded as 0.191, 0.23 and 0.255 at tip speed ratio of 0.64, 0.4 and 0.52 respectively. It indicates that the value of maximum power coefficient is increased by 33.5% as the number of blades increase from four to six at Reynolds number 1.2 x 10^5.

So, it can be concluded that, the value of maximum torque coefficient becomes higher for higher bladed rotor and it is shifted towards the lower value of tip speed ratio at the same Reynolds number. It is to be noted that the variation is more significant for higher Reynolds number.

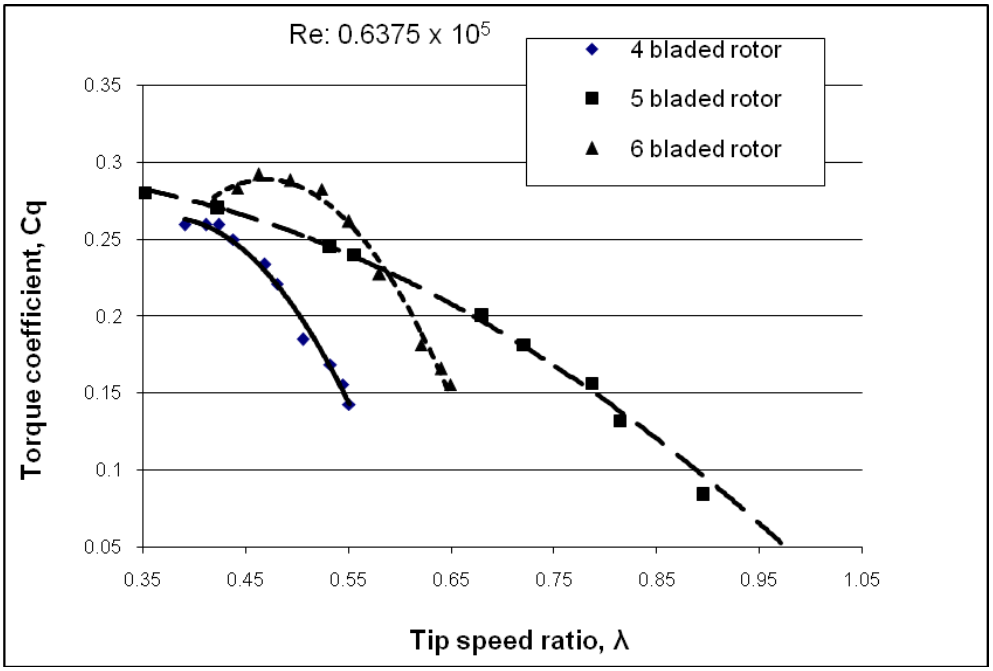

Figure 6. 2. 42: Comparison of torque coefficient vs. tip speed ratio for 4, 5 and 6 Bladed Vane Type Rotor at Reynolds number 0.6375 x 10^5.

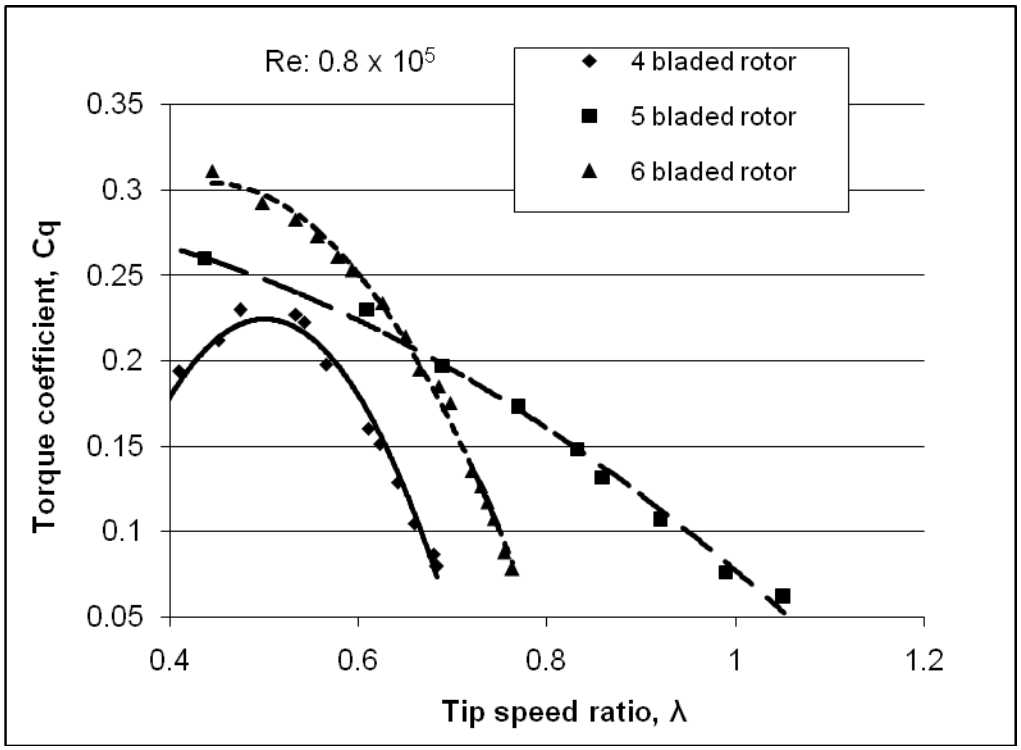

Figure 6. 2. 43: Comparison of torque coefficient vs. tip speed ratio for 4, 5 and 6 Bladed Vane Type Rotor at Reynolds number 0.8 x 10^5.

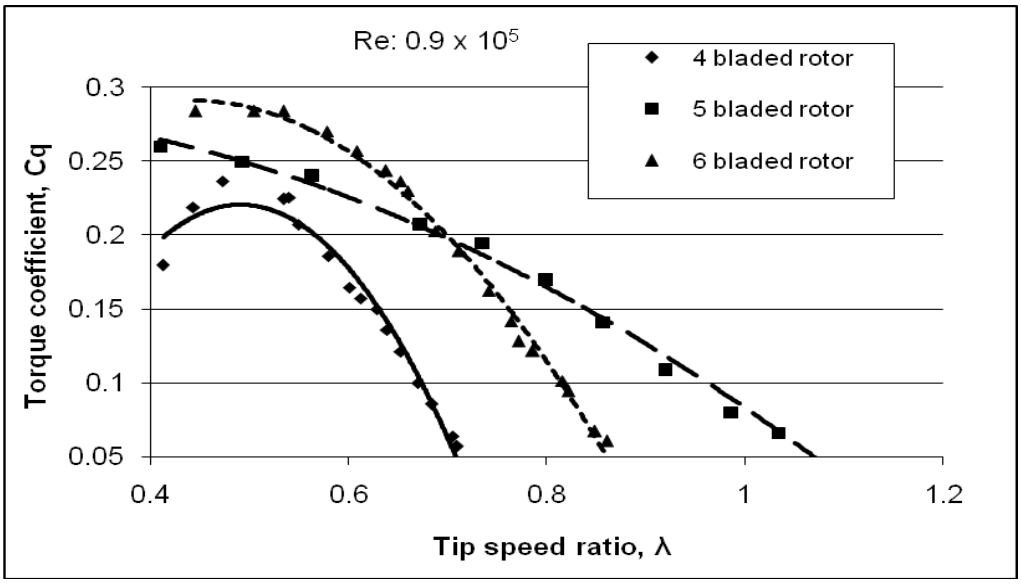

Figure 6. 2. 44: Comparison of torque coefficient vs. tip speed ratio for 4, 5 and 6 Bladed Vane Type Rotor at Reynolds number 0.9 x 10^5.

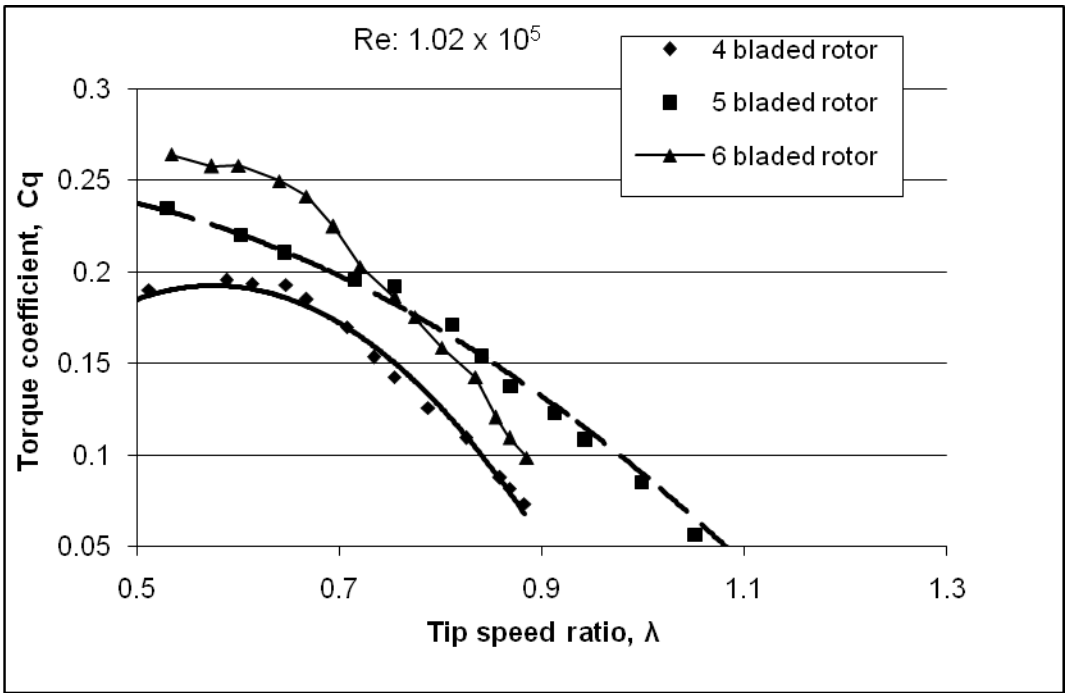

Figure 6. 2. 45: Comparison of torque coefficient vs. tip speed ratio for 4, 5 and 6 Bladed Vane Type Rotor at Reynolds number 1.02 x 10^5.

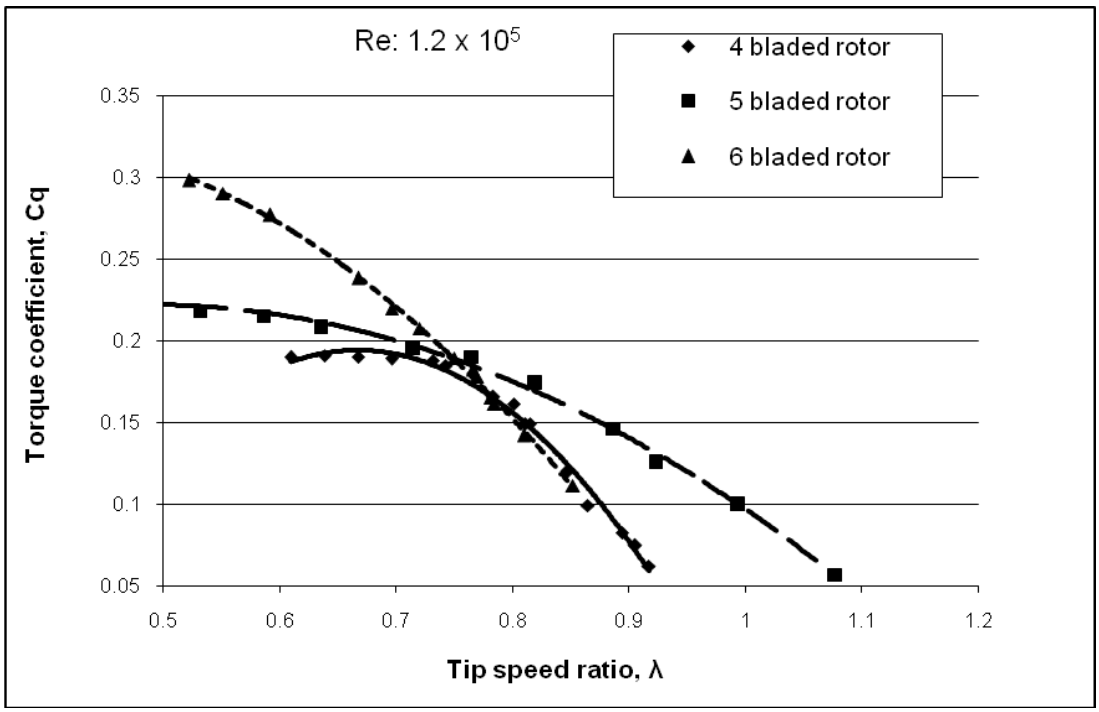

Figure 6. 2. 46: Comparison of torque coefficient vs. tip speed ratio for 4, 5 and 6 Bladed Vane Type Rotor at Reynolds number 1.2 x 10^5.

6.3 A Comparison of Dynamic Characteristics At Static [2] and Present Dynamic Method

6.3.1 Power Coefficient:

A comparison of the experimental results of power coefficients of wind turbines having four, five and six bladed rotors and that of the predicted [2] are shown in Figures 6.3.1, 6.3.2 and 6.3.3 respectively. From these figures, it is observed that the predicted curve and the experimental one follow the same trend even the maximum power coefficient is almost same but there is a deviation in the tip speed ratio.

In Figure 6.3.1 a comparison of power coefficient of the static (predicted[2]) and that of the dynamic (present experimental work) for Four Bladed Vane type Rotor is presented. From this figure it is found that the nature of curve for both case is identical, the maximum value of predicted power coefficient is 0.125 at tip speed ratio 1.1 but experimentally the value of maximum power coefficient is 0.14 obtained at tip speed ratio 0.7.

Figure 6.3.2 shows a comparison of power coefficient vs. Tip speed ratio for the static (predicted[2]) and that of the dynamic (present experimental work), for Five Bladed Vane Type Rotor. Here, also the nature of curve for both cases is identical, maximum power coefficient is almost same. Dynamically the maximum power coefficient is achieved as 0.147 at tip speed ratio 0.76 while the predicted one shows the tip speed ratio as 1.15 for the power coefficient of 0.14.

In Figure 6.3.3 a comparison of power coefficient vs. Tip speed ratio for the static (predicted[2]) and that of the dynamic (present experimental work) for six bladed Vane type Rotor is shown. Here also the same trend is observed i.e the nature of curve for both cases is identical, maximum power coefficient for experimental work is 0.164 at tip speed ratio of 0.6 while the predicted value for the maximum power coefficient is 0.145 achieved at tip speed ratio of 1.2.

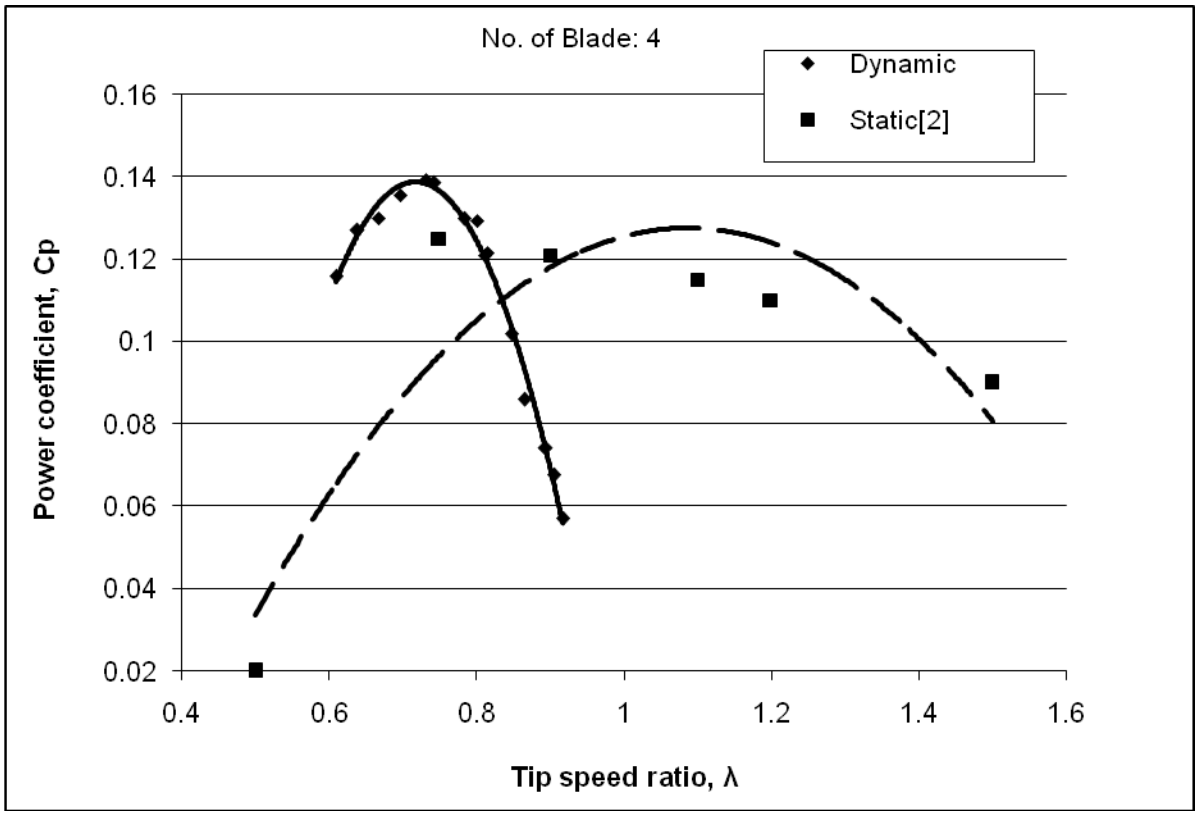

Figure 6. 3. 1: A Comparison of Power Coefficient vs. Tip Speed Ratio of static[2] and dynamic(present experimental work) for 4 Bladed Vane Type Rotor.

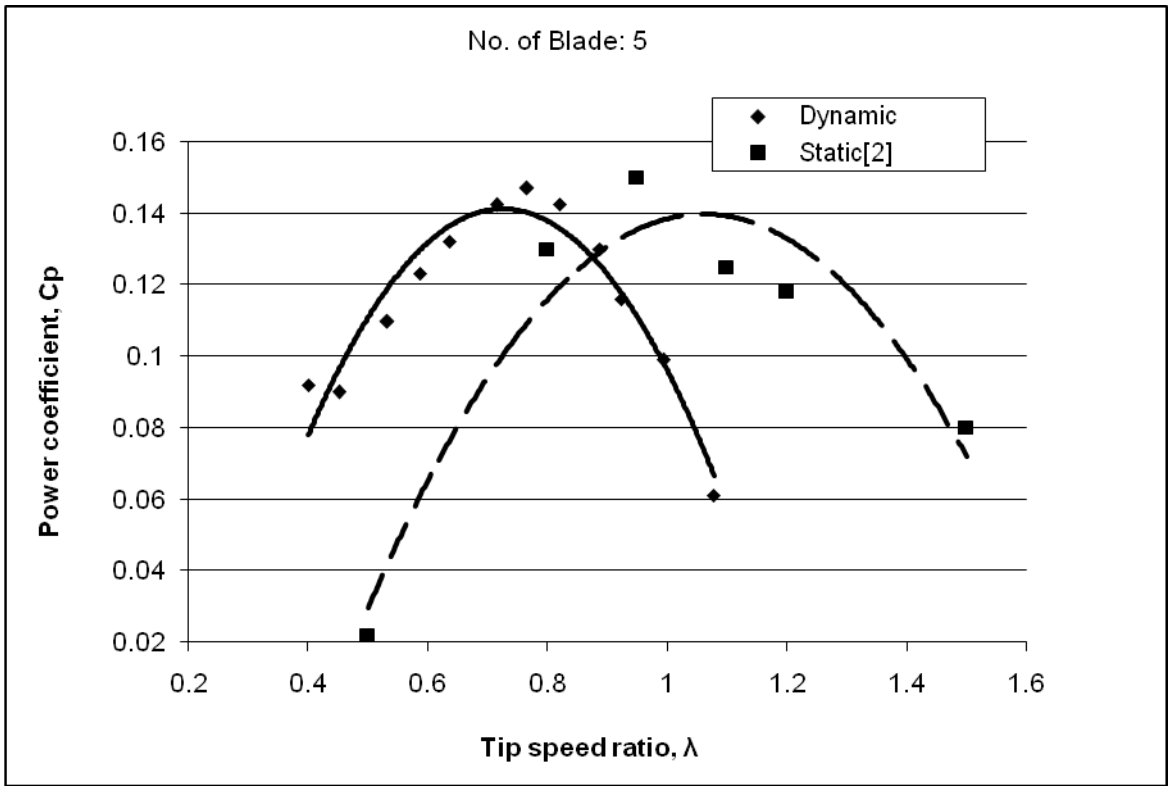

Figure 6. 3. 2: A Comparison of Power Coefficient vs. Tip Speed Ratio of static[2] and dynamic(present experimental work) for 5 Bladed Vane Type Rotor.

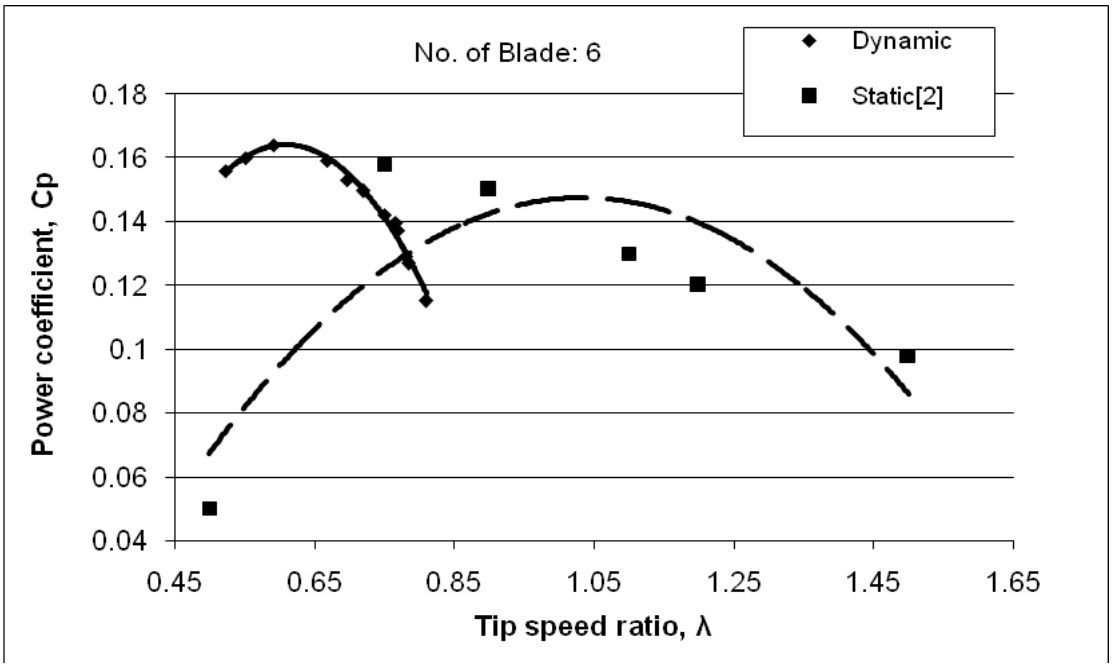

Figure 6. 3. 3: A Comparison of Power Coefficient vs. Tip Speed Ratio of static[2] and dynamic(present experimental work) for 6 Bladed Vane Type Rotor.

6.4 A Comparison among the Existing Research Works and Present Experimental Results

The power coefficients for different tip speed ratios are shown in Figure 6. 4. 1and 6. 4. 2 along with measured data of Kamal [2], Ogawa & Yashida [3], Islam et al [4], Rahman [5] and Bhuiyan [6]. Kamal worked with the same rotor of present work. Ogawa & Yashida [3] and Islam et al [4] both researchers worked with two bladed Savonius rotor. Rahman [5] studied three bladed Savonius rotor and Bhuiyan [6] experimented and analyzed aerodynamic characteristics of four bladed Savonius rotor. The power coefficient obtained in the present dynamic approach matches qualitatively with the measured data, but shows a greater deviation. From the graph it is seen that there is a close correlation between the predicted results and the present experimental result. The predicted maximum power coefficient is achieved at the same overlap tip speed ratio which is 1 but experimentally it is less than 1. There is a variation in the value of maximum power coefficient also. This may because the prediction method assumes a potential vortex and does not consider the wake, however, in reality the flow field around a rotating rotor is governed by time dependent shear layers, separated flows, wake, high turbulence levels and also there is a variation in number of blades, free stream velocities, rotor swept area, shape of the blade, material of the blade etc.,

so the value of power coefficient with respect to tip speed ratio deviates in magnitudes. Yet the nature of curves for all the figures is identical.

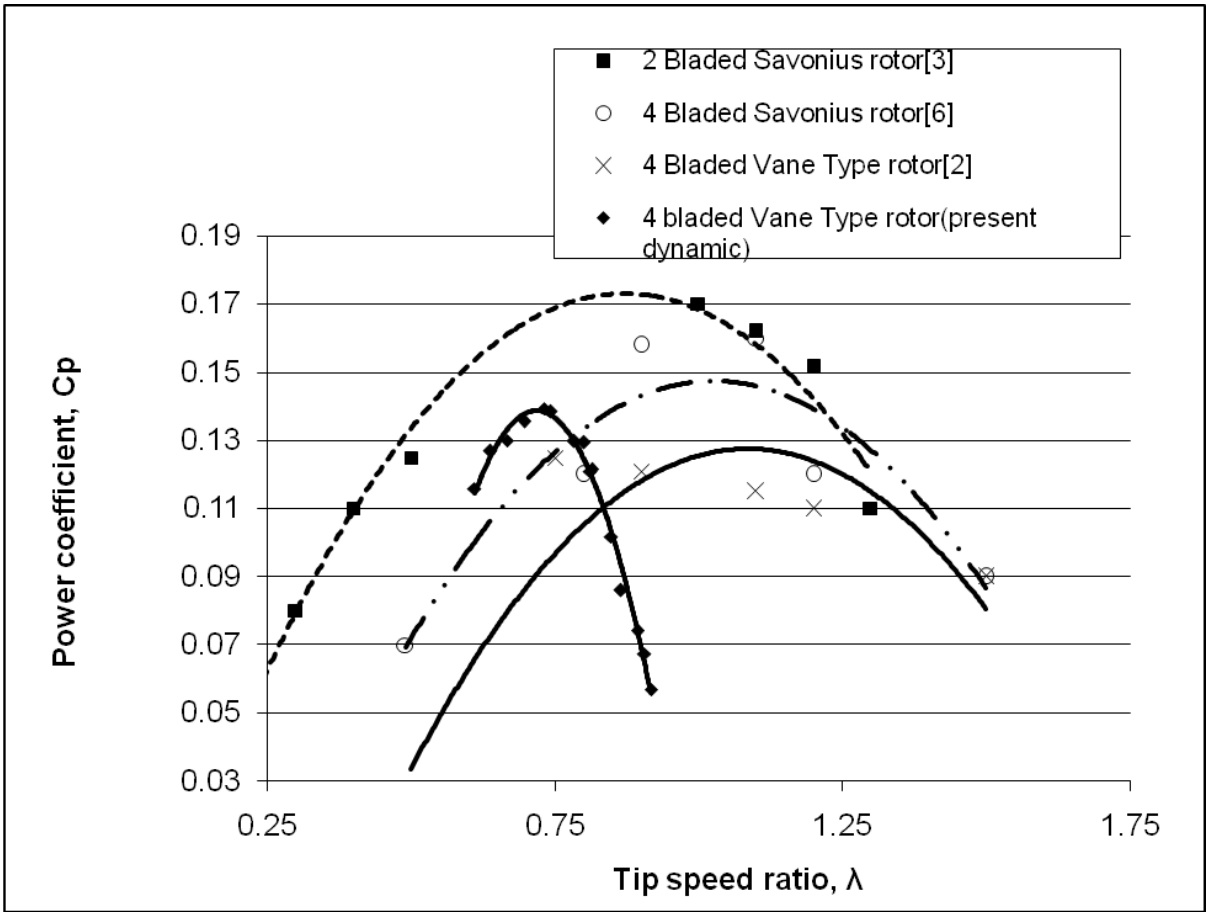

Figure 6. 4. 1: A Comparison of Power Coefficient vs. Tip Speed Ratio between Savonius rotor and Vane Type rotor.

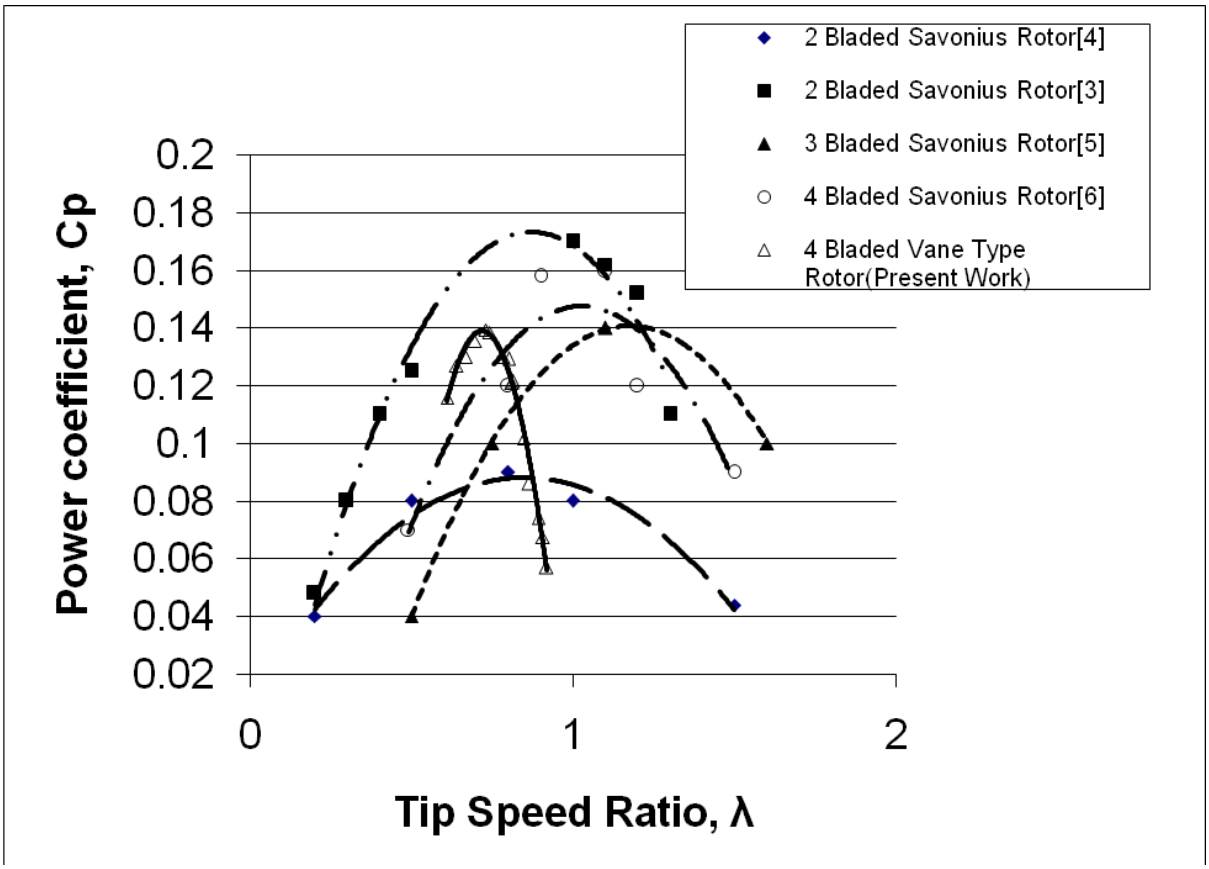

Figure 6. 4. 2: A Comparison of Power Coefficient vs. Tip Speed Ratio for different Bladed Savonius Rotor and 4 Bladed Vane Type of Rotor.

7 CONCLUSIONS AND RECOMMENDATIONS

7.1 Introduction

This chapter presents the conclusions drawn from the experimental investigation of flow over the four, five and six bladed vertical axis vane type rotor.The scope of extension and development of the present study are also included in this chapter.

7.2 Conclusions

The present study concerns with the dynamic conditions of Multi-bladed Vane Type rotor at different Reynolds number. For the purpose of analyzing the dynamic conditions of rotor, the rpm of multi-bladed rotor at different loading conditions and the difference in tensions between two ends of the friction belt for different Reynolds number were measured. Finally, from these data, the changes in tip Speed Ratio, power co-efficient and torque coefficient with the increase in load in the load carrying plate were determined at different Reynolds number of multi-bladed rotor. From the study, analysis and results of this research work, the following conclusions can be made:

1. For any particular bladed rotor, it is observed that the maximum power co-efficient is affected by changing the Reynolds number. For comparatively higher value of Reynolds number the value of maximum power coefficient is comparatively higher and it is shifted towards the higher value of tip speed ratio as the Reynolds number is increased. So, it can be concluded that the increase in Reynolds number make the nature of power co-efficient versus tip speed ratio curve slightly sharper.

2. For the same Reynolds number, it is observed that the maximum power co-efficient is affected by increasing the number of blades. It is seen that with the increase in number of blades the maximum value of power coefficient also increases and it is shifted towards the lower value of tip speed ratio.

3. It can be concluded from the present study that by increasing the number of blades of rotor, the power output can be increased. However, there is an optimum limit that depends on the size and shape of the blades. Simultaneously, it can be said that by increasing Reynolds number, the power output can be increased. Thus it can be concluded that by increasing the number of blades of rotor to the optimum limit considering all significant factors and at the same time by increasing its Reynolds number, the power output can be increased to its maximum level.

4. For any particular bladed rotor the maximum torque co-efficient is affected by changing the Reynolds number. At higher Reynolds number the value of maximum torque co-efficient is slightly lower. So, it can be said that the increases in Reynolds number make the nature of the torque co-efficient versus tip speed ratio curve slightly blunt.

5. At the same Reynolds number, the rotor having higher number of blades, the value of maximum torque coefficient is also higher and it is shifted towards the lower value of tip speed ratio. That means, the increases in number of blades make the nature of torque co-efficient versus tip speed ratio curve sharper. This point is very important for driving the irrigation pump especially positive displacement pump which needs higher starting torque.

6. It is seen that there is a close correlation between the values of present dynamic approach and those of existing research works. However, because of the variation in number of blades, free stream velocities, rotor swept area, shape of the blade, its thickness and material the values of torque and power coefficient with respect to tip speed ratio deviates in magnitude. Yet the nature of all curves in each figure (showing comparison among the nature of predicted dynamic aerodynamic characteristics and similar research works) is identical.

7.3 Recommendations

1. As the number of blades increase so does the value of maximum power coefficient, but the rotor having odd number of blades show a wide range of tip speed ratio, so the rotor with odd number of blades are preferable.
2. The same experiment may be done with rotors having three or seven number of blades to justify the above conclusion.
3. The experiment can be done with flow visualization technique to get a better understanding about the observation of the separation of flow.
4. Further detailed research could be conducted in this field at other Reynolds numbers.

References

[1] Ahmmed, S.(2002), "Investigation and Analysis of Wind Pumping System for Irrigation in Bangladesh", Ph.D. Thesis, Bangladesh University of Engineering and Technology, Dhaka, Bangladesh.

[2] Kamal, F. M. (2008), "Aerodynamic Characteristics of a Vertical Axis Vane Type Rotor ", M.Sc. Engg. Thesis, Dept. of Mech. Engg., BUET.

[3] Ogawa, T. and Yoshida, H. (1986), "The Effects of a Deflecting Plate and Rotor and Plates", Bull. JSME, vol. 29, pp. 2115-2121.

[4] Islam, A.K.M.S, Islam, M.Q., Mandal, A.C. and Razzaque, M.M. (1993), "Aerodynamic Characteristics of a Stationary Savonius rotor", RERIC Int. Energy Journal, Vol. 15, No. 2. pp. 125-135.

[5] Rahman,M. (2000), "Aerodynamic Characteristics of a Three Bladed Savonius Rotor",M.Sc. Engg. Thesis, Dept of Mech. Engg., BUET.

[6] Bhuiyan, H. K. (2003), "Aerodynamic Characteristics of a Four Bladed Savonius Rotor", M.Sc. Engg. Thesis, Dept of Mech. Engg., BUET.

[7] Islam, A.K.M.S, Islam, M.Q., Razzaque, M.M. and Ashraf, R. (1995), "Static Torque and Drag Characteristics of an S-shaped Savonius Rotor and Prediction of Dynamic Characteristics", Wind Engineering, Vol. 19, No. 6, U.K.

[8] Fujisawa, N. (1996), "Velocity Measurements and Numerical Calculations of Flow fields in and Around Savonius Rotors", Journal of Wind Engineering and Industrial Aerodynamics, Vol. 59, U.K.

[9] Gavalda, J.,Massons J.and Diaz, F. (1991) "Drag and Lift Coefficients of the Savonius Wind Machine", Wind Engineering, Vol. 15, No. 5, U.K.

[10] Huda, M.D., Selim, M.A., Islam, A.K., M., S. and Islam, M.Q. (1992), "The Performance of an S-shaped Savonius Rotor with a Deflecting Plate", RERIC Int. Energy Journal, Vol. 14, No. 1, Bangkok, Thailand.

[11] Lysen, E.H., Bos, H.G. and Cordes, E.H. (1978), "Savonius Rotors for Water Pumping", SWD Publication, Amersfoort, The Netherlands.

[12] Aldos, T.K. (1984), "Savonius Rotor Using Swinging Blades as an Augmentation System", Wind Engineering, Vol. 18, No. 4, U.K.

[13] Bowdin, G.J. and McAleese, S.A. (1984), "The Properties of Isolated and Coupled Savonius Rotors", Wind Engineering, Vol. 8, No. 4, pp. 271-288.

[14] Templin, R. J. (1974), "Aerodynamic Performance Theory for the NRC Vertical Vertical-Axis Wind Turbine", National Research Council of Canada, Report LTR-LA-160.

[15] Noll, R.B. and Ham, N.D. (1980), “Analytical Evaluation of the Aerodynamics Performance of a High-Reliability Vertical- Axis Wind Turbine”, Proceedings of AWEA National Conference.

[16] Wilson, R.E. and Lissaman, P.B.S. (1974), “Applied Aerodynamics of Wind Power Machines”, Oregon State University, USA.

[17] Strickland, J.H. (1975), “The Darrieus Turbine: A Performance Prediction Model Using Multiple Streamtubes, Sanida Laboratories Report”, SAND75-0431.

[18] Swamy, N.V.C. and Fritzsche, A.A., “Aerodynamic Studies on Vertical Axis Wind Turbine”, International Symposium on Wind Energy Systems, Cambridge, England, September 7-9, 1976.

[19] Paraschivoiu, I. and Delclaux, F. (1983), “Double Multiple Streamtube Model with Recent Improvements”, Journal of Energy, Vol. 7, No. 3, pp. 250-255.

[20] Paraschiviu, I., Fraunie, P. and Beguier, C. (1985), “Streamtube Expansion Effects on thr Darrieus Wind Turbine”, Journal of Propulsion, Vol. 1, No. 2, pp. 150-155.

[21] Fanucci, J.B. and Watters, R.E. (1976), “Innovative Wind Machines: The Theoretical Performance of a Vertical-Axis Wind Turbine”, Proceedings of the Vertical-Axis Wind Turbine Technology Workshop, Sandia Laboratories, SAND 76-5586, pp. 111-61-95.

[22] Holme, O. (1976), “A Contribution to the Aerodynamic Theory of the Vertical Axis Wind Turbine”, Proceedings of the International Symposium on Wind Energy Systems, Cambridge, pp. c4-55-72.

[23] Wilson, R.E. (1978), “Vortex Sheet Analysis of the Giromill”, ASME Journal of Fluid Engineering, Vol. 100, No. 3, pp. 340-342.

[24] Sawada, T., Nakamura, M. and Kamada, S. (1986), “Blade Force Measurement and Flow Visualization of Savonius Rotors”, Bulletin of JSME. Vol. 29, No.253. Tokyo, Japan.

[25] Aldos, T.K. and Obeidat, K.M. (1987), “Performance Analysis of Two Savonius Rotors Running Side by Side Using The Discrete Vortex method”, Wind Engineering, Vol. 11, No. 5.

[26] Jones, C. N., Littler, R.D. and Manser, B.L. (1979), “The Savonius Rotor Performance and Flow”, 1st BWEA Workshop.

[27] Sivasegaram, S. and Sivapalan, S. (1983), “Augmentation of Power in Slow Running Vertical-Axis Wind Rotors Using Multiple Vanes”, Wind Engineering, Vol. 7, No. 1.

[28] Newman, B.G. (1974), “Measurements on a Savonius Rotor with a Variable Gap”, Proc. Symposium on Wind Energy: Achievements and Potential, Sherbrooke, Canada.

[29] Lysen, E. H. (1983), “Introduction to Wind Energy”, Steering Committee of Wind Energy for Developing Countries, P.O. Box 85, Amersfoort, The Netherlands.

[30] Wilson, R.E. and Walker, S.N. (1981), “Performance Analysis Program for propeller Type Wind Turbines”, Oregon State University, March, USA.

[31] Sivasegaram, S. (1977), “Design Parameters Affecting the performance of Resistance Type Rotors”, Wind Engineering, Vol. 1, pp. 207-217.

[32] Beurskens, H.J.M. (1980), “Low Speed Water Pumping Wind Mills: Rotor Tests and Overall Performance”, Proc. Of 3rd Int. Symp. on Wind Energy Systems, Copenhagen, Denmark.

[33] Islam, M.Q., Hasan, M.N. and Saha, S.(2005), “Experimental Investigation of Aerodynamic Characteristics of Two, Three and Four Bladed S-Shaped Stationary Savonius Rotors” Proceedings of the International Conference on Mechanical Engineering (ICME05-FL-23), Dhaka-1000.

[34] Saha, U.K. and Rajkumar, M.J.(2005), “On the performance analysis of Savonius rotor with twisted blades” Department of Mechanical Engineering, Indian Institute of Technology Guwahati, Guwahati-781 039.

[35] Kamal, F.M. and Islam, M.Q.(2008), “Aerodynamic Characteristics of a Stationary Five Bladed Vertical Axis Vane Type Wind Turbine”, Journal of Mechanical Engineering, Vol. ME39, No. 2, IEB.

[36] Swamy, N.V.C. and Fritzsche, A.A.(1976), “Aerodynamic Studies on Vertical Axis Wind Turbine”, International Symposium on Wind Energy Systems, Cambridge, England.

[37] Ammara, I.,Leclerc, L., and Masson, C.,(2002), “A Viscous Three Dimensional Differential/ Actuator-Disk Method for the Aerodynamic Analysis of Wind Farms“, International Symposium on Wind Energy Systems, Cambridge, England.

[38] Gupta,R., Biswas,A. And Sharma K.K.(2007), “Comparative study of a three bucket Savonius rotor with a combined three-bucket Savonius - three bladed Darrieus rotor”, Department of Mechanicaal Engineering, National Institute of Technology(NIT), Silchar 788010, Assam, India.

[39] Iida, A., Mizuno, A. and Fukudome, K.(2004), “Numerical Simulation of Aerodynamic Noise Radiated form Vertical Axis Wind Turbines”, Proceedings of the 18 International Congress on Acoustics.

[40] Ajedegba, J.O.(2008), “Effects of Blade Configuration on Flow Distribution and Power Output of a Zephyr Vertical Axis Wind Turbine”, M.Sc. Engg. Thesis, Dept of Mech. Engg., The Faculty of Engineering and Applied Science, University of Ontario Institute of Technology.

[41] Saha, U.K. and Maity, D.(2008), “Optimum Design Configuration of Savonius Rotor through Wind Tunnel Experiments”, Journal of Wind Engineering and Industrial Aerodynamics, Volume 96, Issues 8-9, Pages 1359-1375.

[42] Fujisawa, N.(1996), “Velocity Measurements and Numerical Calculations of Flow Fields in and around Savonius Rotors” Journal of Wind Engineering and Industrial Aerodynamics, Vol. 59, Issue 1, Pages 39-50.

[43] Spera, D.A.(1998), “Wind Turbine Technology”, ASME Press.

[44] Patel, M.R.(1999), “Wind and Solar Power Systems”, CRC Press, NY.